HORIBA
Scientific

Multitask Your Microscope™

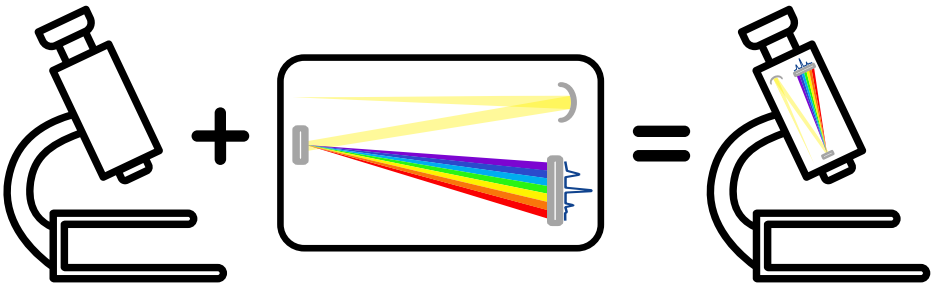

ADD SPECTROSCOPY TO ANY MICROSCOPE

STANDARD MICROSCOPE SPECTROSCOPY SYSTEMS

JOBIN YVON
Technology

Published in the USA by HORIBA Scientific
20 Knightsbridge Rd., Piscataway, NJ 08854

First published November 2019

Table of Contents

INTRODUCTION

Adding Various Spectroscopies to Any Standard Microscope

Microspectroscopy is the practice of performing various spectroscopies at the micro scale, and several trends have converged to make this area of work of current interest. Firstly, research is moving increasingly towards developing a better understanding of materials at the micro and nanoscale in such materials as microplastics [1]. Secondly, many modern materials rely on material engineering at the nanoscale in order to obtain desired properties such as strength and conductivity, as is the case with many 2D materials [2].

The optical microscope from various microscope vendors has, and continues to be, a natural platform for the study of micro materials. The opto-mechanical design of optical microscopes has evolved over many decades, and most of the major manufacturers now have robust, high performing platforms. However, the design of a typical optical microscope has evolved mainly as an imaging device, and many of the enhancements that make them suitable for imaging often interfere with broad-spectrum performance for spectroscopy across the UV, visible and NIR regions of the spectrum. This is mainly because visible imaging only covers a narrow spectrum (typically 400 nm to 700 nm) and many of the components involved in a microscope are transmission components optimized for the visible region of the optical spectrum. This means that using a standard microscope for spectroscopy in the UV or NIR often comes with suboptimal performance. Other more challenging spectroscopies, such as Raman, show this compromise even in the visible part of the spectrum simply because the construction of the typical standard microscope did not consider the requirements of such spectroscopies in their design. So, an important question when considering microspectroscopy on a standard microscope is, *how does one take advantage of the sturdy opto-mechanics and imaging capabilities of the standard microscope and also add high performing spectroscopy to this platform?* Indeed many analytical microspectroscopy manufacturers start with a microscope base and proceed to redesign, and repackage with spectroscopic components, to end up with various benchtop microspectroscopy instruments. This approach is attractive for highly specialized instruments but can be very restrictive and costly when one is interested in an open and flexible microspectroscopy architecture that:

- Can combine multiple spectroscopies on one platform (multimodality)
- Is modular and upgradable
- Retains all the imaging and native functions of the microscope while adding spectroscopy as an additional analytical modality
- Offers high performance levels for both imaging and spectroscopy without compromises

Challenges to implementing microspectroscopy on a standard microscope

The appeal for using a standard microscope for microspectroscopy are many and varied, but are primarily driven by the need for modularity, multimodality, upgradability and sometimes cost. Based on these drivers, researchers have been implementing home-built standard microscope-based microspectroscopy systems for a long time. However, these home-built implementations come with many challenges. Perhaps the most important of these challenges is that of acquiring the skill sets necessary to perform the opto-mechanical and software system integration function necessary to implement a high performing microspectroscopy system. Furthermore, the intrinsic limitations of most standard microscopes for spectroscopic applications described in the first section means that without specialized accessories, most home-built systems are often compromised solutions. The compromise often involves suboptimal performance of spectroscopy, or performing spectroscopy at the expense of some of the other functions of the microscope, including imaging. Finally, a home-built system is also very often a best-effort activity, in which the expected performance outcome is determined by the skill of the system integrator and usually not known in advance. This means that when the outcome is not up to expectations, a lot of time and money can be wasted that could have been used to perform productive work.

Customization without sacrificing performance

The Standard Microscope Spectroscopy (SMS) systems from HORIBA offer a simple proposition – add various spectroscopies to any standard microscope from the major microscope vendors, and do so without sacrificing spectroscopic performance or compromising the performance of the microscope. The SMS systems include uniquely designed accessories that enable microspectroscopy performance at levels comparable to high end specialized benchtop systems while retaining the open framework of a modular and upgradable system.

By decoupling the spectroscopic function from complete reliance on the optical components of the microscope, the SMS systems can separately optimize the spectroscopic functions without compromising the native functions of the microscope. In this regard SMS systems are true value additions to the native functions of the microscope, bringing more analytical capabilities to the microscope.

An SMS system can be obtained as a full turnkey system including the microscope, or as an addition to an end user's existing microscope. In both cases, the SMS system comes with turnkey functionality and various performance guarantees that are often not available for home-built systems.

In subsequent sections of this handbook, we show a sampling of the range of capabilities that can be realized on the SMS platform. With the SMS system you can truly let your imagination take flight!

References

(1) Catarina F. Araujo et al., “Identification of microplastics using Raman spectroscopy: Latest developments and future prospects,” Water Research, Volume 142, 1 October 2018, Pages 426-440
(2) Jiang-Bin Wu et al., “Raman spectroscopy of graphene-based materials and its applications in related devices”, Chem. Soc. Rev., 2018, 47, 1822-1873

Raman spectroscopy is a non-destructive chemical analysis technique, which provides detailed information about chemical structure, phase and polymorphism, crystallinity and molecular interactions. It is based on the interaction of light with the chemical bonds within a material.

Raman is a light scattering technique, whereby a molecule scatters incident light from a light source. Most of the scattered light is at the same wavelength (or color) as the incident light source (likely a laser), and does not provide useful information – this is called Rayleigh Scatter. However, a small amount of light (typically 0.0000001%) is scattered at different wavelengths (or colors), which depend on the chemical structure of the sample under study – this is called Raman Scatter.

A Raman spectrum features a number of peaks, showing the intensity and wavelength position of the Raman scattered light. Each peak corresponds to a specific molecular bond vibration, including individual bonds such as C-C, C=C, N-O, C-H, etc., and groups of bonds such as benzene ring breathing mode, polymer chain vibrations, lattice modes, etc.

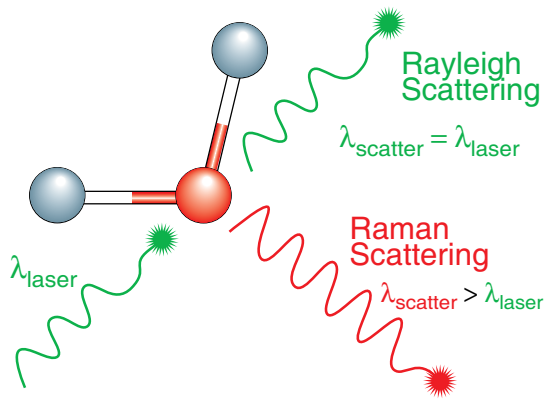

Figure 1: Raman principle

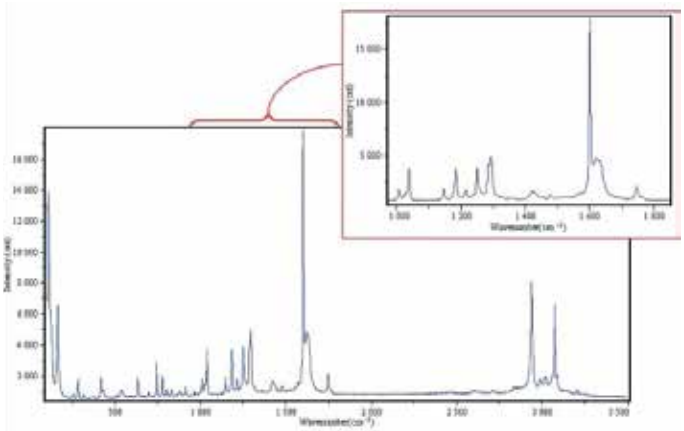

Figure 2: A typical Raman spectrum, in this case, of aspirin. (4-acetylsalicylic acid). The inset image shows the spectral detail present in the spectrum. Information provided by Raman Spectroscopy

Information provided by Raman spectroscopy

Raman spectroscopy probes a material and provides information about its:

- Chemical structure and identity
- Phase and polymorphism
- Intrinsic stress/strain
- Contamination and impurities

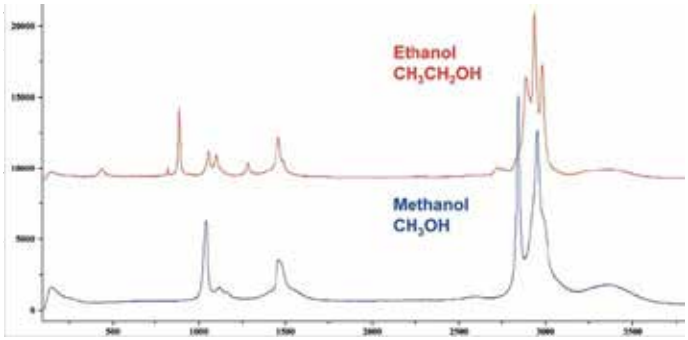

Figure 3: Raman spectra of ethanol and methanol, showing significant spectral differences allowing the two liquids to be distinguished.

When combined with mapping systems, it is possible to generate two-and three-dimensional images based on the sample's Raman spectrum. These images show distribution of individual chemical components, polymorphs and phases, and variation in crystallinity within the sample.

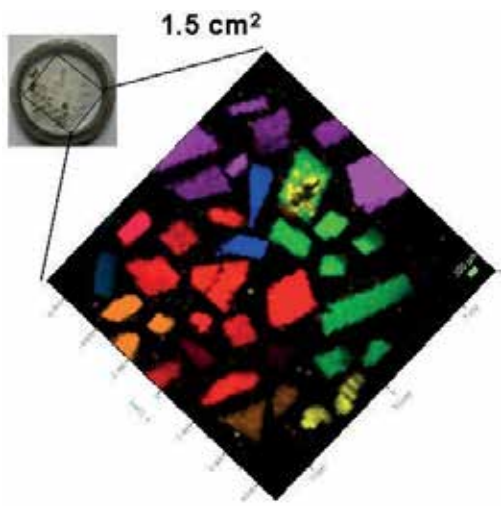

Figure 4: Distribution of different crystals within a mineral sample

Raman spectroscopy is both quantitative and qualitative

The general spectrum profile (peak position and relative peak intensity) provides a unique chemical fingerprint that identifies a material, and distinguishes it from others. Often the actual spectrum is quite complex, so comprehensive Raman spectral libraries can be searched to find a match, and thus provide a chemical identification of the sample under study.

The intensity of a spectrum is directly proportional to concentration. Typically, the relationship between peak intensity and concentration is determined from a calibration procedure and then routine measurements are used to analyze for concentration from the calibration curve. With mixtures, relative peak intensities provide information about the relative concentration of the components, while absolute peak intensities can be used for absolute concentration information.

Raman microspectroscopy

Raman spectroscopy is also used for microscopic analysis, with a spatial resolution in the order 0.5 to 1 µm on standard microscopes. A Raman microscope couples a Raman spectrometer to a standard optical microscope, allowing high magnification visualization of a sample and Raman analysis with a microscopic laser spot. Raman micro-analysis is easy: Simply place the sample under the microscope, focus, and make a measurement.

Motorized mapping stages allow Raman spectral images to be generated, which often contain many thousands of Raman spectra acquired from different positions on the sample. False color images can be created based on the Raman spectrum – these show the distribution of individual chemical components, and variation in other effects, such as phase, polymorphism, stress/strain, and crystallinity.

This chapter focuses on micro Raman systems implemented as a modular addition to any of the common standard microscopes (from Olympus®, Leica®, Zeiss® and Nikon®)... so-called Standard Microscope Spectroscopy (SMS) systems. While the concept of adding various spectroscopies to a standard microscope is not new, the novelty in the HORIBA implementation is in how it is done. By using a unique modular microspectroscopy module, the SMS system enables highly optimized implementation of micro Raman on a standard microscope, without compromising any of the inherent functions of the microscope. In so doing, the SMS enables the standard microscope to serve as a powerful multimodal micro visualization and analytical platform.

Figure 5: A typical modular SMS micro Raman microscope system

Types of samples analyzed with Raman

In general, Raman spectroscopy is suitable for analysis of:

- Solids, powders, liquids, gels, slurries and gases
- Inorganic, organic and biological materials
- Pure chemicals, mixtures and solutions
- Metallic oxides and corrosion.

It is not suitable for analysis of metals and their alloys.

Typical examples of where Raman is used today include:

- Art and archaeology – characterization of pigments, ceramics and gemstones
- Carbon materials – structure and purity of nanotubes,defect/disorder characterization
- Chemistry – structure, purity, and reaction monitoring
- Geology – mineral identification and distribution, fluid inclusions and phase transitions
- Life sciences – single cells and tissue, drug interactions, disease diagnosis
- Pharmaceuticals – content uniformity and component distribution
- Semiconductors – purity, alloy composition, intrinsic stress/strain

Analysis of solids, liquids and gases

Raman spectra can be acquired from nearly all samples that contain true molecular bonding. This means that solids, powders, slurries, liquids, gels and gases can be analyzed using Raman spectroscopy.

Although gases can be analyzed using Raman spectroscopy, the concentration of molecules in a gas is typically very low, so the measurement is often more challenging. Usually specialized equipment such as higher-powered lasers and sample cells with long path lengths are necessary for Raman spectroscopy in gases. In some cases where gas pressures are high (such as gas inclusions in minerals), standard Raman instrumentation can easily be used.

Analysis of mixtures

The Raman spectrum from a material will contain Raman information about all of the molecules that are within the analysis volume of the system. Thus, if there is a mixture of molecules, the Raman spectrum will contain peaks representing all of the different molecules. For known components in the mixture, the relative Raman peak intensities can be used to generate quantitative information about the mixture's composition. In the case of complex matrixes, chemometrics methods might also be employed to build quantitative methods.

Common applications of Raman spectroscopy

Raman spectroscopy is used in many varied fields – in fact, it can be used in any application where non-destructive, microscopic, chemical analysis and imaging is required. Whether the goal is qualitative or quantitative data, Raman analysis can provide key information easily and quickly. It can be used to rapidly characterize the chemical composition and structure of a sample, whether solid, liquid, gas, gel, slurry or powder.

The discussion below highlights some key areas where the use of Raman is well established.

Pharmaceuticals and Cosmetics
- Compound distribution in tablets
- Blend uniformity
- High throughput screening
- API concentration
- Powder content and purity
- Raw material verification
- Polymorphic forms
- Crystallinity
- Contaminant identification
- Combinational chemistry
- In vivo analysis and skin depth profiling
- Dosage, content uniformity

Geology and Mineralogy
- Gemstone and mineral identification
- Fluid inclusions
- Mineral and phase distribution in rock sections
- Phase transitions
- Mineral behavior under extreme conditions
- Chondrite/achondrite meteorites identification

Carbon Materials
- Single walled carbon nanotubes (SWCNTs)
- Purity of carbon nanotubes (CNTs)
- Electrical properties of carbon nanotubes (CNTs)
- sp2 and sp3 structure in carbon materials
- Hard disk drives
- Diamond-like carbon (DLC) coating properties
- Defect/disorder analysis in carbon materials
- Diamond quality and provenance
- Electrical properties and number of layers of graphene

Semiconductors
- Characterization of intrinsic stress/strain
- Purity
- Alloy composition
- Contamination identification
- Superlattice structure
- Defect analysis
- Hetero-structures
- Doping effects
- Photoluminescence micro-analysis
- 2D Transition Metal Dichalcogenide (MoS, WSe, WSe, Phosphorene,...) electrical properties characterization

Life Sciences
- Bio-compatibility
- DNA/RNA analysis
- Drug/cell interactions
- Photodynamic therapy (PDT)
- Metabolic accretions
- Disease diagnosis
- Single cell analysis
- Cell sorting
- Characterization of bio-molecules
- Bone structure

Discrimination of different phases and polymorphs of a material

In most cases, Raman scattering is sensitive to material phase, polymorphism and solid form. Thus, even though two materials may have identical chemical formulae, their different crystal structure or phase will often result in distinct spectra. Phase changes are often clearly distinguished within the spectrum, but other structural differences, such as polymorphism, can reveal themselves only through very subtle spectral changes. In this case, it is often necessary to work with high spectral resolution to allow the minor changes to be confidently characterized.

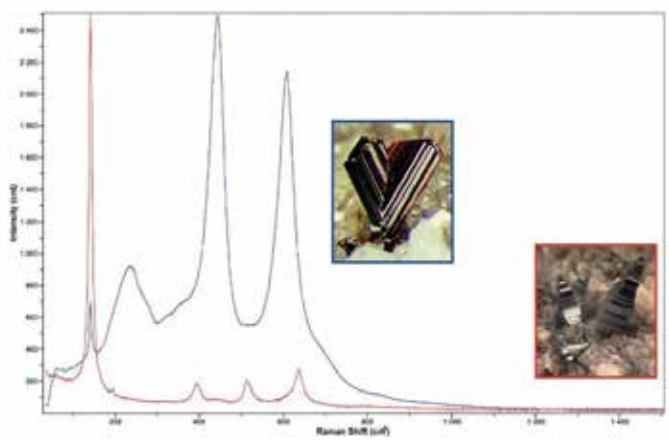

Figure 6: Spectra of TiO2: The difference between Rutile (blue) and Anatase (Red) can be used for fast identification

Analysis of material crystallinity

Raman scattering is also sensitive to the degree of crystallinity in a sample. Typically a crystalline material yields a spectrum with very sharp, intense Raman peaks, while an amorphous material will show broader, less intense Raman peaks. These two states (e.g., fully amorphous, or fully crystalline) can be considered as spectral extremes, and a Raman spectrum from an intermediate state (e.g., partially crystalline) will have characteristics which are intermediate in terms of peak intensity and width (sharpness). Differences between intermediate states can be subtle, and it is often useful to have high spectral

resolution capability so that minor spectral changes can be confidently characterized.

It is possible to accurately calculate peak width and intensity using software peak fitting routines. This information can then be used with calibration and comparison with other techniques, as a quantitative measure of crystallinity. Similar analysis of Raman maps allows images of degree of crystallinity to be produced.

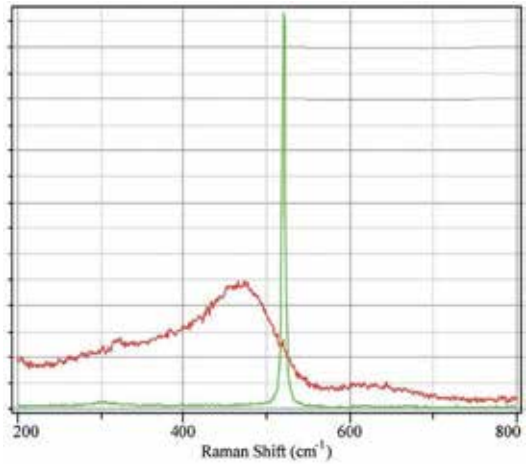

Figure 7: Spectra of polycrystalline (red) and monocrystalline Si (green)

Flexible and Modular Micro Raman Measurement System (SMS)

Introduction

Micro Raman spectroscopy is an increasingly popular technique for molecular analysis and fingerprinting – showing a roughly 9.5% average annual increase in citations over the last decade.[1] This growth comes from the rapid development of new materials, such as graphene and carbon nanotubes, etc., and their use in a vast number of applications. The appeal for micro Raman is the molecular specificity that it provides and the fact that it is a relatively easy and non-contact, non-destructive technique to implement and use. Micro Raman is used extensively in such fields as pharmaceuticals, semiconductors, life sciences, etc., and there are many different instruments targeted to these application areas. However, it is increasingly common to require the addition of micro Raman to a standard microscope, either to leverage an existing microscope and save on cost, or to add micro Raman as one of a multiplicity of techniques on the same microscope platform. In either case, one would require a modular and flexible arrangement of components to accomplish the desired result – and users who have attempted this often realize the result is a compromise solution – in terms of performance between spectroscopy and imaging. The Standard Microscope Spectroscopy (SMS) system from HORIBA is one of the first commercial implementations of such a turnkey modular and flexible micro Raman system based on a standard microscope that do not compromise either the imaging functionality of the microscope or the Raman spectroscopy performance (relative to other high end benchtop systems).

Figure 1 illustrates the configuration of a typical SMS-Raman system with the components for different requirements, including multiple lasers, a UV-Vis-NIR detector, a motorized sample stage, etc. The SMS system is also a comprehensive and flexible platform capable of multiple spectroscopies, such as micro PL, reflectance, TCSPC spectroscopy, etc.

(a) (b)

Figure 1: Experimental setup for micro Raman measurement on a standard microscope. (a) Schematic setup. (b) Front view of HORIBA Standard Microscope Spectroscopy (SMS) system.

Setup

A key enabler for the SMS-Raman system is the universal microspectroscopy adapter from HORIBA that adapts to most standard upright microscopes, and contains uniquely designed reflective optics to direct excitation light to the sample, and a dichroic and long pass filter to separate laser light from the Raman signal from the sample.
The design of the optics in this module enables high performance Raman with the ability to work much closer to the laser line than is achievable with standard microscope filter cubes. The excitation light focuses onto the sample surface through the microscope objective, which also collects the emitted Raman light, collimating and focusing it into the spectrometer. The spectrometer shown in figure 1 is the iHR320 but it could be any other spectrometer and detector from the HORIBA portfolio chosen to meet desired expectations for resolution, spectral range, detector sensitivity and measurement speed. An optional motorized translation stage communicates with the vision camera for sample positioning, scanning and adding spatial distribution to Raman mapping. The entire setup is controlled, and spectral data analyzed by HORIBA LabSpec 6 software.

Results

Figure 2a shows the 520 cm^{-1} Raman peak obtained from a bare silicon sample using this setup. The silicon sample used also contained an area with “HORIBA Scientific” etched in gold lettering. Figure 2b shows a Raman map of this area collected using the motorized stage. The figure shows the peak intensity of the 520 cm^{-1} silicon peak – low intensity on the gold lettering and high intensity on the bare silicon substrate.

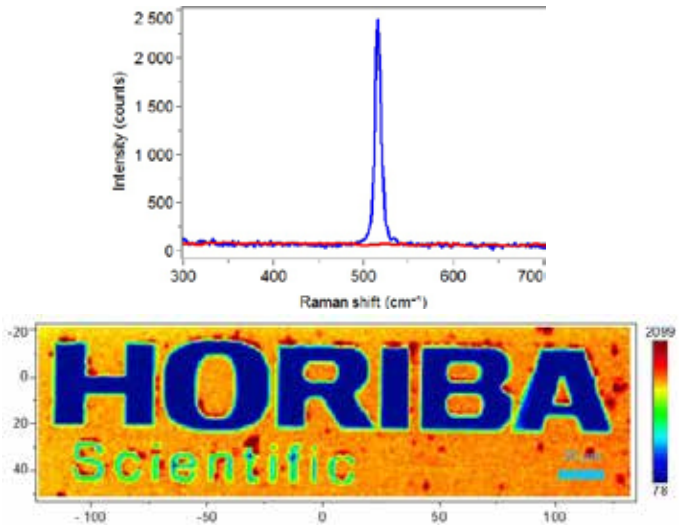

Figure 2: Micro Raman measurement on a Si sample etched with metal "HORIBA Scientific" logo on the surface (excitation wavelength = 532 nm, objective = 50x). (a) Spectra of Si (blue) and metal (red). (b) Raman mapping showing spatial distribution of Si using the peak intensity of the distribution of the 520 cm^{-1} Si peak (pixel size = 255 × 72, resolution = 1 µm).

One of the advantages of using a standard microscope with the SMS system is to take advantage of the native features of the microscope, such as up to five objectives on the turret to perform wide-field mapping at low magnifications and high spatial resolution maps of smaller regions of interest at higher magnifications. Figure 3 shows a wide area Raman map of a carbon nanotube sample (a) and another at higher resolution (b).

Summary

The Standard Microscope Spectroscopy (SMS) system from HORIBA Scientific provides a flexible platform for microspectroscopy, including Raman. The SMS platform includes a universal microspectroscopy adapter that enables obtaining Raman spectra much closer to the laser line than is achievable using the filter cubes that come with the microscope. It offers the flexibility to use different excitation light sources, as well as a choice of spectrometer and detector to satisfy any requirement for spectral resolution, range, sensitivity and measurement speed. The major components used here for Raman measurement are listed to the right.

References

(1) Google Scholar search for "Micro Raman Spectroscopy"

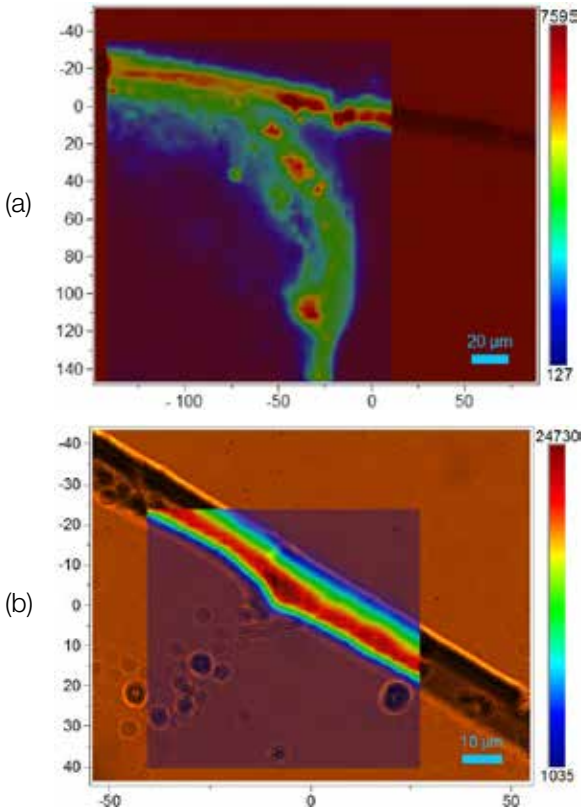

Figure 3: Optical images of carbon nanotubes with Raman mappings overlaid (excitation wavelength = 532 nm). (a) Observed by 10x objective. (b) Observed by 60x objective.

Part No.	Description
LCX-532S-500-CSB-PPA	Laser - 532 nm, 500 mW, SLM DPSS
BX-53-MIC	Olympus BX-53 Upright microscope
VIS-CAM	Vision camera for microscope.
IHR320 Core 3	iHR320 f/4.1, Imaging spectrometer, including patented kinematic triple grating turret with three specified gratings.
SYNCER-1024x256-OE	Syncerity CCD head thermoelectrically (TE) cooled to -60° C using E2V manufactured, spectroscopy grade 1, 1024 x 256 pixel open electrode CCD chip with 26 µm x 26 µm pixels and overall format of 26.6 mm x 6.6 mm.
LabSpec 6	LabSpec Software for Windows XP and above permitting the control of the spectrometer, data acquisition and a wide range of data treatment and storage options.

Advanced Raman Analytics on an SMS

Introduction

Raman spectroscopy is widely used in many fields including pharmaceuticals, life sciences and semiconductors. Its appeal comes from the chemical specificity provided by this technique. Raman spectroscopy is usually able to distinguish between different chemical compounds and molecules, as well identify various states of the same compound or molecule. Such analytical fingerprinting capability is very valuable in many fields to provide a fast and efficient reading of the composition and states of different samples of interest. Vast libraries of Raman spectra for various popular materials have been developed to facilitate material identification using Raman spectroscopy. However, users of home-built or custom Raman solutions are often not exposed to these advanced capabilities of Raman spectroscopy systems that are available on other standard benchtop systems. KnowItAll® is one such reference library of Raman spectra.

The Standard Microscope Spectroscopy (SMS) system from HORIBA is a modular turnkey system that equips a standard microscope with various spectroscopies, including micro Raman, Photoluminescence (PL), reflectance, etc. This system can also be added as a kit to a user's existing microscope. Whether acquired as a complete turnkey solution, or as an upgrade to an existing microscope, the full functionality of KnowItAll® is available for spectral search, analysis and data mining on all SMS systems. In this paper, we demonstrate this capability by measuring micro Raman spectra of silicon, which is commonly used as a calibrating sample. We also measured polystyrene and aspirin, and tested the functionality of KnowItAll® on the resulting datasets.

The HORIBA Edition of KnowItAll® provides an integrated environment for complete spectral searching, analysis and data mining, which complements LabSpec 6's integrated functionality. Over 1,750 Raman spectra from a broad range of materials, including inorganics, organics and polymers, minerals, bio-minerals, semiconductors and pigments/dyes are included in HORIBA's own Raman spectral databases. Furthermore, extensive Raman spectral databases with more than 9,000 spectra from a wide variety of material types can be included as upgrades.

Experiment and results

All the samples were excited using a 532 nm laser, which was free-space coupled to a microscope. The sample emission was collimated and focused into the SMS system. Since KnowItAll® is integrated into LabSpec 6, the acquired spectral data from LabSpec was simply ported over to the KnowItAll® workspace to initiate a search from the spectral databases.

The Raman spectra of silicon, polystyrene and aspirin are shown in Figures 1, 2 and 3 respectively. The blue lines are the results obtained by using an SMS system equipped with Raman components. With one-click exportation to the KnowItAll® environment, the best matched components from Raman spectral databases are shown by the red lines. Although not shown, KnowItAll® is capable of spectral deconvolution of mixtures, identifying different material components present.

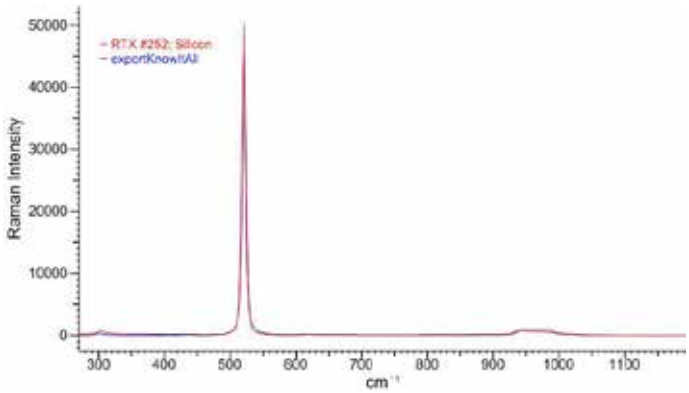

Figure 1: Raman spectrum of Si excited with a 532 nm laser acquired by an SMS system (blue), compared with the known spectra from the HORIBA Edition of KnowItAll® database (red).

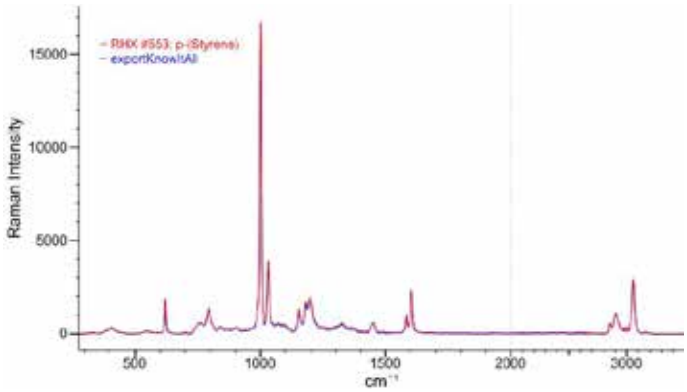

Figure 2: Raman spectrum of polystyrene excited with a 532 nm laser acquired by an SMS system (blue), compared with the known spectra from the HORIBA Edition of KnowItAll® database (red).

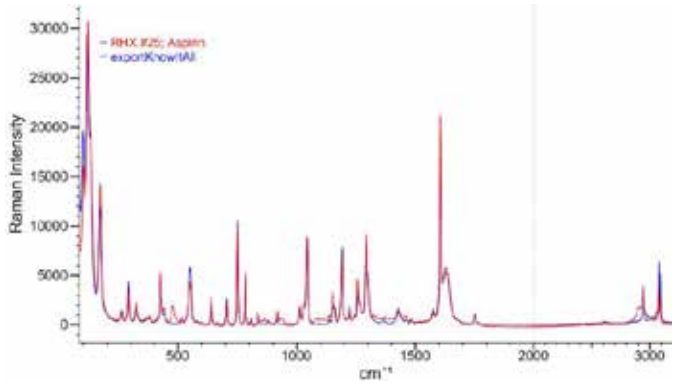

Figure 3: Raman spectrum of aspirin excited with a 532 nm laser acquired by an SMS system (blue), compared with the known spectra from the HORIBA Edition of KnowItAll® database (red).

Summary

The Standard Microscope Spectroscopy (SMS) system from HORIBA Scientific is a comprehensive and flexible platform capable of micro Raman, PL, reflectance, TCSPC spectroscopies, etc. Although modular and customizable, the SMS micro Raman platform offers advanced Raman analytics such as KnowItAll®, which is a powerful and convenient tool to fully understand the origins of spectra and identify the components of a mixture by their spectral signatures. Figure 4 illustrates the system configuration, and the main components used in the setup are listed in the table below.

Figure 4: Front view of a HORIBA Standard Microscope Spectroscopy (SMS) system.

Part No.	Description
LCX-532S-500-CSB-PPA	Laser - 532 nm, 500 mW, SLM DPSS
BX-53-MIC	Olympus® BX-53 Upright microscope
VIS-CAM	Vision camera for microscope.
IHR320 Core 3	iHR320 f/4.1, Imaging spectrometer, including patented kinematic triple grating turret with three specified gratings.
SYNCER-1024x256-OE	Syncerity CCD head thermoelectrically (T\E) cooled to -60° C using E2V manufactured, spectroscopy grade 1, 1024 x 256 pixel open electrode CCD chip with 26 µm x 26 µm pixels and overall format of 26.6 mm x 6.6 mm.
LabSpec 6	LabSpec Software for Windows XP and above permitting the control of the spectrometer, data acquisition and a wide range of data treatment and storage options.
LS6-KIA	KnowItAll HORIBA Edition: Spectral searching and analysis software package. Raman libraries include >1750 spectra for polymers, inorganics, inks/pigments, semiconductors, and biomaterials.

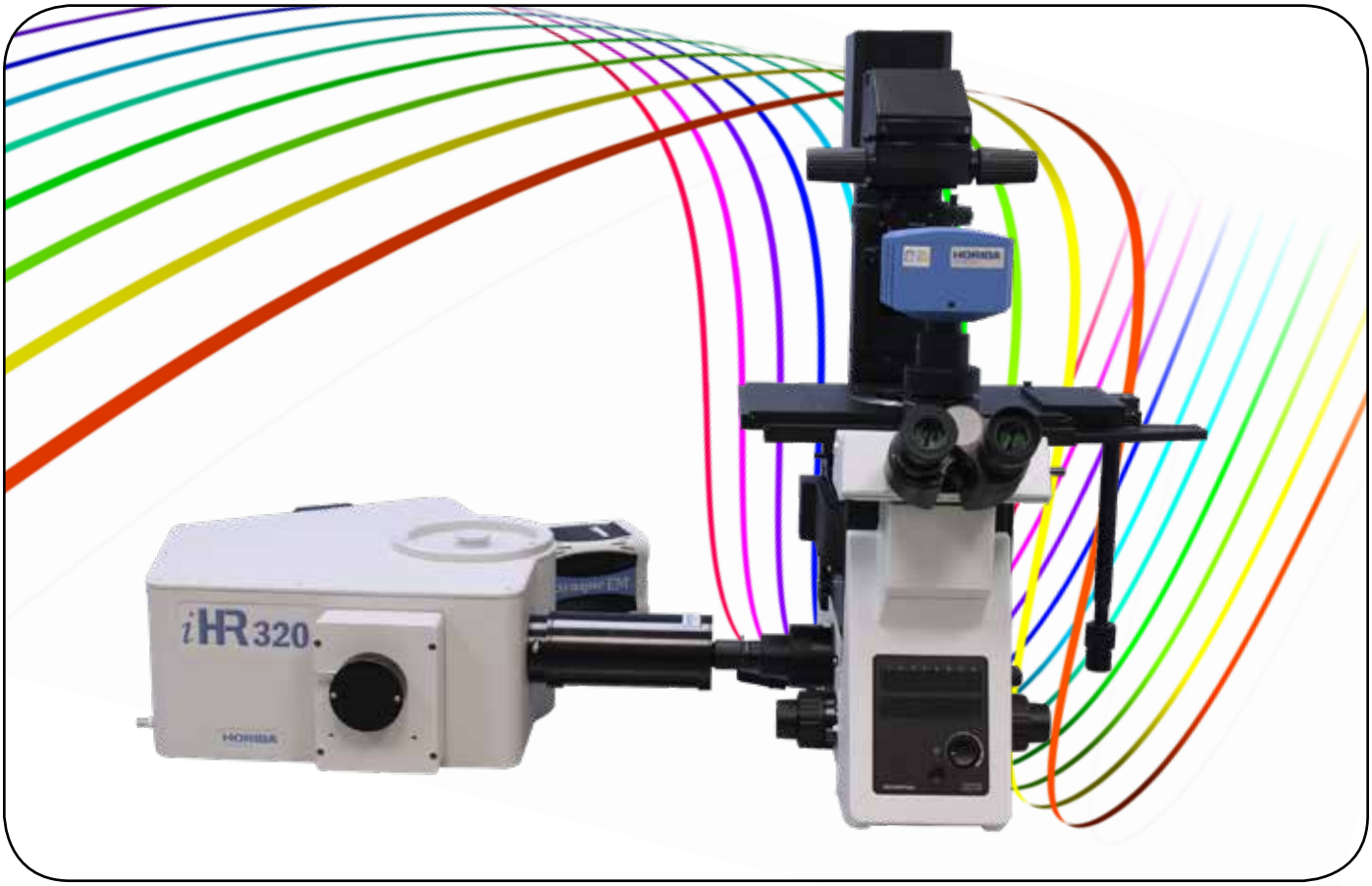

Raman Analysis of 2D Materials on an SMS

Introduction

2D materials are novel structures consisting of a single layer, or at most, a few layers of atoms with material properties that differ significantly from their bulk counterparts. These new material characteristics include enhanced charge mobilities, high tensile strength, etc., and have significant implications for various application fields including photovoltaics, semiconductors, building materials, etc. Since Raman scattering is a result of molecular and crystalline deformations, it is particularly appealing in the study of these new low dimensional materials. Raman spectroscopy is commonly used in the characterization of 2D materials as it provides a contactless and non-destructive technique to identify the structures and allotropes.

It is common to utilize standard microscopes for visualizing these 2D micro and nano structures after, or during, fabrication. However, any further analysis of the sample typically means taking it to one or more specialized systems for that measurement. In this paper, we propose an alternative that takes advantage of the standard microscope as the base evaluation instrument of 2D materials, and instead of moving a sample across different instruments for complementary measurements, we seek to bring these complementary analytical techniques – including Raman, as modular additions to a standard microscope. Furthermore, we seek to do this in a manner that does not compromise the native imaging functionalities of the microscope or degrade the performance of the added spectroscopy.

The Standard Microscope Spectroscopy (SMS) system from HORIBA is a modular turnkey system that equips a standard microscope with the capability to perform micro Raman spectroscopy with high performance, but without any compromises to the other imaging functions of the microscope. In this work, we show the capability of the SMS system by performing micro Raman measurements on two popular 2D materials: Molybdenum disulfide (MoS_2) and graphene oxide (GO).

Instrumentation and results

The SMS system is a comprehensive and flexible platform capable of multiple spectroscopies, such as micro PL, reflectance, TCSPC spectroscopy, etc. Figure 1 shows the SMS equipped with a universal microscopy adapter – MicroSpex. The MicroSpex is a self-contained spectroscopy module with the Raman excitation and filtering optics pre-installed. In this case, the filter was for a 532 nm laser. The filter module design for the MicroSpex is different from that of the filter cubes that come with most standard microscopes. This design change is intentional and enhances Raman performance, especially regarding working close to the laser line (see section 2.3.4). The MicroSpex effectively decouples the imaging and spectroscopy functions on the microscope, enabling both to work optimally and without compromises to either. The excitation light is focused onto the sample surface by the objective, which also collects the emission light collimating and focuses it into the iHR320 spectrometer. The SMS includes white light illumination and a color camera for sample visualization. An optional motorized translation stage communicates with the vision camera for sample positioning, scanning and adding spatial resolution to Raman mapping. HORIBA LabSpec software is used for instrument control and data analysis.

(a) (b)

Figure 1: Experimental setup for micro Raman measurement on a standard microscope equipped with MicroSpex. (a) Schematic setup. (b) Front view of HORIBA Standard Microscope Spectroscopy (SMS) system.

1. Molybdenum disulfide (MoS_2)

The 2D structure of MoS_2 shows interesting properties with possible applications in the production of fast transistors and photodetectors. Raman spectroscopy is commonly used to characterize its crystal structure, as shown in Figure 2. The Raman frequencies of E^1_{2g} (~ 382 cm^{-1}) and A_{1g} (~ 407 cm^{-1}) peaks (1) are observed in Figure 2(b). By utilizing the motorized translation stage, spatial information is added to the measured data set and the 2D and 3D images of Raman mapping based on the emission intensity of A1g peak are produced (see Figure 2(a) and 2(d), respectively). The intensities of the Raman peak at the defects, whose diameters are less than 0.5 µm, drop significantly. At such high spatial resolution, the microstructure of the sample can be immediately determined.

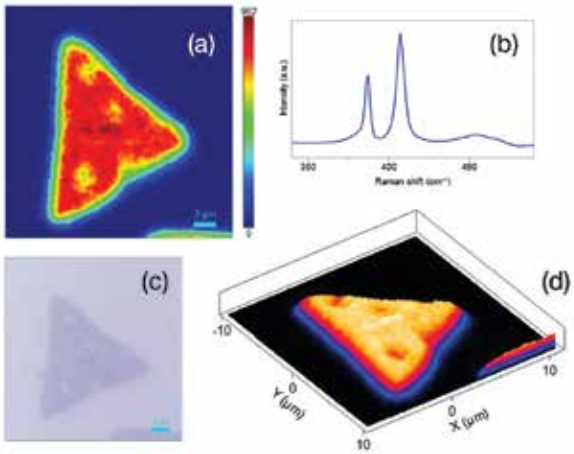

Figure 2: Raman characterization of a monolayer MoS_2 using 532 nm laser line (objective = 100x, spatial resolution = 0.3 µm). (a) 2D image of Raman map of A_{1g} peak intensity. (b) A Raman spectrum showing sharp and intense E^1_{2g} and A_{1g} peaks of MoS_2 sample. (c) Optical image of the MoS_2 flake. (d) 3D image of Raman map of A_{1g} peak intensity.

2. Graphene oxide (GO)

A similar measurement as in section 1 above was performed on a graphene oxide (GO) sample. The results are shown in Figure 3. The Raman frequencies of the D band (1350 cm^{-1}) and G band (1580 cm^{-1}) (2) caused by the electron-phonon scattering mechanism can be observed in Figure 3(b). They are used to characterize the properties of graphene, as well as graphene-based materials such as GO. The 2D and 3D images of Raman mapping based on the emission intensity of the G peak are illustrated in Figure 3(a) and 3(d), respectively.

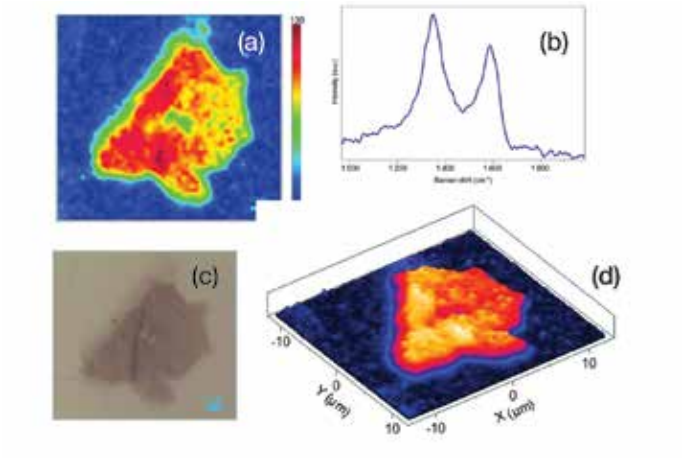

Figure 3: Raman characterization of a GO flake using 532 nm laser line (objective = 100x, spatial resolution = 0.5 µm). (a) 2D image of Raman map of the G peak intensity. (b) A Raman spectrum showing D and G peaks. (c) Optical image of the GO flake. (d) 3D image of Raman map of the G peak intensity.

Summary

The Standard Microscope Spectroscopy (SMS) system from HORIBA Scientific provides a modular microspectroscopy solution for performing high resolution micro Raman. Samples of monolayer MoS2 and GO were used to assess the system capabilities. The MicroSpex accessory on the SMS is the key enabler for this functionality, and can be added as a kit to a user's existing microscope. The SMS configuration adds significant analytical capability to most standard microscopes without compromising the quality of either imaging or spectroscopy. The major components used here for micro Raman measurement are listed below.

Part No.	Description
LCX-532S-500-CSB-PPA	Laser - 532 nm, 500 mW, SLM DPSS
BX-53-MIC	Olympus BX-53 Upright microscope
MicroSpex-UMA	Universal Microscope Spectroscopy Adapter.
VIS-CAM	Vision camera for microscope.
IHR320 Core 3	iHR320 f/4.1, Imaging Spectrometer, including patented kinematic triple grating turret with three specified gratings.
SYNCER-1024x256-OE	Syncerity CCD head thermoelectrically (TE) cooled to -60° C using E2V manufactured, spectroscopy grade 1, 1024 x 256 pixel open electrode CCD chip with 26 µm x 26 µm pixels and overall format of 26.6 mm x 6.6 mm.
LabSpec 6	LabSpec Software for Windows XP and above permitting the control of the spectrometer, data acquisition and a wide range of data treatment and storage options.

References

(1) H. Li, et al., Adv. Funct. Mater., 22, 1385 (2012).
(2) R. Saito, et al., Adv. Phys., 60, 413 (2011)

Low Wavenumber Raman Material Characterization on an SMS system

Introduction

Raman microspectroscopy is a popular analytical technique in such fields as pharmaceuticals, life science, semiconductors, etc. Raman spectroscopy provides composition, as well as structural fingerprinting of various molecular structures, with very high specificity. Research is moving increasingly into development and engineering of novel materials at the micro and nano scales, and various specialized micro Raman instrumentation have been developed to address this need. Unfortunately, the highly specialized nature of many of these instruments often means less flexibility to adapt to changing requirements for the measurement. These changes could include demand for higher spectral resolution or enhanced sensitivity in a different spectral range, or even the need to multiplex micro Raman with another complementary technique on the same platform. Such changes in measurement requirements are the main drivers for a more flexible and modular platform for performing micro Raman spectroscopy, and the standard microscope is a natural candidate for building such modular systems. However, in their native form, most standard microscopes are imaging devices and often show poor spectroscopic performance when the native microscope optics is used for spectroscopy – especially Raman. Worse, implementation of microspectroscopy on a microscope can sometimes lead to a compromise of the imaging properties of the microscope itself.

In this work, we describe a modular turnkey system that equips a standard microscope with high performance micro Raman without any compromises to the other imaging functions of the microscope. The Standard Microscope Spectroscopy (SMS) system includes a universal microspectroscopy adapter (MicroSpex) that enables high performance Raman – specifically working close to the laser line. This performance feature is not readily achievable when using the filter cubes that come standard with the microscope. Since the MicroSpex is a self-contained spectroscopy module, it effectively decouples the imaging and spectroscopy functions on the microscope, enabling both to work optimally and without compromises to either.

Instrumentation

Figure 1 shows an illustration of the MicroSpex mounted on a standard microscope (in this case equipped for a fiber-coupled excitation and emission). The module shown includes laser-coupling optics to direct excitation light to the sample and a dichroic and long pass filter to separate laser light from sample emission. The SMS system is a comprehensive and flexible platform capable of multiple spectroscopies, such as micro PL, reflectance, TCSPC spectroscopy, etc.

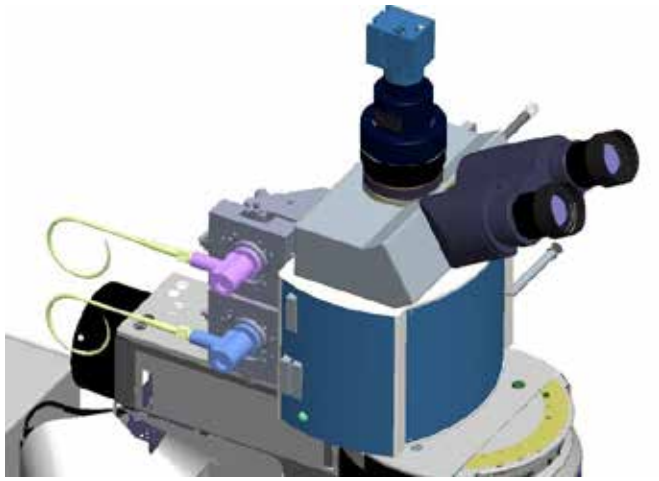

Figure 1: MicroSpex mounted on a HORIBA Standard Microscope Spectroscopy (SMS) system. Free space and fiber coupling are available for both excitation and emission.

In this work we show the SMS's capability of performing Raman measurements at relatively low wavenumbers from the laser line. Samples with peaks in this region of the spectrum such as sulfur, polystyrene, and aspirin were measured on the SMS equipped with the MicroSpex and compared to similar results measured on other systems. Figure 2 illustrates the schematic setup of the SMS system equipped with MicroSpex.

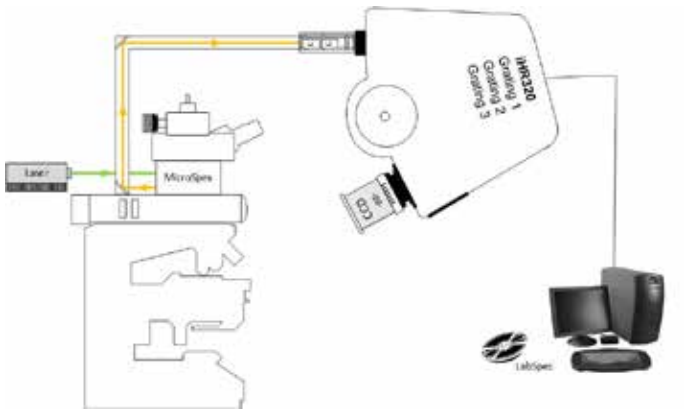

Figure 2: Experimental setup for micro Raman spectroscopy using MicroSpex on a standard microscope.

Results

The Raman spectra of a sulfur powder sample are shown in Figure 3. The blue line was the result obtained for the same sample using a prob- based Raman system with identical acquisition conditions as the SMS with MicroSpex. In this case, the Raman peaks near 100 cm^{-1} are barely visible. The red line is the result from SMS with MicroSpex. In this case, the sulfur peak at 27.37 cm^{-1} is distinguishable!

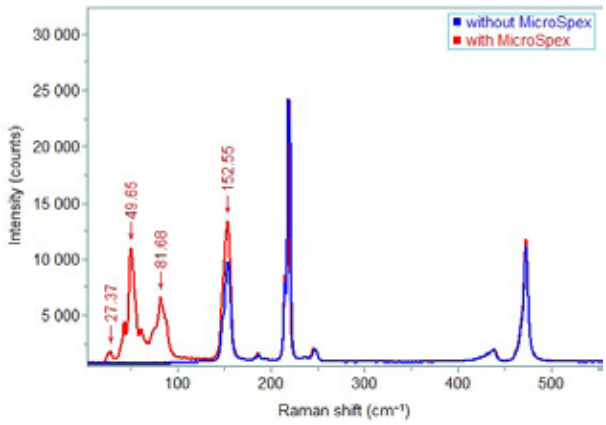

Figure 3: Raman spectra of sulfur exhibits prominent peaks below 100 cm^{-1} using MicroSpex on a standard microscope (red), which is not able to be observed by using a standard microscope only (blue).

Figure 4 shows a similar comparative measurement for polystyrene. Once again, the peaks below 50 cm^{-1} are quite distinct on the SMS system.

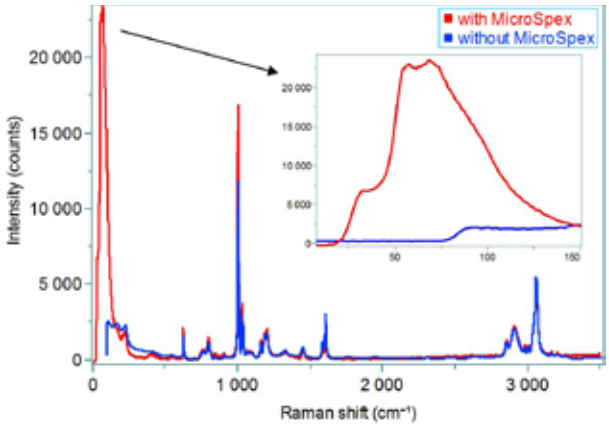

Figure 4: Comparison of Raman spectra of polystyrene between using MicroSpex (red) and not using MicroSpex (blue).

Finally, figure 5 shows the Raman spectra of an aspirin sample – with a clear sensitivity and resolution of the low wavenumber peaks discernible from the measurements on the SMS system.

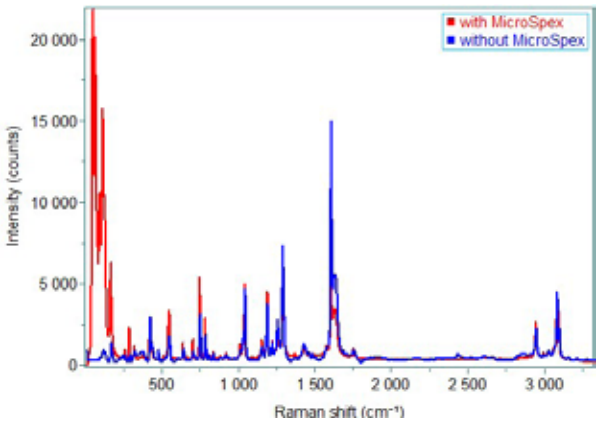

Figure 5: Raman spectra of aspirin. (Red) Microscope equipped with MicroSpex. (Blue) Standard microscope without MicroSpex.

Summary

The MicroSpex used on a Standard Microscope Spectroscopy (SMS) system from HORIBA Scientific provides an outstanding solution for measuring low wavenumber Raman spectroscopy. Sulfur, polystyrene and aspirin samples were tested and compared by using an SMS system equipped with the MicroSpex accessory and another probe based Raman system. The results show a superior advantage using MicroSpex in the measurement of Raman spectra, especially at low wavenumber. The major components used here for Raman measurement are listed below.

Part No.	Description
LCX-532S-500-CSB-PPA	Laser - 532 nm, 500 mW, SLM DPSS
BX-53-MIC	Olympus BX-53 upright microscope
MicroSpex-UMA	Universal microscope spectroscopy adapter.
IHR320 Core 3	iHR320 f/4.1, Imaging spectrometer, including patented kinematic triple grating turret with three specified gratings.
SYNCER-2048x70-NIR	Syncerity CCD head thermoelectrically (TE) cooled to -50° C using spectroscopy grade 1, 2048 x 70 pixel back-Illuminated NIR CCD chip with 14 µm x 14 µm pixels and overall format of 28.7 mm x 0.98 mm.
LabSpec 6	LabSpec Software for Windows XP and above permitting the control of the spectrometer, data acquisition and a wide range of data treatment and storage options.

Best Practices for Micro Raman Spectroscopy

Introduction

Raman microscopy provides an informative technique in the characterization of molecular structures. The rapid development of new materials contributes to the fast growth of Raman instruments. Raman spectroscopy is a non-contact and non-destructive technique, contributing to its appeal in many applications. HORIBA Scientific provides a wide variety of Raman spectroscopy instrumentation to suit different needs. Amongst these is the Standard Microscope Spectroscopy (SMS) system that equips most standard microscopes with micro Raman capability. The SMS platform is a modular and flexible system capable of multitasking any standard microscope by adding multiple functionalities such as Raman, PL, TCSPC spectroscopy, etc. The modularity and flexibility of the SMS platform means that a user needs to be more aware of the options available in order to customize a system to a particular need. In this write up, we describe the best practices for micro Raman measurement, including selection of lasers, filters and objectives, etc.

Choice of laser

The selection of the laser wavelength can be one of the most important considerations for Raman measurement. Since Raman light is a shift from a known laser line, one typically uses a stable, narrow linewidth, monochromatic laser as the excitation source for Raman spectroscopy. Raman quality lasers can have high intensities and retain a high degree of collimation so that a tightly focused spot can be achieved at the sample for spatially resolved micro measurements. The choice of laser wavelength is especially important for samples that can fluoresce. For instance, a green laser (532 nm) may promote the much more intense and broader fluorescence emission from biological samples, which may swamp the underlying Raman spectrum and make it non-detectable. In such a case, a red (633 nm) or NIR (785 nm) laser with the lower photon energy, may be more appropriate since the degree of fluorescence excitation would be lower at such wavelengths. However, with the laser wavelength increasing (green – red – NIR) the Raman scattering efficiency decreases, requiring longer integration times or higher power lasers to achieve good signal-to-noise (SNR) spectra for Raman. Thus, it is often practical to employ several laser wavelengths on the equipment to match the various sample properties and obtain the best detection of the Raman signal.

In addition to wavelength, using a narrow linewidth laser is important for efficient Raman measurements. A broad linewidth laser may convolve with the measured Raman signal and obscure features of interest in the measurement. Finally, the laser power should be chosen to obtain a good SNR of the measured Raman signal, over a reasonable integration time and without damaging the sample. Our Standard Microscope Spectroscopy (SMS) system uses lasers that pass our stringent QC tests, fully evaluated over many projects.

Raman filters

In Raman microspectroscopy, the optical isolation of the excitation light from emitted light is of great importance, and can be very challenging, as these wavelength ranges are often quite close to each other. Most standard fluorescence microscopes include filter cubes accommodating a bandpass filter, dichroic and notch or edge long pass filters. These filters are usually not adequate for Raman measurement as the filter edges are often not sharp enough to block laser light from the back-scattered Raman signal. A proper Raman filter set requires a narrow bandpass filter to suppress all but the laser line going to excite the sample, a sharp-edged dichroic filter to block the laser line and pass the Raman signal and sometimes another sharp-edged long pass filter to eliminate remnants of the excitation laser from the Raman signal.

The above “conventional” filter set is sometimes still not satisfactory in some instances where one needs to measure Raman very close to the laser line or so-called low wavenumber Raman spectroscopy. The SMS system is equipped with an innovative universal microspectroscopy adapter (MicroSpex) with a unique design that enables low wavenumber Raman filtration facilitating micro Raman measurements down to a few tens of wavenumbers on a standard microscope. The MicroSpex is a self-contained spectroscopy module, as shown in figure 1, which includes all required optics for Raman filtering, and can effectively separate the laser line from emission. The MicroSpex adapts simply to most standard microscopes.

Objectives

Micro Raman spectroscopy commonly uses objectives for laser illumination and collection of the scattered Raman signal. Consequently, the performance of objectives also needs to be considered. Generally, high magnification objectives provide higher power densities and produce stronger Raman signals for a given laser power and spectral acquisition time. High magnification objectives also typically have high numerical apertures (NA) and therefore perform better in collecting back-scattered Raman signal over a larger solid angle from the sample. Finally, for spatially resolved micro Raman measurements, a high magnification objective also enhances the spatial resolution of the sample. For the above reasons, it is recommended to use an objective that transmits well at both the laser and Raman spectral range and with as high an NA (magnification) as possible. This, of course, does not mean

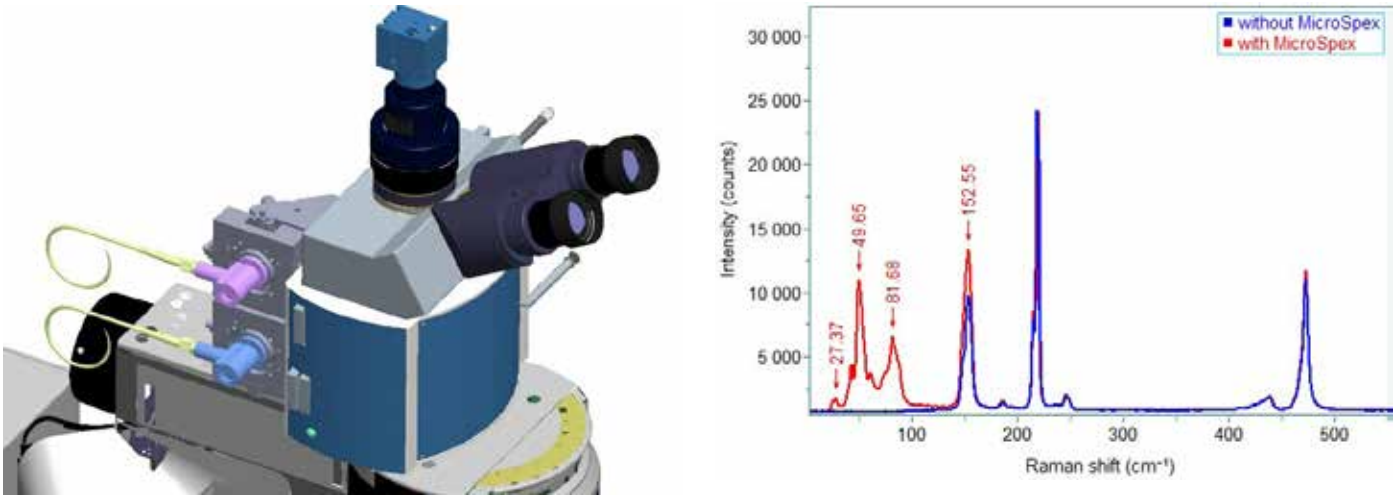

(a) (b)

Figure 1: (a) Fiber-coupled MicroSpex on a HORIBA Standard Microscope Spectroscopy (SMS) system. Free space and fiber coupling are available for both excitation and emission. (b) Raman spectrum of sulfur exhibits prominent peaks below 100 cm^{-1} using MicroSpex on SMS (red). The spectrum measured with the Microspex shows features below 100cm^{-1} that are not observed by using Raman filters in the filter cube that comes with a standard microscope.

one should always use a 100x objective, as that also limits the field of view of the objective. Moreover, the choice of objective may also affect Raman peak position and relative intensities for some polarization sensitive Raman measurements [1].

Optical etaloning in CCDs

Charge coupled detectors (CCDs) are commonly used for Raman spectroscopy, and the quantum efficiency (QE) of these detectors are often used as guides in the selection of the CCD. There are two major categories of CCDs: Front-illuminated and back-illuminated CCDs. As the name implies, front-illuminated detectors sense light from the front of the sensor. However, other pixel structures on the front of the sensor often interfere with the photons, preventing them from reaching the photosensitive part of the sensor, thereby lowering the QE of the sensor. This is especially true in the UV and NIR regions of the spectrum. For this reason, back-illuminated (BI) CCDs were introduced, where light enters the photosensitive part of the detector through the relatively uncluttered back of the sensor, which improved the UV response. Furthermore, a variant of the BI sensors uses a thicker photosensitive area, which enhances the NIR response (so-called deep depleted BI sensors). However, one negative side effect of using a thicker photosensitive layer for the deep depleted BI sensors is the introduction of etaloning. Etaloning results in a modulation of the QE response of the sensor mainly in the NIR region of the spectrum. This modulation can sometimes show and corrupt Raman spectra in this region. For this reason, one usually uses a front-illuminated (etalon-free) sensor for Raman measurement. If using a back-illuminated sensor in the NIR, ensure that the detector includes anti-fringing technology to suppress the etaloning effects. HORIBA provides many different CCDs with such anti-fringing technology that are excellent for Raman spectroscopy.

Use of EMCCDs for Raman spectroscopy

Another recent introduction is the use of Electron Multiplying CCD (EMCCD) detectors in Raman spectroscopy. EMCCDs are CCDs with built-in gain to improve signal-to-noise (SNR) ratio. The built-in gain in EMCCDs can be used to improve SNR for very low photon flux Raman measurements, or to high speed Raman measurements such as mapping, where the need for speed results in low photon flux per unit time of measurement.

References

(1) David Tuschel, Spectroscopy, 32, 14 (2017)

In general, **luminescence** refers to light emission from a material following some type of stimulation or excitation. **Photoluminescence (PL),** in particular refers to luminescence emission that results from excitation or stimulation of the material by light of often-shorter wavelength.

Figure 1 shows a Jablonski diagram - an energy level schematic of the various electronic state transitions involved in photoluminescence. The left axis shows increasing energy, where a typical photo luminescent molecule has an absorbance spectrum. This spectrum shows the energy or wavelengths, where the molecule will absorb light.

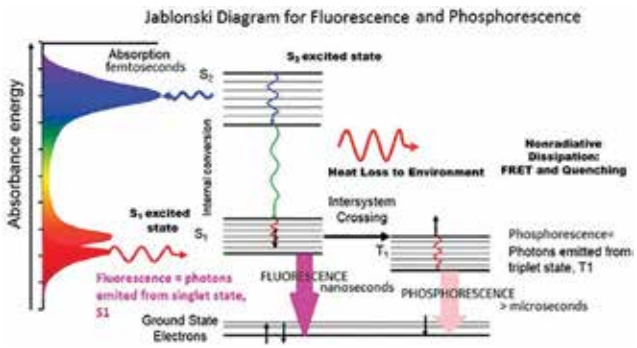

Figure 1: The Jablonski Diagram of molecular absorbance and photoluminescence

If the incident light is at a wavelength where the molecule will absorb the photon, the molecule is then excited from the electronic ground state to a higher excited state, denoted S_2 here. The electrons then go through internal conversion, affected by vibrational relaxation and heat loss to the environment. As shown in the figure, the final photo-emission transition can either occur through a fast singlet state (fluorescence) or through a slower triplet state (phosphorescence). In conventional photoluminescence, photons are emitted at higher wavelengths (lower energy) than the wavelength of the absorbed photons.

The diagram in figure 1 is extremely important to understand for any photoluminescence spectroscopist. When measuring a photoluminescence spectrum, one is typically looking at the intensity of the emission, its wavelength or energy, and the time over which the emission occurs. The latter is the photoluminescence lifetime, explained further in a subsequent section. Any number of things can affect these PL observables, including energy transfer to and from other molecules, quenching by other molecules, temperature, pH, local polarity, aggregation or binding. Understanding the mechanisms of these interactions can provide insight into what is being observed with a change in photoluminescence spectra and its associated observables.

Photoluminescence spectrum

Steady state photoluminescence results from excitation by light of a constant (steady) intensity, and spectrum is the intensity of the emission measured as a function of wavelength. A photoluminescence emission spectrum is when the excitation wavelength is fixed and the emission wavelength is scanned to get a plot of intensity vs. emission wavelength. A photoluminescence excitation spectrum is when the emission wavelength is fixed and the excitation monochromator wavelength is scanned. In this way, the spectrum gives information about the wavelengths at which a sample will absorb in order to emit at the single emission wavelength chosen for observation. It is analogous to absorbance spectrum, but is a much more sensitive technique in terms of limits of detection and molecular specificity. Excitation spectra are specific to a single emitting wavelength/species as opposed to an absorbance spectrum, which measures all absorbing species in a solution or sample. The emission and excitation spectra for a given fluorophore are mirror images of each other. Typically, the emission spectrum occurs at higher wavelengths (lower energy) than the excitation or absorbance spectrum.

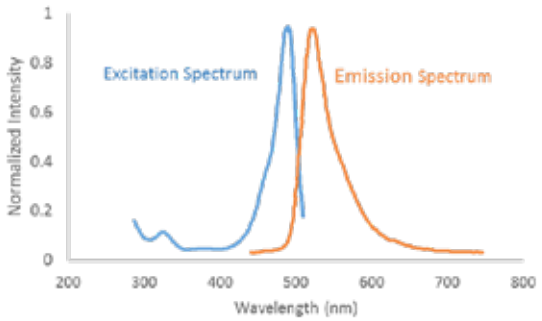

Figure 2: A photoluminescence excitation spectrum (blue) and an emission spectrum (purple) are mirror images of each other.

These two spectral types (emission and excitation) are often used to observe changes in a sample under study. The spectral intensity and/or peak wavelength may change with variants such as temperature, concentration, or interactions with other molecules around it. This includes quencher molecules, and molecules or materials that involve energy transfer. Some fluorophores are also sensitive to solvent environment properties such as pH, polarity, and certain ion concentrations.

What type of materials exhibit photoluminescence?

Fluorescent molecules and materials come in all shapes and sizes. Some are intrinsically fluorescent, such as chlorophyll and the amino acid residue tryptophan (Trp), phenylalanine (Phe) and tyrosine (Tyr). Others are molecules synthesized specifically as stable organic dyes or tags to be added to otherwise non-fluorescent systems. There are entire catalogs of these available. Typically, organic fluorescent molecules have aromatic rings and pi-conjugated electrons in them. Depending on their size and structure, organic dyes can emit from the UV out into the near-IR. Here is a random sampling of a few common fluorochromes that span the UV-visible range. Others are highly engineered for very specific uses of photoluminescence spectroscopy. A few of the categories of fluorescent molecules and materials are:

- Amino acids (Trp, Phe, Tyr)
- Base pair derivatives (2-AP, 3-MI, 6-MI, 6-MAP, pyrrolo-C, tC)
- Chlorophylls
- Fluorescent proteins (FPs)
- Organic dyes (fluorescein, rhodamine, N-aminocoumarins and derivatives of these)
- Rare earth elements (lanthanides)
- Semiconductors
- Quantum dots
- Single walled carbon nanotubes (SWCNTs)
- Solar cells
- Pigments, brighteners
- Phosphors
- Many more…

Other molecules and materials such as fluorescent proteins, semiconductors, phosphors, and rare earth elements are among the commonly used fluorescent samples. Polymers with conjugated aromatics or dienes also commonly have fluorescent properties.

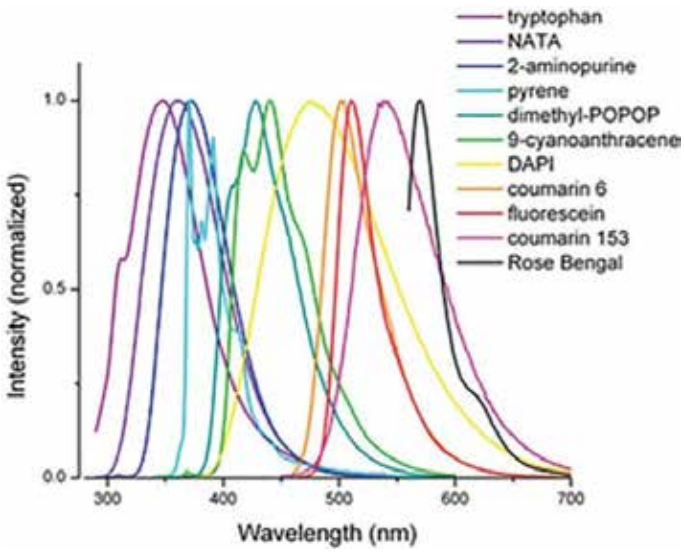

Figure 3: Photoluminescence emission spectra of some common fluorochromes across the UV and visible spectrum

Advantages of photoluminescence spectroscopy

Firstly, photoluminescence is a very sensitive technique. Photoluminescence signals are extremely strong in intensity compared to vibrational spectroscopies such as Raman or infrared. In comparison to UV-visible absorption spectra, the sensitivity of photoluminescence is much higher even if the incident and measured signals used in UV-Vis absorbance spectroscopy are much stronger than photoluminescence. In absorption, one is using a derived signal (ratio) which limits the sensitivity when both signals are nearly equal. Because direct signal measurement of photoluminescence is strong, only small amounts and/or concentrations of sample are required for such measurements.

Secondly, photoluminescence is selective. Probes report photoluminescence on a molecular level. For example, by tagging a protein that is only located in the nucleus or the cell membrane, one can measure specifically what is going on in those areas, as opposed to other organelles, or the cytoplasm. Photoluminescence makes it easy to see what is going on at the molecular level specifically, without the guesswork.

Furthermore, many molecules are fluorescent naturally, so there is no need to change these types of samples in any way in order to study them. For samples that are not naturally fluorescent, there is a whole range of molecular probes and dyes that can be added for a specific application, without significant sample preparation. For the most part, samples can be measured as is, without having to prepare them in special pellets or media. Photoluminescence can be measured for samples that are solids, liquids, solutions, powders, films, cell cultures, tissue samples, and even whole animals. Photoluminescence measurements of gaseous samples are difficult and uncommon but have been done, requiring special sample handling and flow cell optics and in some cases, extreme temperature conditions. Most gases measured by photoluminescence are dissolved gas molecules.

Disadvantages of photoluminescence spectroscopy

Unlike techniques with very narrow and characteristic spectra such as Infrared, Raman, and NIR reflectance spectroscopy, photoluminescence spectra are often very broad peaks. For this reason, photoluminescence is not efficient for sample identification. Furthermore, photoluminescence peak intensity and wavelength are sensitive to a whole host of physical properties, including temperature, concentration, aggregation, solvent polarity, pH, and many more. While such environmental sensitivity is very useful when using PL as an environmental probe, it has an adverse effect when the interest is in following the evolution of a luminescent sample regardless of its environment.

Flexible and Modular Micro PL Measurement System (SMS)

Introduction

Photoluminescence (PL) is one of the most commonly used contactless and non-destructive techniques to investigate such materials as semiconductors and nanotubes. The absorption and emission spectra can be used to identify atoms and molecules with specific energy level structure. In research environments, it is common for experimental requirements to change with the variety of materials under study. Changes such as spectral coverage range, resolution, temperature, size, etc., are the primary drivers of the type and capabilities of the instrumentation used. Therefore, a flexible system with high performance is of great importance for such environments.

Here we describe a modular turnkey system that equips a standard microscope for micro PL measurement. Figure 1 illustrates the configuration of a typical Standard Microscope Spectroscopy (SMS) system with the components for different requirements, including multiple lasers UV-Vis-NIR detectors, a motorized sample stage, etc. The SMS system is also a comprehensive and flexible platform capable of multiple spectroscopies, such as micro-reflectance, Raman, TCSPC spectroscopy, etc.

(a) (b)

Figure 1: Experimental setup for micro PL measurement on a tandard microscope. (a) Schematic setup. (b) Front view of HORIBA Standard Microscope Spectroscopy (SMS) system.

Setup

The SMS system includes a universal microspectroscopy adapter, which is a key enabler of its performance. This unique accessory contains reflective optics to direct excitation light to the sample, and a dichroic and long pass filter to separate laser light from sample emission. The excitation light is focused onto the sample surface by the objective, which also collects the emission light collimating and focusing into the iHR320 spectrometer. Two exit ports can be used for different detectors, such as CCD, PPD, PMT, and solid state detector to cover an extended spectral range. The motorized translation stage communicates with the vision camera for sample positioning, scanning and adding spatial distribution information to PL mapping. The entire instrument is controlled by HORIBA LabSpec software.

Results

Flexibility of light source and detector

Both free-space and fiber-coupled ports for a light source are available on the microscope. The pre-aligned fiber coupler adapts any fiber-coupled light source for different measurement or wavelength without additional alignment. Figure 2 shows the steady state PL measurement of the biological convallaria sample using a free space coupled cw laser with CCD detector.

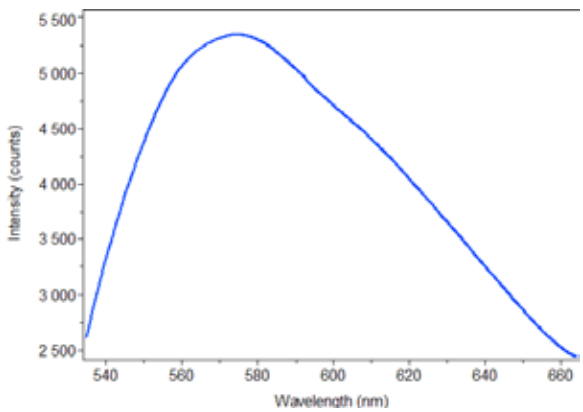

Figure 2: (a) Steady state PL measurement using cw 532 nm laser and CCD.

Different sample scales or experimental conditions require different objectives, and the SMS system takes advantage of the standard features of the microscope, with typically 5 objectives, to measure the sample's different spatial resolutions and fields-of-view. Figure 3 shows the optical images of the convallaria sample observed by different objectives. The spot size is much smaller using the objective with the higher numerical aperture. Other objectives are also available for different applications; for example, super long working distance objectives often work for a cryostat, and objectives with enhanced transmission at NIR range for NIR light source and emission.

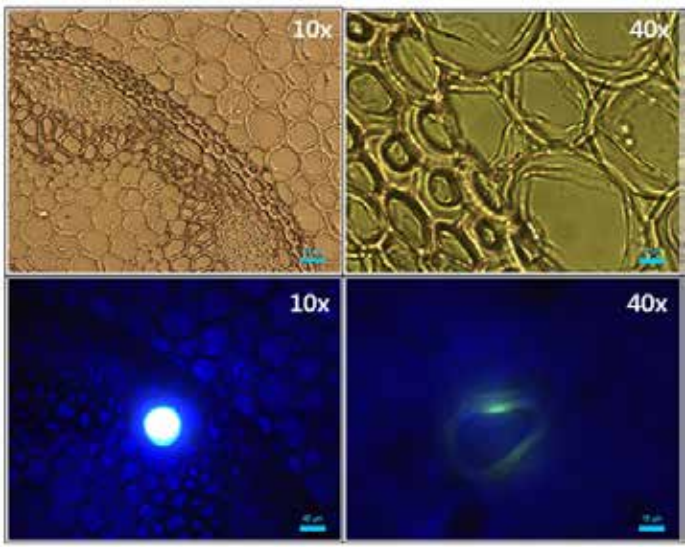

Figure 3: Optical image of convallaria sample using 10x and 40x objectives. Top: illuminator on and laser off. Bottom: illuminator off and laser on.

By using a motorized translation stage, which can also be adapted to hold a microscope-compatible cryostat for low temperature measurement, spatial information can be obtained from a PL map. PL maps can provide such information as the distribution of luminescent materials and fluorophores concentration, etc. An example of the contrast of optical image and PL mapping of a convallaria sample is shown in Figure 4.

Summary

The Standard Microscope Spectroscopy (SMS) system from HORIBA Scientific provides a flexible platform for photoluminescence and other spectroscopies. The SMS system can accommodate various requirements, such as coupling multiple light sources, using multiple objectives for different resolutions, PL mapping, and extended wavelength range with multiple detectors, etc. This system is obtainable as a turnkey system or as an upgrade to a user's existing microscope. The major components used here for PL measurement are listed to the right.

(a)

(b)

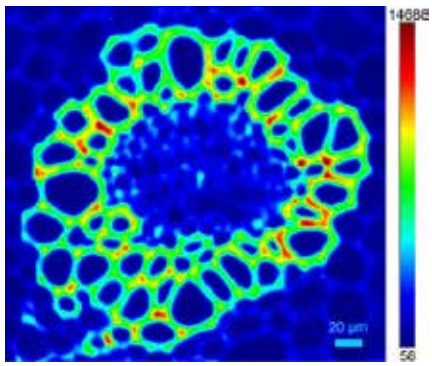

Figure 4: Convallaria sample observed by 20x objective. (a) Optical image. (b) PL mapping (excitation wavelength = 532 nm, emission wavelength ~ 566 nm, step size = 1 µm).

Part No.	Description
LCX-532S-500-CSB-PPA	Laser - 532 nm, 500 mW, SLM DPSS
DeltaDiode-485L	Pulsed laser diode 488 nm (+/-10 nm) w/active temp control
BX-53-MIC	Olympus BX-53 upright microscope.
VIS-CAM	Vision camera for microscope.
IHR320 Core 3	iHR320 f/4.1, imaging spectrometer, including patented kinematic triple grating turret with three specified gratings.
SYNCER-2048x70-NIR	Syncerity CCD head thermoelectrically (TE) cooled to -50° C using spectroscopy grade 1, 2048 x 70 pixel back-Illuminated NIR CCD chip with 14 µm x 14 µm pixels and overall format of 28.7 mm x 0.98 mm.
LabSpec 6	LabSpec Software for Windows XP and above permitting the control of the spectrometer, data acquisition and a wide range of data treatment and storage options.

Photoluminescence Characterization of GaAs and Other Semiconductor Materials on an SMS System

Introduction

To fabricate high quality semiconductor devices, the microelectronics industry has to measure fundamental material properties, such as basic band structure, transport parameters, bandgap values, carrier scattering times and concentrations of impurities and defects, etc [1].

Among the various measurement methods, optical characterization techniques such as photoluminescence (PL), stand out because they are non-destructive and require minimal sample preparation. These features are of great importance for production use, for on-line applications, and for examination of finished devices.

PL depends on the fact that electrons residing in the valence band of a semiconductor can be excited via optical absorption to the conduction band, to an impurity, or to a defect level in the energy gap. The corresponding relaxation of the excited species leads to emission of light that can offer an optical fingerprint of the sample or process. PL can be used to determine the energy gap of a semiconductor sample. This technique is especially useful for III-V and II-VI ternary and quaternary alloys like $Al_xGa_{1-x}As$ or $Al_xGa_{-x}AsySb_{1-y}$ because the energy gap of these alloys varies with the compositional parameters x and y. When this process is inverted, x and y can be found from the gap value thereby establishing a calibration between the gap energy and the composition. PL can also detect the presence of impurities and crystalline defects in semiconductors, which affect material quality and device performance. A full-width-half-maximum (FWHM)of a PL peak could provide a qualitative measure for impurity concentration, carrier concentration and crystalline structure perfection. In this paper we show how an SMS system can be used to characterize a variety of semiconductor materials from different groups, emitting PL peaks with wavelengths varying from 200 nm to 2200 nm.

Experimental setup

Different free-space-coupled excitation lasers were used to excite a wide range of materials. These lasers were mounted on a laser combiner and free-space coupled to the microscope using HORIBA's universal microspectroscopy adapter that enables the addition of various spectroscopies to any standard microscope without compromising the existing microscope's functionality. The microspectroscopy adapter conveys the pulsed excitation light to the microscope objective and onto the sample surface. The photoluminescence emission from the sample is collected with the same microscope objective and free-space or fiber-coupled to a spectrometer passing through the dichroic and long-pass filter for cleaning up the excitation laser from the emission signal. An iHR320 spectrometer with multiple gratings, SynapsePlus CCD and InGaAs array detector detected the emission signal. LabSpec software is used for steady state PL measurement and post processing of the signal.

Results

Figure 1 shows a variety of different semiconductor materials including ZnO, GaN, GaAs, CdTe, CIGS, InP and GaSb characterized with the SMS system emitting photoluminescence from 200 nm to 2000 nm. These PL peak positions are associated to material bandgap and the peak's full-width-half-maximum is a measure of crystallinity, as well as other structural parameters. Typically, broadening of the PL peak happens as crystal structure is deformed by the presence of impurities and defects.

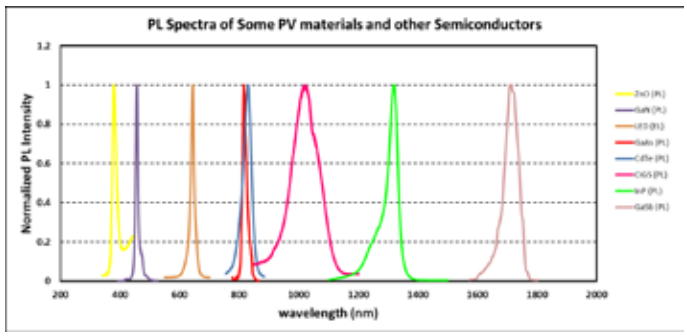

Figure1: Different semiconductor materials such as ZnO, GaN, GaAs, CdTe, CIGS, InP and GaSb characterized with an SMS system emitting photoluminescence from 200 nm to 2000 nm.

Conclusion

In this paper, we demonstrate a modular and flexible system to characterize a wide variety of semiconductors with PL emission ranging from 200 nm to 2200 nm on one standard microscope platform.

References

(1) "Optical Characterization in Microelectronics Manufacturing"; Journal of Research of the National Institute of Standards and Technology; Volume 99, Number 5, September-October 1994

UV Photoluminescence Material Characterization on an SMS system (GaN)

Introduction

GaN is a popular wide bandgap semiconductor used in many applications. With a bandgap of 3.4 eV at room temperature and excellent thermal stability and conductivity, it lends itself particularly well to high-power and high-frequency applications, where these properties help mitigate device deterioration or damage under extreme conditions of use [1,2]. Its wurtzite crystal structure (lattice constants: a = 3.189 Å, c = 5.186 Å) enables doping with various elements such as magnesium or silicon to create n or p type materials [3]. GaN also forms various alloys with engineered bandgaps to serve particular needs, such as heterojunction formation in tandem solar cells for photovoltaic applications [4,5].

As an engineered material, GaN and its various alloys usually require very controlled processes for their fabrication in order to display desired properties, and having a fast, non-contact characterization technique is essential for proper monitoring and performance characterization of such materials. Photoluminescence (PL) spectroscopy is a popular technique to achieve this. PL is easy to perform, nondestructive, fast, contactless and an effective technique that provide valuable data on device architecture, bandgaps and defects density, etc. However, performing PL measurements of these materials can be challenging due to strong UV absorption in most materials used in the optics of the typical UV-Vis spectroscopy system. The SMS from HORIBA is designed on minimally absorbing reflective optics, which enables the easy and effective study of wide bandgap material such as GaN.

Experimental setup

The SMS system is a comprehensive and flexible platform capable of multiple spectroscopies, such as micro PL, reflectance, TCSPC spectroscopy, etc. The key enabler for the SMS is the universal microspectroscopy adapter – MicroSpex. It is a self-contained spectroscopy module with the PL excitation and filtering optics pre-installed. The MicroSpex effectively decouples the imaging and spectroscopy functions on the microscope, enabling both to work optimally and without compromises to either. The excitation light is focused onto the sample surface by the objective, which also collects the emission light, collimating and focusing it into the iHR320 spectrometer. The SMS includes white light illumination and a color camera for sample visualization. An optional motorized translation stage communicates with the vision camera for sample positioning, scanning and adding spatial resolution to the PL measurement. HORIBA LabSpec software is used for instrument control and data analysis.

Results

Measurements were made on a GaN thin layer grown on sapphire. Figure 1 shows the PL spectrum for a point measurement on the sample. The shape of the PL peak is directly related to the quality of the grown layer and the amount of defects embedded in the structure. The main observed band at 387 nm results from direct band-to-band recombination between the electrons in the conduction band with holes in the valence band. The broadening and the side band can be attributed to defects and impurities introduced in the middle of the band gap while growing the GaN thin layer with the MOCVD technique.

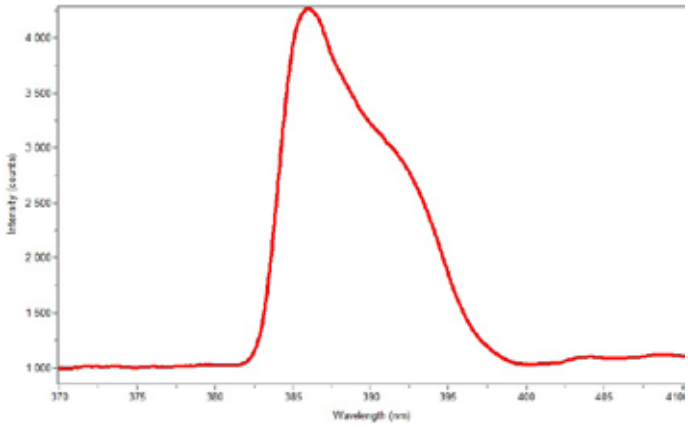

Figure 1: GaN PL peak spectrum taken with SMS using 266 nm laser excitation

Figure 2 shows the results for a rectangular 1 mm × 1 mm PL map of a similar sample. All spectra are shown in the top plot while the lower three plots show the spatial distribution of different PL spectrum parameters (peak intensity, broadening and peak wavelength position) using the data analysis features of LabSpec 6. Each of these characteristics provide valuable data on the quality (uniformity and defect density) of the wafer or the fabricated device.

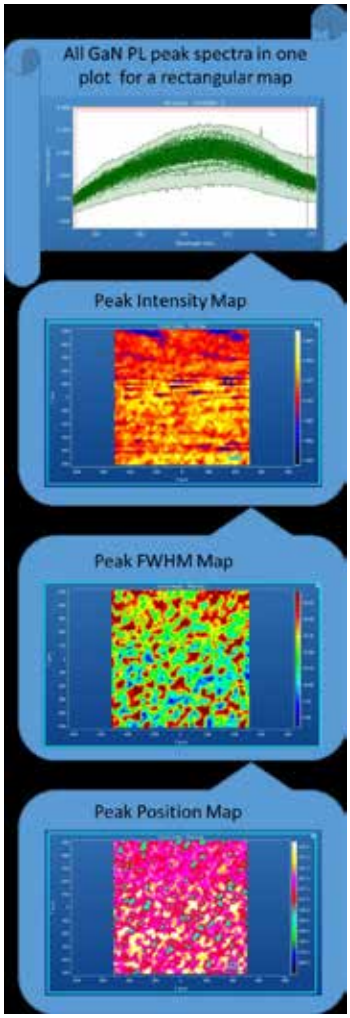

Figure 2: Photoluminescence data (all spectra in one plot) of a 1 mm × 1 mm GaN accompanied with peak intensity, peak FWHM and peak position colored distributions.

Conclusion

In this article, SMS is used to characterize a GaN wafer. Materials such as GaN can be challenging to characterize due to the tendency of most optical material to absorb the UV radiation region of the light. SMS is designed with mostly reflective optics with almost no UV absorption which makes characterizing wideband gap materials like GaN easy and efficient.

References

(1) Guillermo Santana, et al., Photoluminescence Study of Gallium Nitride Thin Films Obtained by Infrared Close Space Vapor Transport, Materials 2013, 6, 1050-1060; doi:10.3390/ma6031050

(2) Asgari, A.; Khalili, K. Temperature dependence of InGaN/GaN multiple quantum well based high efficiency solar cell. Solar Energy Mater. Solar Cells 2011, 95, 3124–3129.

(3) Gherasoiu, I.; Yu, K.M.; Reichertz, L.A.; Kao, V.M.; Hawkridge, M.; Ager, J.W.; Walukiewicz, W. High quality InxGa1–xN thin films with x > 0.2 grown on silicon. Phys. Status Solidi B 2010, 247, 1747–1749.

(4) Tran, B.-T.; Chang, E.-Y.; Trinh, H.-D.; Lee, C.-T.; Chandra, K.S.; Lin, K.-L.; Huang, M.-C.; Yu, H.-W.; Luong, T.-T.; Chung, C.-C.; Nguyen, C.-L. Fabrication and characterization of n-In0.4Ga0.6N/p-Si solar cell. Solar Energy Mater. Solar Cells 2012, 102, 208–211.

(5) Saron, K.M.A.; Hashim, M.R. Broad visible emission from GaN nanowires grown on n-Si (1 1 1) substrate by PVD for solar cell application. Superlattices Microstruct. 2013, 56, 55–63.

Fluorescence Imaging and Photoluminescence Spectroscopy on an SMS system

Introduction

Fluorescent labels are often used to study activity in various materials in which they can be embedded. Fluorescence imaging on a microscope is a popular method to visualize these labels within the material system under study.
Use of such fluorescent markers ranges from biological applications, such as gene expression to quality control applications, such as anti-counterfeit technology, etc.
Fluorescence imaging is a filter-based technique that is only capable of resolving wide bands of wavelengths. The demands on the filters become quite challenging when there are multiple fluorophores in the sample with potential overlaps in their spectral signatures. In such situations, a system with a higher ability to discriminate between the spectra from different fluorophores is required – typically this means using a spectrometer to select a very narrow band of spectra corresponding to the fluorophore of interest and registering an image at that wavelength.
In this work, we demonstrate a modular turnkey system that adds both components of fluorescence imaging and PL imaging spectroscopy to a standard microscope. We used convallaria, which is a commonly available biological sample to assess the capabilities of the system.

Setup

(a)

Figure 1: Experimental setup for fluorescence imaging and PL spectroscopy on a standard microscope. (a) Schematic setup. (b) Front view of HORIBA Standard Microscope Spectroscopy (SMS) system.

Figure 1 illustrates the configuration and picture of the Standard Microscope Spectroscopy (SMS) system for fluorescence imaging and PL spectroscopy.
A key component of this system is the universal microspectroscopy adapter from HORIBA that adapts to most standard microscopes and adds various spectroscopic capabilities without compromising the other functions of the microscope. The SMS system also includes adapters to couple one or more excitation lasers to the microscope, intensity and polarization controls, a vision camera and an optional mapping stage, as well as coupling accessories to channel the emission to the spectrometer for analysis. The entire system is controlled by HORIBA LabSpec 6 software.

Measurements

The measurement uses two optical pathways: Fluorescence imaging, and photoluminescence spectroscopy pathways. Fluorescence imaging relies mainly on the filter cube that comes with the microscope. The typical filter cube contains a set of three filters – a bandpass filter for selecting a narrow band of excitation wavelengths, a dichroic beam splitter to separate the excitation and emission beams and a long pass edge filter to remove remnants of the excitation light from the emission light, which is detected by the imaging camera. Figure 2 below shows the transmission properties of a typical filter set used for fluorescence imaging superimposed on the absorption and emission spectra of acridine orange fluorescent dye in use on the Convallaria sample.[1]

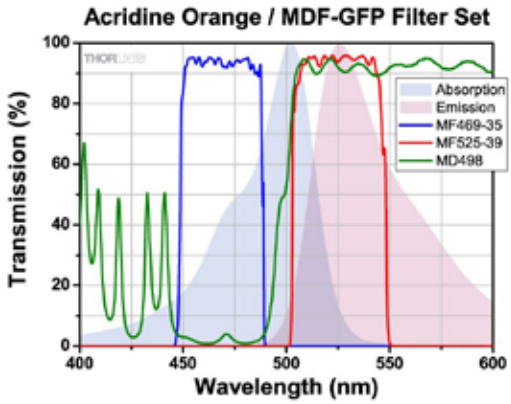

Figure 2: Fluorescence spectra of acridine orange dye on a sample and transmission properties of the filter set used in fluorescence imaging.

The area under the red curve in figure 2 shows all the emission wavelength from the sample that gets detected by the fluorescence imaging camera on the microscope as shown in figure 3b. A limitation of the fluorescence imaging pathway is that it cannot distinguish between any of the wavelengths that are transmitted by the emission filter – they all get imaged by the camera.

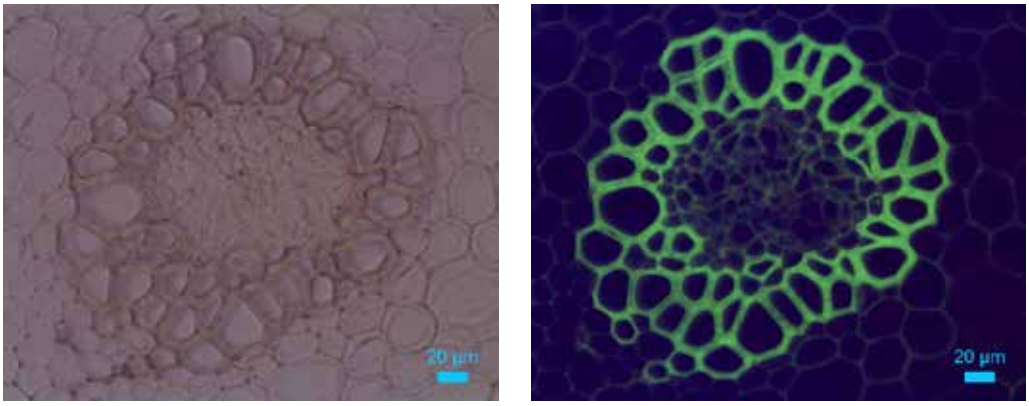

(a) (b)

Figure 3: (a) Optical image of the convallaria sample observed by 20x objective. (b) Fluorescence image of the convallaria sample by using the filter set, including a 472/30 nm bandpass filter, 488 nm dichroic beam-splitter, and 510 nm long-pass filter.

The photoluminescence pathway on the other hand uses a 532 nm laser to selectively excite the convallaria sample through a filter module in the microspectroscopy adapter. The excitation light was collimated into the microscope by free-space and focused onto the sample surface by a 20x objective, which also collected the emission light. The emission from the sample goes back through the same filter module and, unlike the fluorescence imaging case, where this emission is sent to a camera, the emission is now coupled to an iHR320 spectrometer equipped with a CCD array detector where an actual spectrum can be measured as shown in figure 4b below.

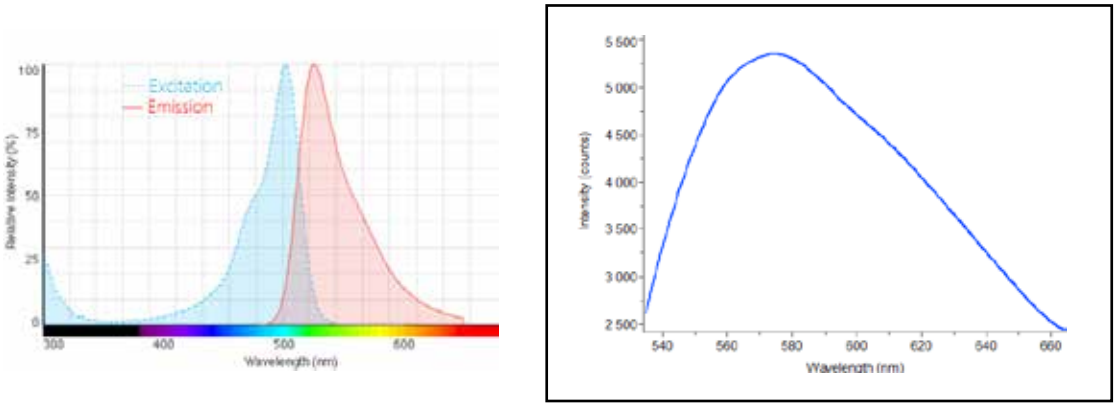

(a) (b)

Figure 4: Fluorescence spectra of acridine orange. (a) Certified excitation and emission spectra (2). (b) Experimental emission spectrum (excited by 532 nm laser, detected by CCD, integration time = 0.01s).

With the fully resolved spectrum in figure 4b, it is possible to generate a photoluminescence spectral image at any of the wavelengths, unlike the case of filter-based fluorescence imaging. Figure 5 shows one such spectral map showing PL intensity distribution at 566 nm. This map data was collected by parking the spectrometer at 566nm and moving the sample stage in a raster pattern so that the PL is collected over a discrete array of points on the sample. The total mapping process of the area of 258 × 275 pixel size with the resolution of 1 µm, took around 20 min.

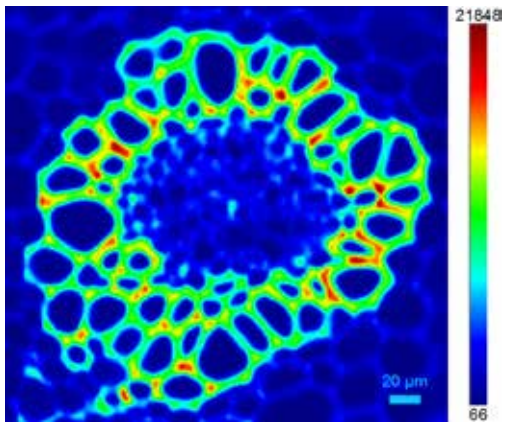

Figure 5: (a) Optical image of the convallaria sample observed by 20x objective. (b) Fluorescence image of the convallaria sample by using the filter set, including 472/30 nm bandpass filter, 488 nm dichroic beam-splitter, and 510 nm long-pass filter.

Summary

In this work, we investigated both the fluorescence imaging and photoluminescence spectroscopy on the same platform of a standard microscope. The Standard Microscope Spectrometer (SMS) system from HORIBA Scientific provides a solution accommodating almost all major spectroscopies, such as micro-reflectance, Raman, Photoluminescence (PL), TCSPC spectroscopy, etc. The major components used in this work are listed to the right.

References

(1) https://www.thorlabs.com/newgrouppage9.cfm?objectgroup_ID=2990
(2) www.thermofisher.com/order/catalog/product/A1301

Part No.	Description
LCX-532S-500-CSB-PPA	Laser - 532 nm, 500 mW, SLM DPSS
BX-53-MIC	Olympus BX-53 upright microscope
VIS-CAM	Vision camera for microscope.
IHR320 Core 3	iHR320 f/4.1, imaging spectrometer, including patented kinematic triple grating turret with three specified gratings.
SYNCER-1024x256-OE	Syncerity CCD head thermoelectrically (TE) cooled to -60° C using E2V manufactured, spectroscopy grade 1, 1024 x 256 pixel open electrode CCD chip with 26 µm x 26 µm pixels and overall format of 26.6 mm x 6.6 mm.
LabSpec 6	LabSpec Software for Windows XP and above permitting the control of the spectrometer, data acquisition and a wide range of data treatment and storage options.

CCD-based Steady State and Time-resolved Micro PL Spectroscopy on an SMS System

Introduction

Time-resolved photoluminescence (TRPL) provides a powerful technique for tracking the dynamics of spectra, which adds one dimension (time) to static or steady state photoluminescence (PL) spectroscopy. TRPL is widely applied in various fields, including probing kinetic processes of photo-reactions, observing absorbance sensitivity of nanoparticles [1], investigating thermally activated delayed fluorescence (TADF) in OLEDs [2], etc.

The temporal characteristics of luminescence phenomena covers a broad range of time, from sub picoseconds to several minutes. In this paper, we are concerned with luminescence effects that occur over milliseconds and longer and therefore can be resolved with a fast CCD array detector. Specifically, we investigate the dynamics of photo-bleaching as an illustration of transient luminescence phenomena. It is common to use single channel detectors (SCDs) such as PMTs for kinetic measurements of this type due to their speed. However, when one is interested in obtaining kinetic data over a wide spectral range, the SCD-based measurements are no longer viable because the rate-limiting step becomes the slow scanning of the spectrometer. Hence, the CCD-based measurements as described here become viable alternatives.

The setup considered is one used for steady state PL measurements, but because the CCD detector involved is fast, one is also able to use the same set up for time-resolved studies of this type. The Standard Microscope Spectroscopy (SMS) system is a comprehensive and flexible platform capable of adding multiple spectroscopies, such as micro-reflectance, Raman, photoluminescence (PL), TCSPC spectroscopy, etc. on most standard microscopes.

Method

The SMS system included a 532 nm cw laser as the excitation light source and coupled into the standard microscope by free space. The universal microscope spectroscopy adapter from HORIBA contains reflective optics to direct excitation light to the sample and a dichroic and long pass filter to separate laser light from sample emission. The excitation light was focused onto the sample surface by a 40x objective, which also collected the emission light. The collimated emission light was directed into the iHR320 spectrometer with 600 gr/mm grating blazed at 750 nm. The SMS system also includes a vision camera to visualize the sample under study. The Syncerity CCD on the spectrometer measured both steady state and time-resolved micro PL spectra at selected points on the sample. LabSpec 6 software was used for instrument control and data analysis. Figure 1 illustrates the configuration and picture of the SMS system.

(a) (b)

Figure 1: Experimental setup for steady state and time-resolved micro PL measurement on a standard microscope. (a) Schematic setup.(b) Front view of HORIBA Standard Microscope Spectroscopy (SMS) system.

Results

Figure 2(a) shows the vision camera image of the sample. Figure 2(b) shows the PL signal with a peak near 638 nm from the region of interest.

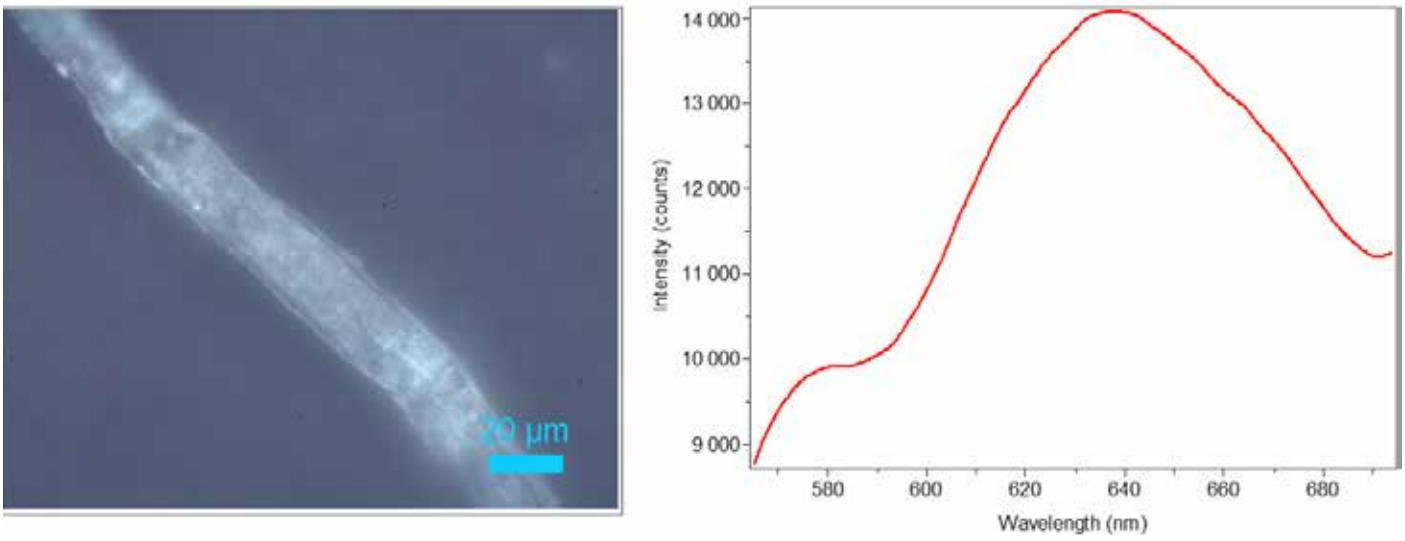

(a) (b)

Figure 2: (a) Vision camera image of the photo-bleaching sample observed by a 40x objective. (b) PL spectrum from region of interest on the sample.

To investigate the dynamic process of photo-bleaching, the Syncerity CCD was used to capture a kinetic series of spectra covering the spectral range of 560 nm to 700 nm. Figure 3(a) shows the series of spectra captured. Each PL spectrum was acquired with an integration time of 0.1 sec and a delay of 0.5 sec between successive spectra. The total measurement time was 20 minutes. Figure 3(b) shows the time evolution of the peak intensity of the spectra shown in 3(a).

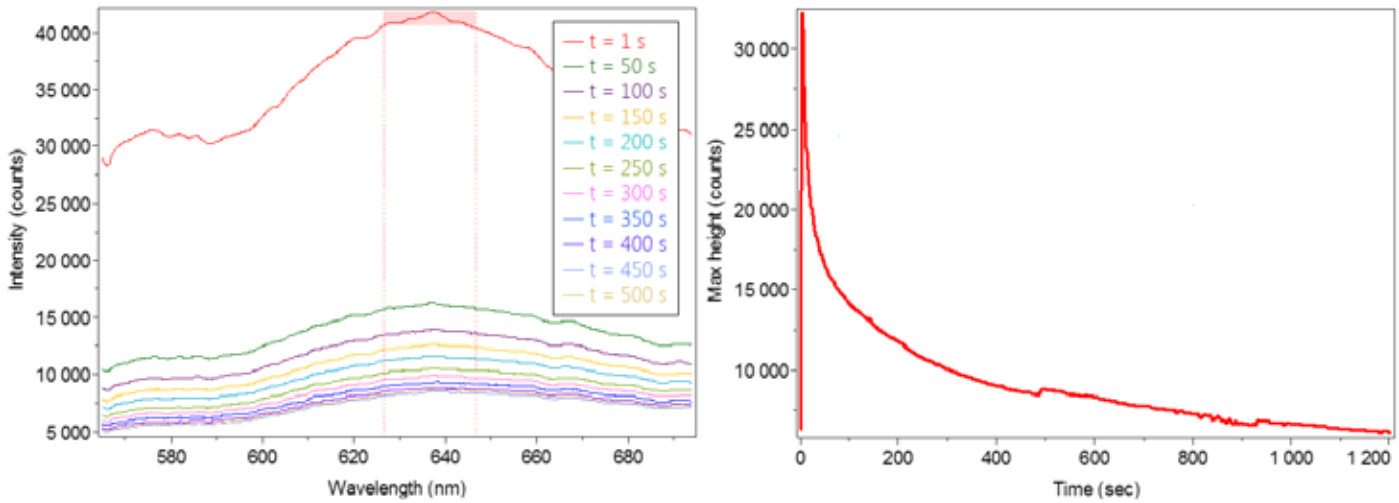

(a) (b)

Figure 3: (a) PL spectral response due to photo-bleaching effect at selected times. (b) Temporal response of PL intensity on the photo-bleaching sample surface.

The standard microscope equipped with a CCD offers key benefits such as high efficiencies, and are cost effective for measuring both steady state and time-resolved PL on one platform. The newer and faster CCDs provided by HORIBA are a key enabler of this capability.

Summary

In this work, we investigated both the steady state and time-resolved photoluminescence of a micro-scale photo-bleaching sample using a continuous laser and CCD array detector on a standard microscope. The Standard Microscope Spectroscopy (SMS) system from HORIBA Scientific provides a solution accommodating almost all major spectroscopies, such as micro-reflectance, Raman, photoluminescence (PL), TCSPC spectroscopy, etc. The major components used in this work are listed below.

Part No.	Description
LCX-532S-500-CSB-PPA	Laser - 532 nm, 500 mW, SLM DPSS
BX-53-MIC	Olympus BX-53 upright microscope
VIS-CAM	Vision camera for microscope.
IHR320 Core 3	iHR320 f/4.1, imaging spectrometer, including patented kinematic triple grating turret with three specified gratings.
SYNCER-1024x256-OE	Syncerity CCD head thermoelectrically (TE) cooled to -60° C using E2V manufactured, spectroscopy grade 1, 1024 x 256 pixel open electrode CCD chip with 26 µm x 26 µm pixels and overall format of 26.6 mm x 6.6 mm.
LabSpec 6	LabSpec Software for Windows XP and above permitting the control of the spectrometer, data acquisition and a wide range of data treatment and storage options.

References

(1) V.V.R. Sai *et al.*, Biosensors and Bioelectronics, 24, 2804 (2009)
(2) P. Pander *et al.*, Display and Imaging, 0, 1 (2017)

Semiconductor Characterization using Photoluminescence Mapping

Introduction

Many of today's technologies rely on semiconductor optoelectronic devices, and there is an increasing drive to make these devices at low cost in order to access more consumer markets. Therefore, the need for yield improvement in the fabrication of these devices is of great interest. Semiconductor devices are very sensitive and their performance can be affected by the introduction of small amounts of impurities or compositional changes in the material structure. As a result, there is a need to assess quality and performance at the various stages in the fabrication, from wafer growth to actual device performance, quality control and failure analysis.

Photoluminescence (PL) mapping is one of the more popular semiconductor characterization techniques. PL is very sensitive, fast, non-invasive and often requires no sample preparation [1]. Furthermore, its appeal derives from being useful at all levels of the device fabrication chain, from material engineering where properties such as material bandgaps can be engineered, to process and product quality control where properties such as homogeneity of wafer deposition can be monitored and controlled. Finally, PL plays an important role in failure analysis and defects characterization.

Why is PL appealing for semiconductor characterization?

From a Photoluminescence (PL) map, the PL peak position, PL peak intensity and PL peak FWHM or full-width-half-maximum, can be inferred. These parameters contain much information about the material being mapped. PL peak position changes may be attributed to variations of the device active layer thickness, the composition alloys in ternary and quaternary epitaxial layers or changing quantum well widths. As an example, changing the amount of Al in $Al_xGa_{1-x}As$ will change the peak wavelength position by changing the energy associated to the bandgap transition. PL peak intensity contains information on the purity and quality, i.e., the presence of competing radiative and/or non-radiative recombination centers at that location of the sample. Peak FWHM is an indicator of a number of factors including doping, layer disorder and layer grading effects [2], and also yields information about changes in the alloy composition of ternary and quaternary materials and is in many cases a better indicator, at room temperature, than the peak wavelength. The reason for this is that the FWHM is not sensitive to excitation power density, unlike the peak wavelength [3].

The Standard Microscope Spectroscopy (SMS) system from HORIBA Scientific offers a versatile and modular microspectroscopy solution for PL characterization of semiconductors, including mapping. SMS offers a wide range of excitation wavelengths and covers emission from 200 to 2200 nm without compromising any functionality of a conventional microscope. The SMS can be provided as a turn-key solution including the microscope, or added as an upgrade to an existing microscope.

Experimental setup

Figure 1 shows a typical SMS system for micro PL. A 980 nm laser was used to excite plain unprocessed InP wafer and fabricated InP devices. The laser (not shown in figure 1) was mounted on a laser train and free-space coupled to the microscope using HORIBA's universal microspectroscopy adapter that enables addition of various spectroscopies to any standard microscope without compromising existing microscope functionality. The microspectroscopy adapter conveys the pulsed excitation light to the microscope objective and onto the sample surface. The same excitation objective collects the PL emission from the sample and free-space or fiber couples to a spectrometer. An iHR320 spectrometer with multiple gratings and InGaAs array detector were used to detect the emission signal. LabSpec software is used for steady state PL measurement, which not only automates data-collection, but also offers an array of analytical tools for data processing and interpretation.

Figure 1: Typical SMS system for micro PL.

Results

Figure 2 shows various PL parameters for a plain InP wafer (peak intensity, peak wavelength, and FWHM of the emission), all of which can be correlated to material properties of the wafer, as described in the introduction. The plots on the right hand side of the figure show the histogram of the distribution for the mapped data providing users with very useful statistical information about their wafer quality.

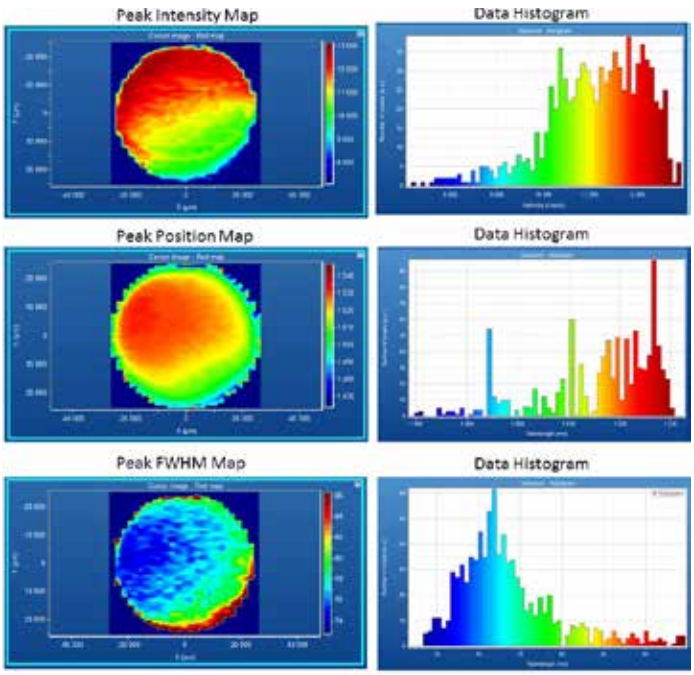

Figure 2: PL mapping performed on a fabricated InP device showing PL peak intensity, peak position and FWHM of the emission and its attributed histogram of the data.

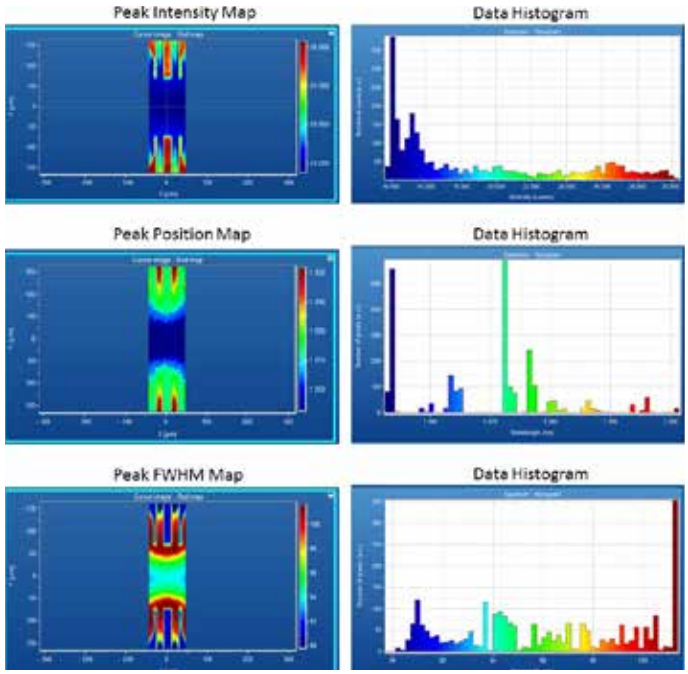

Figure 3: PL mapping performed on a fabricated InP device showing PL peak intensity, peak position and FWHM of the emission and its attributed histogram of the data distribution.

Conclusion

In this paper, we demonstrated the ability of performing PL mapping on a plain wafer and different semiconductor devices. These types of measurements are particularly useful for device engineering, process and product quality control, as well as device failure analysis.

References

(1) Shane Francis White “Spatial and Spectral Photoluminescence Characterization of Semiconductor Wafers”, A thesis for the degree of Master of Science, March 1996.

(2) C.J.L. Moore and C.J. Miner “A Spatially Resolved Spectrally Resolved Photoluminescence Mapping System”, Journal of Crystal Growth, Vol. 103, pp. 21-27, 1990.

(3) I.C. Bassignana, C.J. Miner and N. Puetz “Photoluminescence and Double-Crystal X-Ray Study of InGaAs/InP: Effect of Mismatch Strain on Band Gap”, Journal of Applied Physics, Vol. 65, Issue 11, pp. 4299-4305, June 1989.

Defect Characterization in Semiconductor Materials and Devices using Photoluminescence Mapping

Introduction

Semiconductor materials are vital to the fabrication of active photonic devices such as light sources and detectors. Successful fabrication of such devices relies on the high quality of the underlying materials and precise deposition of intended geometries on a wafer substrate [1]. Defective materials and imperfections in geometries adversely affect yield, and usually increase cost and development times. The cost and delay penalties compound when such defects in either material or device-geometry are not caught early enough in the fabrication cycle. Defects exist in a large variety and can be epitaxial or non-epitaxial, visible or non-visible. Some of these defects can be caught using ordinary inspection tools, but this is impossible for sub-micron or non-visual defects (NVD). NVD is a category of semiconductor material and process induced defects that cause device failures. Luminescence-based characterization of semiconductor devices and materials is vital to detect and quantify these defects, especially for NVDs. Photoluminescence characterization can reduce semiconductor devices production cost and performance variance, and allow improved understanding of their physical properties. In addition, PL is advantageous since it is non-destructive, and provides rapid spatially resolved evaluation of defects, either at room temperature conditions or low temperatures. PL measurement is made by exciting a material or device with light energy above their bandgap and recording the emitted light that results from relaxation. HORIBA's SMS instrumentation offers a versatile and modular platform for semiconductor devices' quality control and defect failure analysis. Because the SMS design relies mainly on reflective optics, it offers a wide range of excitation wavelengths and covers emission from 200 to 2200 nm without compromising any functionality of a conventional microscope.

Results

Figure 1 shows various PL parameters for a defect caused by extra tension on a GaSb thermo-photovoltaic device. These parameters include peak intensity, peak wavelength, and FWHM of the emission. These PL parameters can be correlated to material properties of the wafer. The plots on the right hand side of the figure show the histogram of the distribution for the mapped data providing users with very useful statistical information about how the defect is affecting the device under the test.

Figure 2 is an example of a defect on GaSb TPV caused by thermal annealing of the implanted dopants. This figure shows PL peak intensity, peak position and FWHM of the emission and its associated histogram of the data distribution. This information is very useful to perform device failure analysis and device defect study.

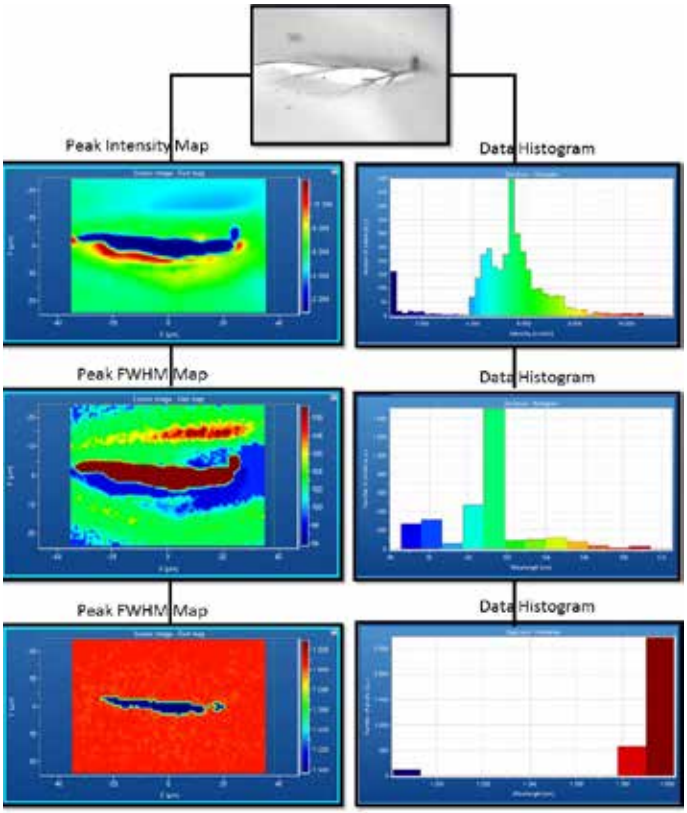

Figure 1: Various PL maps for a defective GaSb TPV device (peak intensity, peak wavelength, and FWHM of the emission) with the associated data histograms.

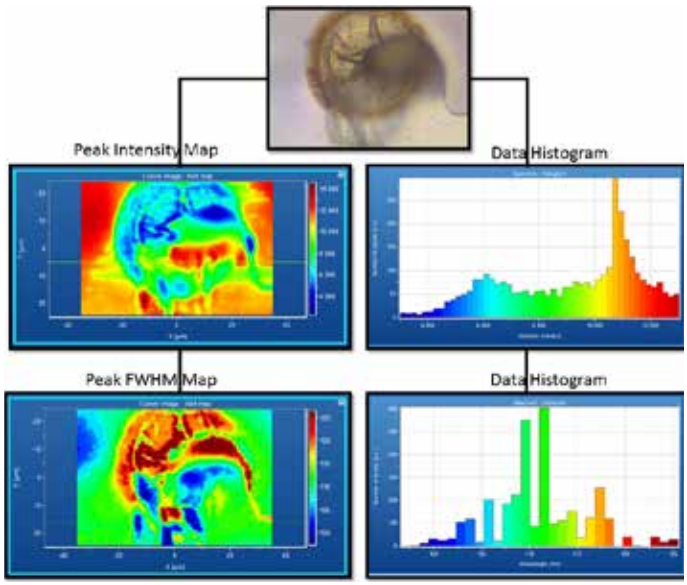

Figure 2: A PL mapping performed on a fabricated GaSb device with a defect caused by thermal annealing of the implanted doping, showing PL peak intensity, peak position and FWHM of the emission and its attributed histogram of the data distribution.

Figure 3 is demonstrating a defect caused by epitaxial growth of a multilayer detector structure.

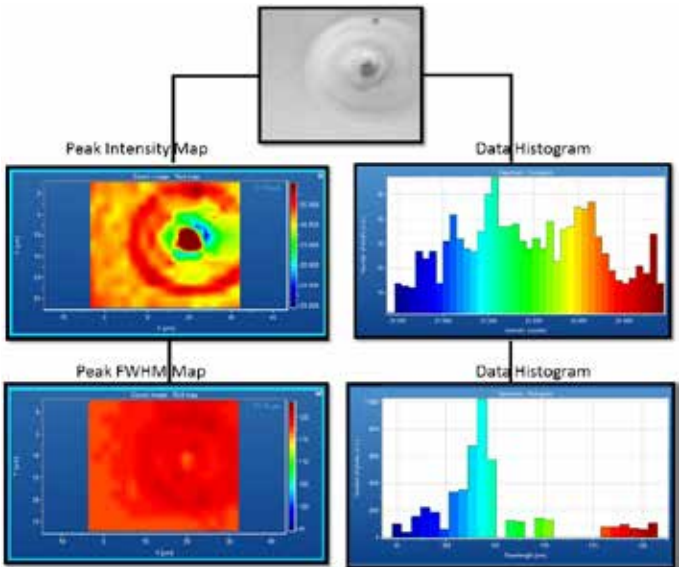

Figure 3: PL mapping performed on a fabricated multilayer device showing PL peak intensity, peak position and FWHM of the emission and its attributed histogram of the data distribution.

Conclusion

In this paper, we demonstrated the ability to perform PL mapping on different semiconductor devices for quality control and device failure analysis, including defect characterization.

References

(1) S. Perkowitz' and D. G. Seller "Optical Characterization in Microelectronics Manufacturing", J. Res. Natl. Inst. Stand. Technol. 99, 605 (1994)

Introduction to Time-Resolved Photoluminescence

As mentioned in the previous section, **luminescence** refers to light emission from a material following some type of stimulation or excitation. **Photoluminescence (PL),** in particular refers to luminescence emission that results from excitation or stimulation of the material by light of often-shorter wavelengths, as illustrated in figure 1.

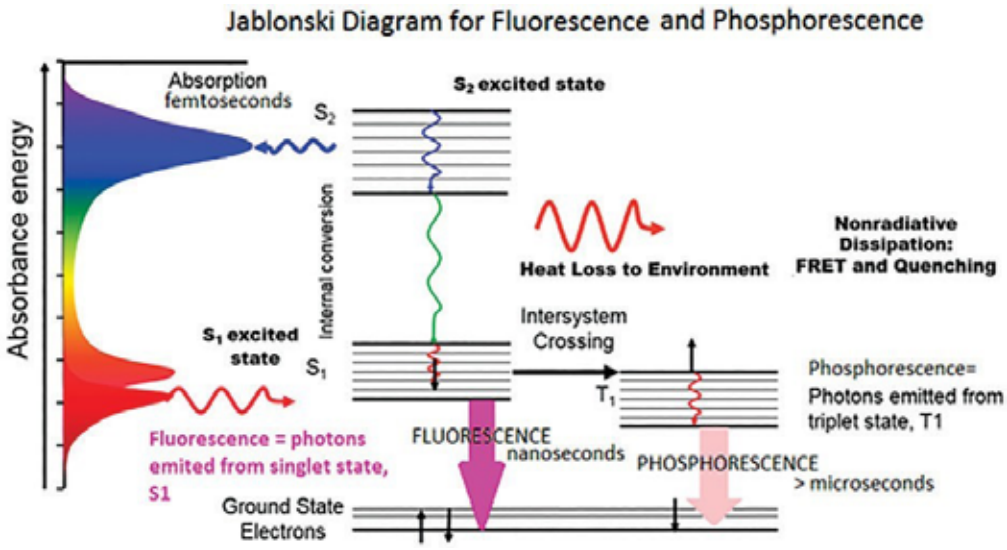

Figure 1: The Jablonski diagram of molecular absorbance and photoluminescence

Time-resolved photoluminescence (TRPL) is a measure of the time evolution of the photoluminescence process in a given sample. In simple terms, TRPL can be thought of as the average length of time an excited species spends in the excited state. This depends on the type of molecule and its local environment. Typically, the excited state decays in an exponential manner, as indicated in figure 2 below. The decay lifetime τ is a spectroscopic fingerprint that is characteristic of the sample. In addition, the photoluminescence lifetime can be dependent on the environment in which the emitting species is located, and can therefore be used as a local environmental probe for material characterization.

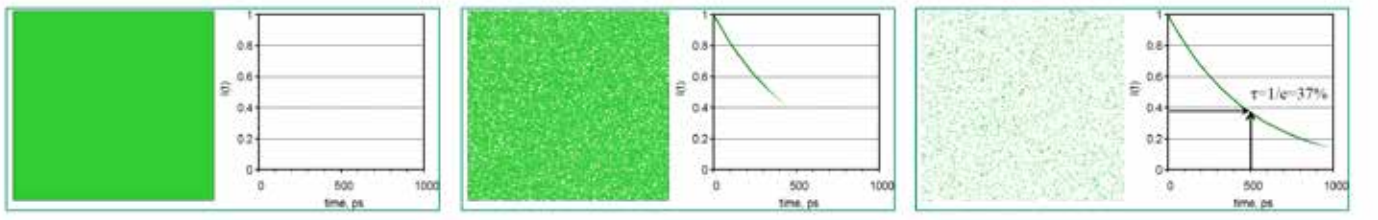

Figure 2: Illustration of time-resolved photoluminescence. Each figure shows the state of excitement of the sample on the left and the photoluminescence decay intensity as a function of time on the right. (a) Following excitation, the sample is fully excited. (b) As time evolves, the excited states decay to the ground state by emitting photons. (c) The measured emission intensity typically follows, an exponential or multiple exponentials. The lifetime is defined as the time it takes for 37% of the excited population to decay to the ground state.

Photoluminescence decay lifetimes can vary significantly – from picoseconds to several seconds. Fast decays range from picoseconds to microseconds and are called fluorescence phenomena, while slower decays range from microseconds to seconds and are called phosphorescence phenomena.

TRPL has a number of advantages over steady state PL, which is an intensity measurement. TRPL is an “absolute” measurement, rather than the “relative” steady state measurement (which gives a time-averaged signal) – This attribute means that TRPL is background-free. Furthermore, TRPL can provide the additional degree of freedom necessary to distinguish between photoluminescence species that emit at the same wavelength.

Due to the wide range of time scales involved in TRPL measurements, there is correspondingly a variety of techniques used for their measurement. Time Correlated Single Photon Counting (TCSPC) is one of the more popular techniques for TRPL measurement. TCSPC is commonly used for measuring short lifetimes in the sub picosecond to microsecond time range. Recent changes in TCSPC electronics has enabled an extension of the measurement range to seconds using such techniques as Multichannel Scaling (MCS).

TCSPC

TCSPC stands for time correlated single photon counting. It is a method of using the timing of a pulsed excitation source (i.e. laser or LED) with the timing of the arrival of single (photoluminescence) photons on a detector to reconstruct the lifetime decay over many events (repetition of pulses and photons detected) as seenin figure 3. This technique is based on the fact that the probability of detecting a single photon at time, t, after an excitation pulse is proportional to the fluorescence intensity at time t. The repetition of a laser or LED pulsed at relatively high repetition rates (10 kHz to 100 MHz) is synchronized with the time the next photon arrives at a detector (i.e. PMT). Timing electronics in the form of a time-to-digital converter or time-to-amplitude converter (TAC) are used to record these events over and over again until sufficient statistics are collected to reconstruct the decay. The decay is then fit to an exponential function to model the lifetime deca (figure 4).

There are other techniques for TRPL measurements, such as boxcar, single shot transient digitizer (SSTD) and strobe. In the current context for microspectroscopy, we have limited the exposure to TCSPC-based implementation on a standard microscope. We also show time resolved measurements based on the use of fast CCD array detectors.

As described above, TCSPC measures the time-evolution of a photoluminescence signal at one wavelength or a narrow band of wavelengths. Often one is interested in seeing the time evolution of the entire photoluminescence spectrum, so-called Time Resolved Emission Spectroscopy (TRES).

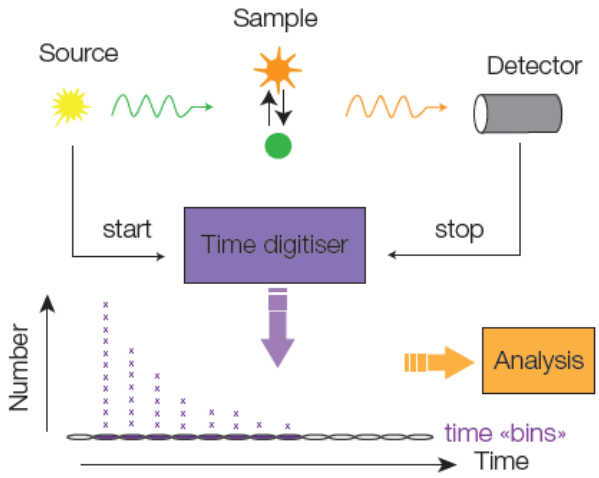

Figure 3: TCSPC photoluminescence lifetime measurement principle.

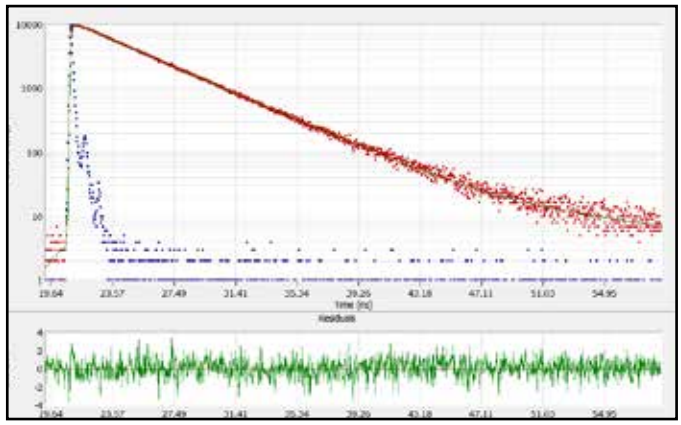

Figure 4: Fluorescence lifetime decay of fluorescein (red), instrument response (blue) and fit (green). Error residuals is shown in lower graph.

Fluorescence and Phosphorescence Time Resolved Photoluminescence Spectroscopy on an SMS System

Introduction

Fluorescence and phosphorescence are two popular luminescence phenomena used for material characterization. The primary difference between these two phenomena is in the way the electronic transitions that result in the luminescence occur, as shown in figure 1 below. This difference in decay relaxation pathways is manifested in the time scales involved – with fluorescence being a relatively fast effect occurring over picoseconds to microseconds, while phosphorescence is much slower, occurring over microseconds to seconds.
Due to the difference in time scales, fluorescence and phosphorescence lifetimes are usually measured on separate instruments with different technologies for time resolution of the luminescence. HORIBA's Standard Microscope Spectroscopy system for time resolved photoluminescence (SMS-TCSPC) is capable of combining both micro fluorescence and phosphorescence measurements on one platform, measuring luminescence lifetimes from the picoseconds range associated to fluorescence phenomena, to several seconds for phosphorescence. Furthermore, the SMS-TCSPC system is built on standard commercial microscopes, making this an open and flexible configuration that can be acquired as a turnkey system or added to an existing microscope.

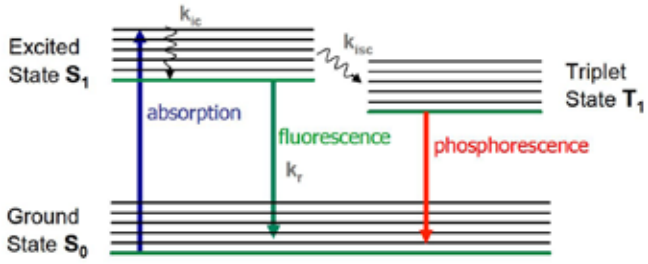

Figure 1: Jablonski diagram illustrating absorption, fluorescence and phosphorescence phenomena in a molecule. Both fluorescence and phosphorescence processes absorb incoming photons, resulting in change of electron distribution and moving the molecule to an excited electronic state. The excited molecule relaxes back to the ground state via emission of light. In fluorescence, this occurs between singlet energy levels (fast), but in phosphorescence the relaxation is via a triplet state (slow).

Time correlated single-photon counting (TCSPC) is the most popular method of determining picosecond to microsecond fluorescence lifetimes. It is based on the fact that the probability of detection of a single photon at a certain time after an excitation pulse is proportional to the fluorescence intensity at that time [1]. TCSPC is a pulsed technique that builds up a histogram of fluorescence photon arrival times from successive excitation-collection cycles. The histograms obtained give an immediate qualitative indication of lifetimes and can show the presence of more than one decay pathway. It can be fitted with an appropriate decay model and provides the lifetimes and the goodness of fit.

In this article, we show that the same HORIBA hardware and software used for TCSPC lifetime measurement (fluorescence timescale) can also be used for determination of lifetime on a phosphorescence timescale. For these longer lifetime measurements, the Multichannel Scaling (MCS) technique is used. MCS works by counting all events occurring within a specified time interval t to t + Δt (the dwell time or bin width). The overall measurement time T for each time sweep is divided into i histogram points (number of bins) and T is quantized by the relation T = iΔt. At the start of a measurement, all photon counting events are collected into the first time channel. At the end of the dwell time photon counting starts in the next channel, and so on. This continues until all i channels have been utilized (called a sweep). This process can be repeated for a prerequisite number of sweeps, specified time or peak number of counts. The resulting histogram can be fitted with an appropriate decay model to determine lifetimes.

Experimental setup

A 375 nm DeltaDiode laser is used as an ultrafast pulsed excitation source with 45 ps pulse width and maximum repetition rate of 100 MHz. This light source is free-space or fiber-coupled to a microscope using HORIBA's universal microspectroscopy adapter that enables the addition of various spectroscopies to any standard microscope without compromising existing microscope functionality. The microspectroscopy adapter conveys the pulsed excitation light to the microscope objective and onto the sample surface. The photoluminescence emission from the sample is collected with the same microscope objective and free-space or fiber-coupled to a spectrometer passing through the dichroic and long-pass filter for cleaning up the excitation laser from the emission signal. An iHR320 spectrometer with a 600 gr/mm grating blazed at 750 nm and SynapsePlus CCD is used to detect the emission signal. LabSpec software is used for steady state PL measurement and EzTime software is used for TCSPC and MCS lifetime measurement.

The same electronics are used for both fluorescence (TCSPC) and phosphorescence (MCS) lifetime measurement by using the DeltaDiode in "burst" mode for the latter. The use of "burst mode" enables a DeltaDiode laser to be used to measure lifetimes on longer time ranges. Burst mode works by operating the DeltaDiode at its maximum repetition rate (100MHz in this case). The resulting "train of pulses" can then be "gated" ON or OFF. At 100 MHz there is an excitation pulse every 10 ns, so on

the first software preselected phosphorescence time range of 340 µs with a bin width of 83 ns, each time bin can contain 8 excitation pulses. Since the emissions studied using this technique are long-lived, each gated stream of pulses would appear as one long excitation pulse of roughly 83 ns, as shown in figure 2a. The duration of the gated pulse is software controlled. The longer the duration, the more photons are incident on the sample, but there are fewer time bins over which to analyze the decay. Since the pulse train is turned off almost instantaneously, there is no need to analyze using deconvolution (the process of recording an instrument response function or IRF, and using it to remove the effect of the excitation pulse itself have a finite duration). Data can be "tail-fitted" beginning at the end of the excitation pulse train as demonstrated in figure 2b.

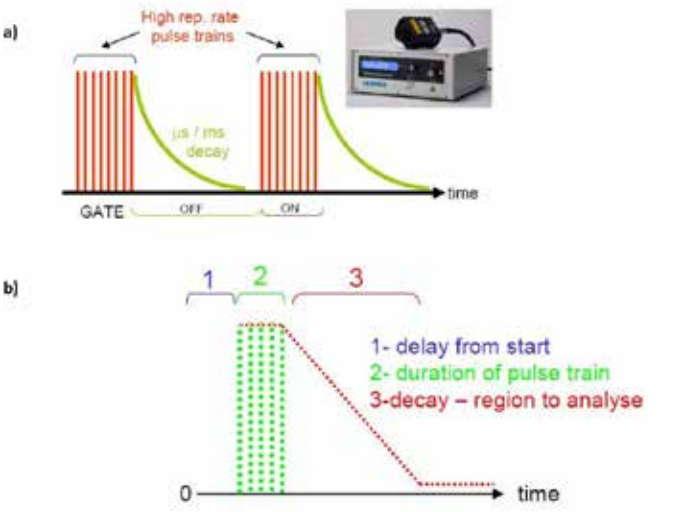

Figure 2: (a) Illustration of DeltaDiode operation in burst mode. (b) Schematic of the resulting decay plot expected to be recorded by EzTime software from the start to the end of measurement set time.

Experiment results

1. Fluorescence lifetime (TCSPC)

The sample used for fluorescence lifetime measurement was a green Chroma filter slide with PL peak at 550 nm. The decay time measurement at 550 nm is shown in figure 3. The red dotted line is the intensity decay, and the blue dotted line is the instrument response function (IRF). The green line in the upper plot is the fitted decay and in the lower plot is the standard deviation of the residuals for the fit. The calculated lifetimes by EzTime are shown in table 1 with a goodness of fit of X^2=1.04.

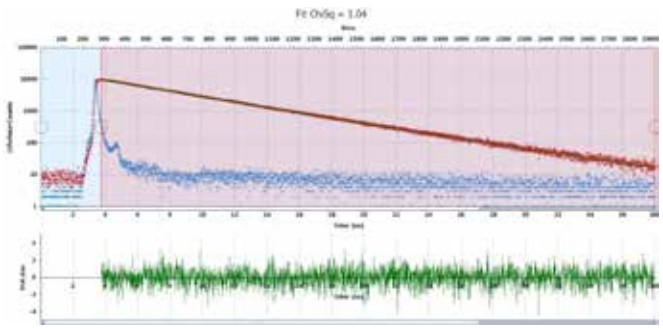

Figure 3: Experimental and simulated intensity decay of a green Chroma slide in log scale, with emission at 550 nm.

Results			
Name	Value	Std Dev	Units
T1	2.68	0.10	ns
T2	5.00	0.05	ns
T3	24.23	5.94	ns

Table 1: Calculated lifetimes by EzTime for the green Chroma slide.

2. Phosphorescence lifetime (MCS)

The sample used for phosphorescence lifetime was a glow in the dark crème with PL peak at 565 nm. Figure 4 shows the delay (5% of the experiment time), pulse train (15% of the experiment time) and the lifetime decay. To calculate the lifetime, only the decay section is analyzed and there is no need to include IRF correction.

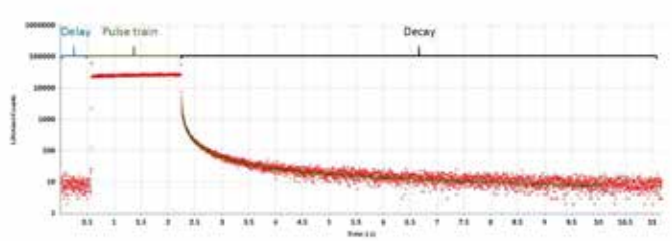

Figure 4: The data collected by EzTime for the experiment time of 11s. The delay is set to be 5% of the experiment time, pulse train is 15% of the experiment time and lifetime decay will be recorded for the remaining 80% of the experiment time.

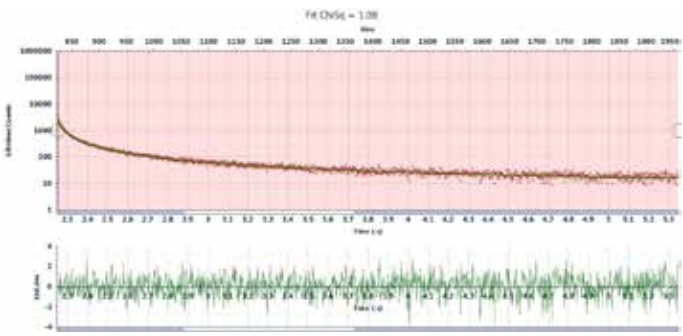

Figure 5: Experimental and simulated intensity decay of a glow in the dark crème in log scale, with emission at 565 nm.

As shown in Figure 5 the data is tail-fitted and the standard deviation of residuals plotted. Table 2 shows lifetime values after fitting the decay by EzTime software and the goodness of fit is X^2=1.08.

Results			
Name	Value	Std Dev	Units
T1	0.072	0.005	ns
T2	0.36	0.012	ns
T3	2.48	0.10	ns
T4	0.012	0.00051	ns

Table 2: Calculated lifetimes by EzTime for the glow in the dark creme.

The second sample used was Europium Chloride with pl peak at 590 nm and an expected lifetime of 117±3 µs. The lifetime decay plot is shown in figure 6 and the measured lifetime as expected is 117.2 µs ± 2.4 µs with goodness of fit of X^2=1.

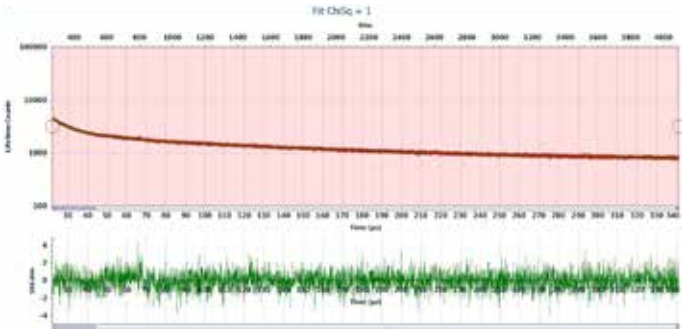

Figure 6: Experimental and simulated intensity decay of Europium Chloride in log scale, with emission at 590 nm.

Results			
Name	**Value**	**Std Dev**	**Units**
T1	117.23	2.39	µs

Table 3: Calculated lifetimes by EzTime for the Europium Chloride.

Conclusion

In this paper, we show an open and flexible system for both short-lived fluorescence and long-lived phosphorescence characterization on a single standard microscope platform. This system takes advantage of new developments in HORIBA's family of ultrashort lifetime sources, electronics and detectors to extend their capability to longer lifetimes thereby eliminating the need for multiple systems and enhancing measurement efficiency.

References

(1) HORIBA Jobin Yvon Ltd, Glasgow, Scotland, UK; "A practical guide to time-resolved luminescence lifetime determination using dedicated Time-Correlated Single-Photon Counting systems."

Micro Photoluminescence Lifetime Measurement on Semiconductor Sample for Device Characterization and Defect Study

Time resolved photoluminescence is another powerful technique that can provide a wealth of complementary information that is not readily accessible through steady state measurements. For example, while defects may be identified with steady state photoluminescence, time-resolved PL can provide more information on the nature of the defect. It can also provide a probe into the dynamics happening within the material such as minority carrier lifetimes and recombination processes in the bulk or at the interface.

Experimental Setup

AnSMS system as described in previous articles was used with TCSPC components, a PPD-650 detector and a 375 nm DeltaDiode laser as an ultrafast pulsed excitation source with 45 ps pulse width and maximum repetition rate of 100 MHz.

Results

Figure 2 shows PL lifetime measurements (and their correspondent residuals) for two locations marked as 1 and 2 in Figure 1. Location 1 is selected at the edge of the device and location 2 is closer to the center between the two metallic fingers where the PL peak intensity is maximum. Time correlated single photon counting (TCSPC) is the most popular method of determining picosecond to microsecond fluorescence lifetimes [1]. TCSPC is a pulsed technique that builds up a histogram of fluorescence photon arrival times from successive excitation-collection cycles. The histograms obtained give an immediate qualitative indication of lifetime, and can show the presence of more than one decay pathway. It can be fitted with an appropriate decay model and provides the lifetimes and the goodness of fit. As can be seen in figure 3, the data is fitted and the standard deviation of the residuals are plotted for decays attributed to position 1 and 2. Decay spectra in figure 3 contain multiple lifetime components which can be caused by the inhomogeneous distribution of gallium and aluminum in AlGaInP [2].

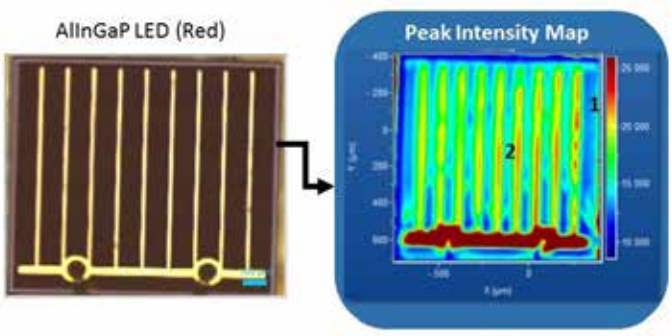

Figure 1: PL peak intensity map for AlInGaP LED (red).

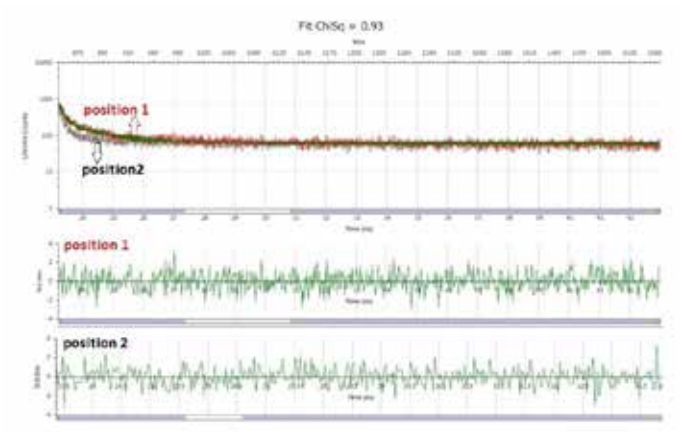

Figure 2: Experimental and simulated intensity decay of AlGaInP (red) LED in log scale, with emission at 630 nm.

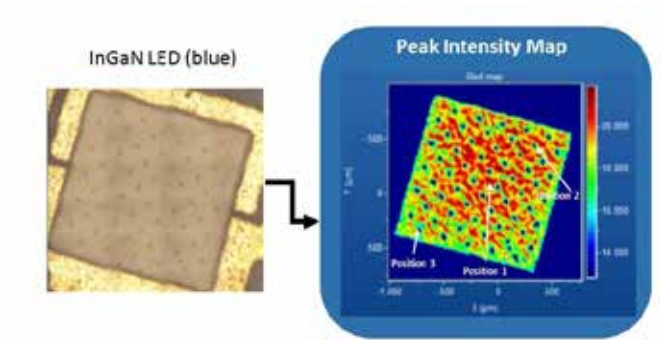

Figure 3: PL intensity map for InGaN LED (blue).

Figure 4 shows the lifetime decays for a blue LED (InGaN) at 3 locations marked in Figure 3 PL intensity map. These decays were recorded for 450 nm PL peak emission. Location 1 is at the center of the device where PL peak is strong and narrow; location 2 is on the contact pattern on the surface where PL peak is much weaker and location 3 is on the side of the device where a visual defect was observed. After fitting the decay spectra, the longest excess carrier lifetime belongs to position 1 at the center of the device with average lifetime of 27.93 ± 2.69 ns. Meshed pattern on the surface displayed shorter average lifetime of 19.89 ± 1.67 ns and the visual defect on the side of the device had the shortest lifetime of 3.86 ± 2.62 ns.

The shorter lifetime caused by the presence of the defect in the structure is possibly due to the trap-assisted recombination process that happens when an electron falls into an energy level within the bandgap (traps) introduced by the presence of a defect or foreign atoms like doping [3]. For all the decays several lifetime components were observed as shown in Table 2 which can be due to the inhomogeneous distribution and phase segregation of

the indium in InGaN structure of the blue LED. Excessive carriers (photo generated electrons and holes) with higher energies can perform a direct recombination or relax to lower energy states caused by excessive indium. All of these relaxation channels have different decay times and probabilities.

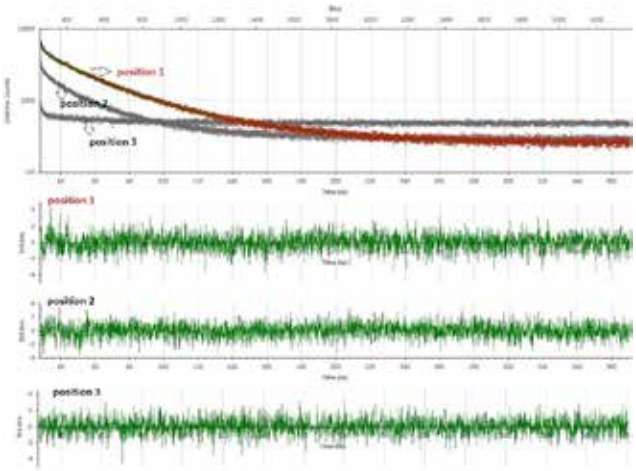

Figure 4. Experimental and simulated intensity decay of InGaN (blue) LED in log scale, with emission at 450 nm.

Table 1 shows lifetime values after fitting the decay by EzTime software and the corresponding values for the goodness of fit (chi sq.). It was expected to observe a shorter lifetime for the PL peak at the edge of the device (1.01 ± 0.78 ns) compared to the center (5.98 ± 0.23 ns) due to the observed higher concentration of defects in the PL map (see figure 1 intensity map). The reason for this phenomena is that the lifetime of the excess carriers strongly depends on the concentration of the defects present in the semiconductor device. These defect points introduce intermediate bandgaps between the conduction and valence bands, therefore acting as recombination centers in the bandgap and making the carrier lifetimes shorter.

Results for position 1 (chi sq. = 0.093)			
Name	Value	Std Dev	Units
T1	0.26	0.03	ns
T2	1.97	0.57	ns
Average Lifetime	1.01	0.78	ns
Results for position 2 (chi sq. = 1.09)			
T1	1.09	0.14	ns
T2	7.92	0.26	ns
Average Lifetime	5.98	0.23	ns

Table 1. Calculated lifetimes by EzTime for the AlGaInP (red) LED

Results for position 1 (chi sq. = 1.05)			
Name	Value	Std Dev	Units
T1	24.00	2.38	ns
T2	55.74	1.23	ns
T3	2.18	0/23	ns
Average Lifetime	27.93	2.69	ns
Results for position 2 (chi sq. = 1.09)			
T1	18.39	3.05	ns
T2	1.73	0.30	ns
T3	46.36	2.01	ns
Average Lifetime	19.89	1.67	ns
Results for position 3 (chi sq. = 1.02)			
T1	0.04	0.2	ns
T2	1.61	0.64	ns
T3	37.57	4.57	ns
Average Lifetime	3.86	2.62	ns

Table 2: Calculated lifetimes by EzTime for the InGaN (blue) LED

Conclusion

In this paper, we demonstrated the ability to perform lifetime measurements on different commercial LED devices. The sample luminescence was resolved spectrally and spatially, and lifetimes of the same luminescence was studied. Multiple time spectra at different photon emission energies was recorded. These time spectra showed multiple exponential decays likely attributable to inhomogeneous distribution of gallium and indium for InGaN or gallium and aluminum in AlGaInP in the samples. It was observed that the presence of defect will shorten the excess carrier lifetimes perhaps due to the trap-assisted recombination process caused by an electron falling into an energy level within the bandgap. These traps are introduced by the presence of defects or foreign atoms like doping. This method can be used as a complementary technique for PL measurement to provide more information regarding the device degradation and defects.

References

(1) HORIBA Jobin Yvon IBH Ltd, Glasgow, Scotland, UK; "A practical guide to time-resolved luminescence lifetime determination using dedicated Time-Correlated Single-Photon Counting systems"
(2) Morkoç H., [Handbook of nitride semiconductors and devices, Materials Properties, Physics and Growth], John Wiley & Sons, 670-750 (2009).
(3) Queisser, Hans J., and Eugene E. Haller. "Defects in semiconductors: some fatal, some vital." Science 281.5379 945-950 (1998).

Fluorescence Lifetime Imaging on a Standard Microscope Spectroscopy (SMS) System

Introduction

Fluorescence lifetime spectroscopy is an increasingly popular technique for material analysis. This is partly because it is a background-free technique and partly because it offers complementary insights that are not readily accessible through steadystate methods. In addition, fluorescence lifetime imaging microscopy (FLIM) adds spatial information to the measured data set, providing another form of contrast to the image. A FLIM image consists of the fluorescence lifetime at each pixel of the image rather than just the fluorescence intensity as in steady-state fluorescence [1]. Fluorescence lifetime typically does not depend on concentration but is highly dependent on the fluorophores' local environment. The spatial information provided by FLIM enables measurement of variables such as pH, viscosity, and temperature [2] to be made. In the case of perovskite materials, local differences in the lifetimes reflecting the radiative recombination can be ascertained [3].

Here we describe a modular turnkey system that equips a standard microscope with FLIM components for lifetime imaging. The lifetime measurement is based on time-correlated single-photon counting (TCSPC) for recording the time-resolved fluorescence decay. This system is capable of lifetime imaging measurements from picoseconds to microseconds, as well as single point phosphorescence measurements. The components, shown below in Figure 1 can be added as a kit to a user's existing microscope.

Figure 1: Photograph of FLIM-capable TCSPC components (FiPho timing electronics, DeltaDiode lasers, HPPD detector). Images are collected and analyzed using EzTime Image software.

To assess the system's capabilities, we tested a commonly used biological sample - convallaria. Figure 2 illustrates the configuration and picture of our Standard Microscope Spectrometer system for FLIM (SMS-FLIM). It is a comprehensive and flexible platform capable of multiple spectroscopies, such as micro-reflectance, Raman, photoluminescence (PL), TCSPC spectroscopy, etc.

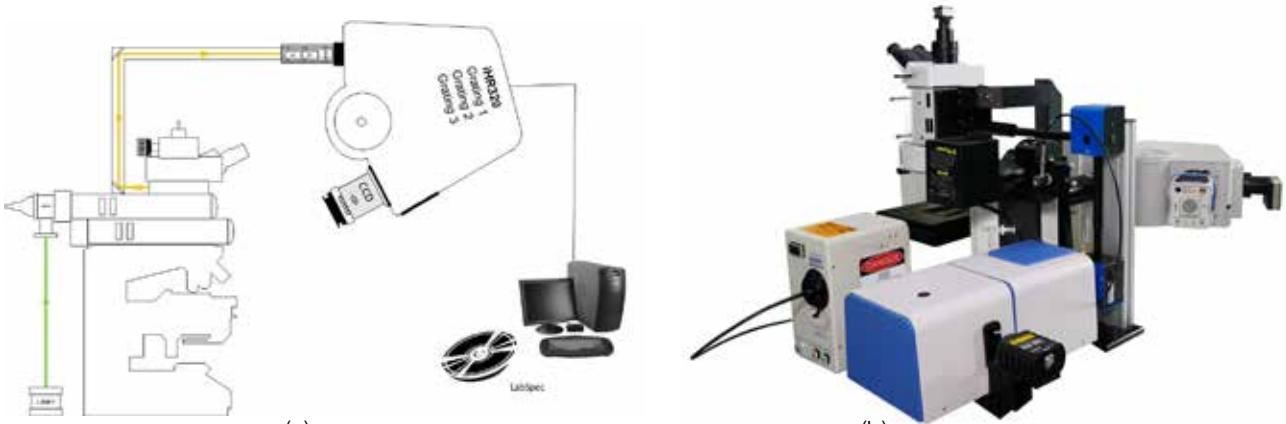

(a) (b)

Figure 2: Experimental setup for micro luminescence lifetime mapping using FLIM technique on a standard microscope. (a) Schematic setup. (b) Rear view of HORIBA Standard Microscope Spectroscopy (SMS) system.

Experiment

A 481 nm DeltaDiode laser was used as the fast-pulsed excitation light source with optical pulse width of less than 80 ps and repetition rates up to 100 MHz. The excitation source was coupled into the microscope by either free-space or a multimode fiber. The custom laser-coupling accessory provided by HORIBA contains reflective optics to direct excitation light to the sample and a dichroic and long pass filter to separate laser light from sample emission. The objective focused the excitation light onto the sample surface. A motorized XY translation stage communicates with the vision camera for sample positioning and scanning. The stage movement was synchronized with the FiPho TCSPC timing electronics.

The emission light was collected by the objective, collimated and focused into the iHR320 spectrometer with 600 gr/mm grating blazed at 750 nm. The SynapsePlus CCD was used to measure the steady state luminescence and a fast PPD-900 detection module on the side exit port of the spectrometer was used to measure the time-resolved emission. The resultant image from the FLIM measurement comprised of time-resolved decays recorded at each point of the map grid and analyzed using HORIBA EzTime Image software.

The emission spectrum of the convallaria sample stained by acridine orange (AO), which has been certified around 530 nm, was confirmed by a steady state measurement, shown in Figure 3. The FLIM measurement was then performed at this peak fluorescence emission accordingly.

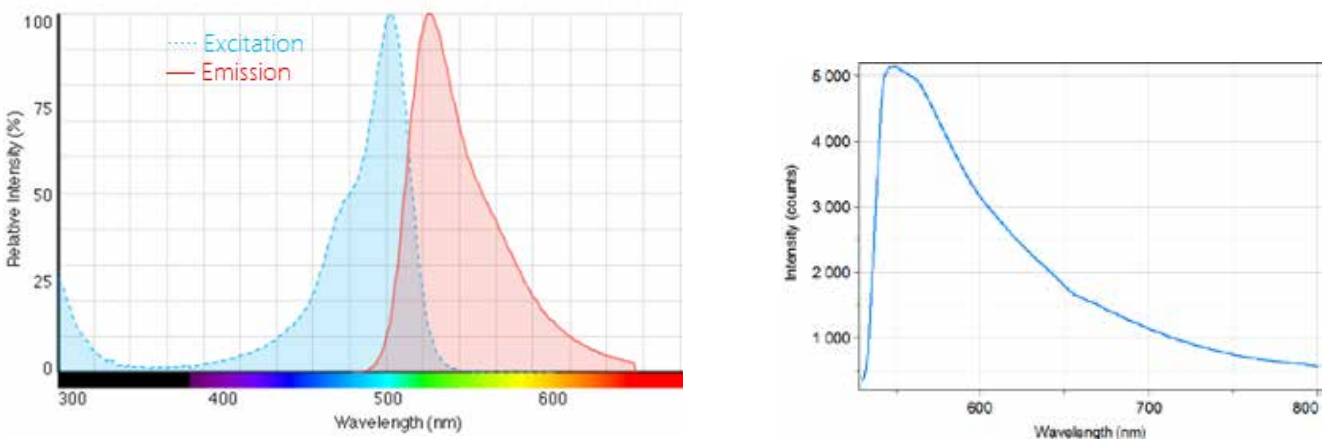

(a) (b)

Figure 3: Fluorescence spectra of acridine orange. (a) Certified spectra[4]. (b) Experimental spectrum (affected by cut-on slope of 532 PL filter and dichroic).

Figure 4(a) shows the optical image recorded by a monochrome camera on the microscope. The desired imaging area was set to 244 µm ×184 µm, with a step size of 2 µm. The runtime for each point was 200 ms. The acquisition of total 11224 points was accomplished in around 20 minutes. Figure 4(b) gives the image of emission intensity. The concentration of AO is apparently much higher in cell walls.

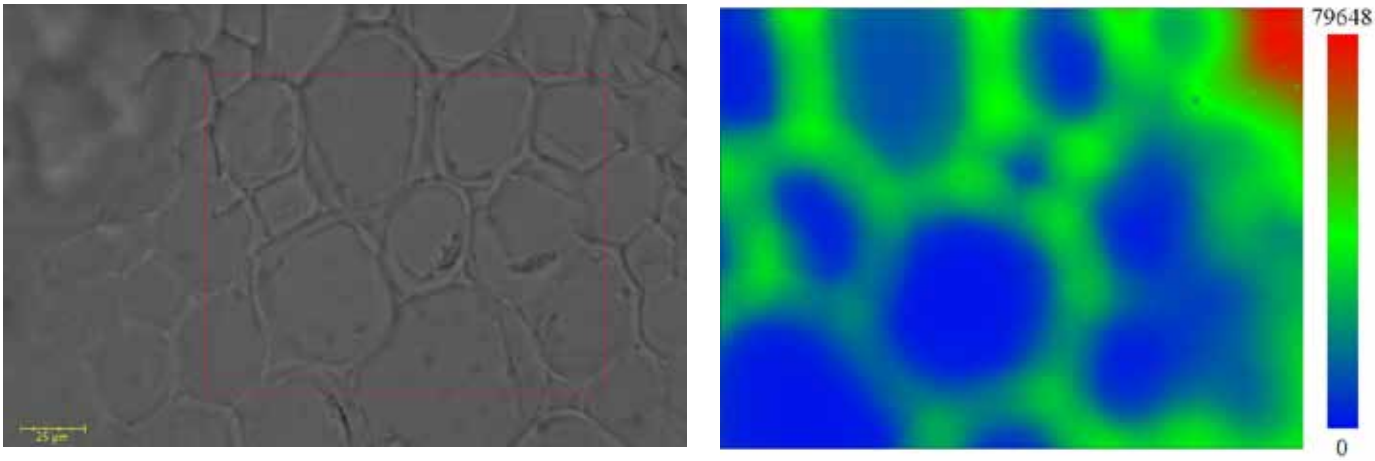

(a) (b)

Figure 4: (a) Optical image of the convallaria sample observed by 40x objective. (b) Mapping of emission intensity at selected area. (Excitation light = 481 nm DeltaDiode laser, fiber coupled. Repetition rate = 16 MHz. Time range = 50 ns. Objective = 40x. Slit = 2000 µm. Runtime = 200 ms. Size (pixels) = 122 x 92. Step size = 2 µm.)

Results

The time-dependent decay at each point was fitted to a three-exponential-decay model.

$$I(t) = A + B_1 \exp(-t/\tau_1) + B_2 \exp(-t/\tau_2) + B_3 \exp(-t/\tau_3)$$

where τ_i are the lifetimes, B_i are the pre-exponentials. The normalized pre-exponentials are calculated by,

$$\alpha_i = \frac{Bi}{\sum_i B_i}$$

The average lifetime at each point of the FLIM image was determined by the amplitude-weighted lifetime of this three-lifetime model,

$$(\tau) = \sum_i \alpha_i \tau_i$$

The lifetimes were quantitatively analyzed by EzTime Image software. The lifetime of each exponential component was estimated about τ_1 = 4.62 ns, τ_2= 1.37 ns, τ_3 = 0.31 ns, respectively. Figure 5 illustrates the spatial distribution of emission intensity and average lifetime, respectively, at the selected area.

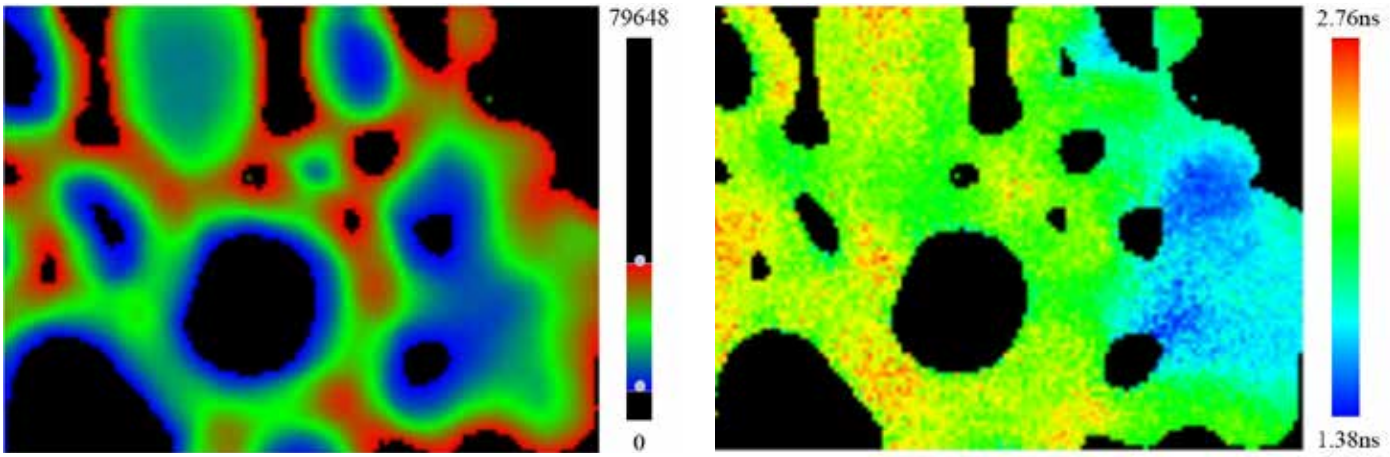

(a) (b)

Figure 5: (a) Artificially set the thresholds to select the area for analysis on emission intensity. (b) Spatial distribution of average lifetime of the selected area.

The normalized pre-exponential mapping of each lifetime component is shown in Figure 6, in order to represent the distribution of the weight for each component, which can be further used to contrast the variables related to the local environment. The scale applies to all three images. The sum of the normalized pre-exponential values of the three lifetimes is "1" at each point. It was observed that the emission with lifetime of τ_2 = 1.37 ns dominates around the area of cell walls, and the right region produces more emission with shorter lifetimes of τ_3 = 0.31 ns.

Conclusion

The above procedure validates the capability of the fluorescence lifetime imaging measurement based on standard microscope platform, with convallaria as the example. EzTime Image software provides a powerful tool for recording and analyzing the lifetimes from both single point and imaging measurements.

Reference

(1) Joseph R. Lakowicz, Principles of Fluorescence Spectroscopy, Third Edition (Springer, New York, 2010)
(2) K. Okabe, et al., Nature Communications, 3, 705 (2012)
(3) G. Namkoong, et al., Solar Energy Materials & Solar Cells, 155, 134 (2016)
(4) www.thermofisher.com/order/catalog/product/A1301

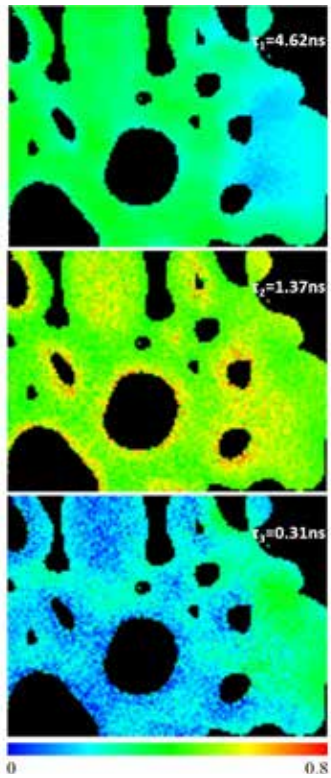

Figure 6: FLIM images of the normalized pre-exponential for each lifetime component.

Steady State and Time-Resolved Micro PL Spectroscopy on a Standard Microscope Spectroscopy (SMS) System

Introduction

Time correlated single photon counting (TCSPC) provides a commonly used technique for luminescence lifetime measurement [1]. HORIBA provides a wide range of TCSPC instruments covering various wavelengths and time ranges – from picoseconds to seconds. In this work, we demonstrate a modular turnkey system that adds both steady state and time-resolved micro PL to a standard microscope. The time-resolved capability is based on TCSPC technology. The system is capable of measuring lifetimes from picoseconds to seconds and can be added as a kit to a user's existing microscope. We illustrate its capabilities by testing on three different common samples. Figure 1 shows the system configuration and picture.

(a) (b)

Figure 1: Experimental setup for micro luminescence lifetime measurement using the TCSPC technique on a standard microscope. (a) Schematic setup. (b) Front view of HORIBA Standard Microscope Spectroscopy (SMS) system, a comprehensive and flexible platform capable of multiple spectroscopies, such as Micro-reflectance, Raman, Photoluminescence (PL), TCSPC spectroscopy, etc.

Measurement Configuration

A 481 nm DeltaDiode laser, was used as an ultra-fast pulsed excitation light source with an optical pulse width of 80 ps and repetition rates up to 100 MHz. The light source was coupled into the microscope by either free-space or a multi-mode fiber. The custom laser-coupling accessory provided by HORIBA contains reflective optics to direct excitation light to the sample, and a dichroic and long pass filter to separate laser light from sample emission. The objective focused the excitation light onto the sample surface. The system includes an optional motorized XY translation stage communicating with the vision camera for sample positioning and mapping. The emission light was collected by the objective collimated and focused into the iHR320 spectrometer with 600 gr/mm grating blazed at 750 nm. The Synapse CCD was used to measure the steady state luminescence while the fast PPD-900 on the side exit port of the spectrometer was used to measure the time-resolved luminescence. The decay rates were analyzed using HORIBA EzTime software.

Experiment and result

Sample number one was a filter slide whose photoluminescence (PL) spectrum showed a peak at 591 nm. The steady state PL spectrum was measured with the CCD (Figure 3b). The decay time measurement at awavelength of 591 nm is shown in Figure 2. The red-circled data points are the experimental data of the intensity decay. The blue-circled plot is the instrument response function (IRF). The IRF measures the response of the system to the excitation pulse, which can be deconvolved from the sample signal to isolate the pure response from the sample. The green line in the upper plot is the fitted curve using a single-decay model. The lower plot is standard deviation of the residuals from the fitted curve – showing the goodness of fit of the green curve to the red data points.

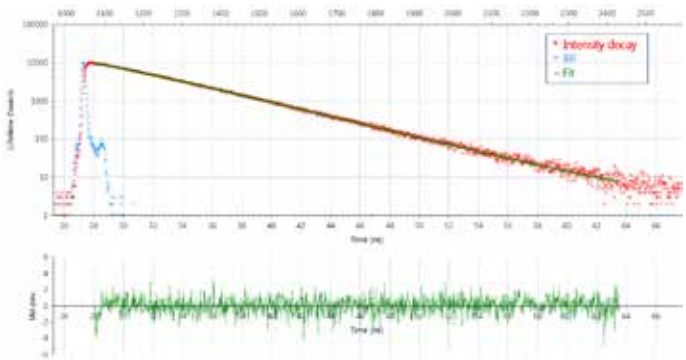

Figure 2: Experimental and simulated intensity decay of a pink Chroma slide in log scale, with emission at 591 nm. (Excitation light source = DeltaDiode laser of 481 nm, free-space coupled. Repetition rate = 10 MHz. Time range = 100 ns. Objective = 10x. Slit = 100 µm.)

For a single exponential decay, the intensity can be expressed as[1]: $I(t) = I_0 \exp(-t/\tau)$ where I_0 is the intensity when $t = 0$, τ is the lifetime. The calculated liftetime by EzTime was $\tau = 4.95 \pm 0.0063$ ns, with a goodness-of-fit parameter x^2=1.02.

Representing biologicals, we also measured a convallaria sample stained by acridine orange (AO), an organic compound with an excitation maximum around 500 nm and an emission maximum around 530 nm, as shown in Figure 3a. This sample represented multi-exponential decays.

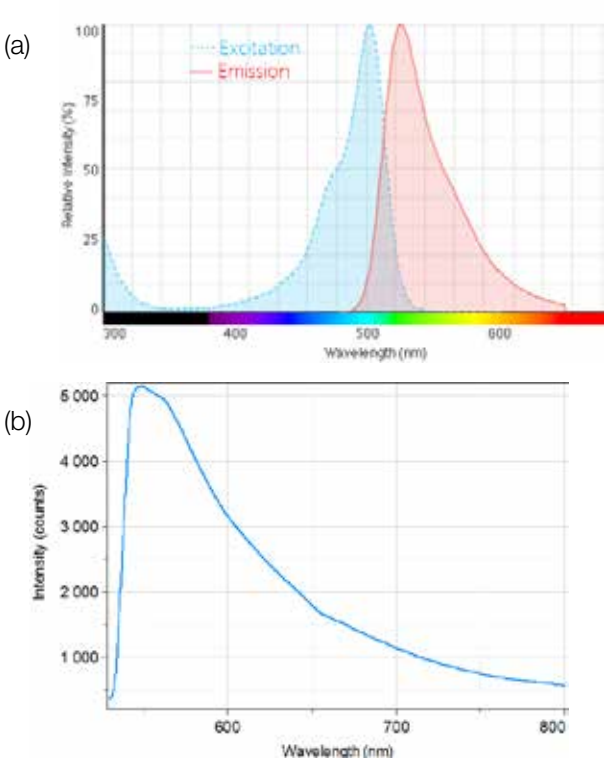

Figure 3: Fluorescence spectra of acridine orange. (a) Certified spectra [2]. (b) Experimental spectrum (affected by cut-on slope of 532 PL filter and dichroic).

The multi-lifetime model commonly considers the intensity as the sum of individual exponential decays [1]:

$$I(t) = A + \sum_{(i=1)}^{n} B_i \exp(-t/\tau)$$

where τ_i are the lifetimes, the pre-exponentials B_i are the amplitudes of the components at t=0, n is the number of lifetime components. The normalized pre-exponentials are calculated by:

$$\alpha_i = \frac{Bi}{\sum_i B_i}$$

The relative amplitudes are the fractional contribution of each decay time to the steady state intensity,

$$f_1 = \frac{\alpha_i \tau_i}{\sum_i \alpha_i \tau_i}$$

The amplitude-weighted lifetime is used to determine the average lifetime:

$$(\tau) = \sum_i \alpha_i \tau_i$$

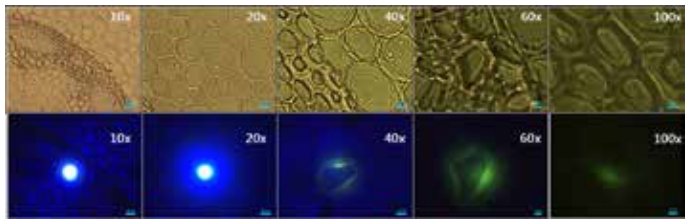

Figure 4: Vision camera image of convallaria observed by various objectives. Top row: Detected region with bottom illuminator on and laser off. Bottom row: Photoluminescence with illuminator off and laser on.

Figure 4 shows vision camera images of sample under different magnifications (top row) and the excitation laser spot size on the sample at corresponding magnifications. The spectrometer was parked at the emission peak of 562 nm where the lifetime was measured. We used EzTime to fit the curve. A three-decay-time model resulted in a best reduction of x^2=1.05, as shown in figure 5. The average lifetime (τ) ≈1 ns. The fitted parameters of the three-decay-time model are listed in Table 1.

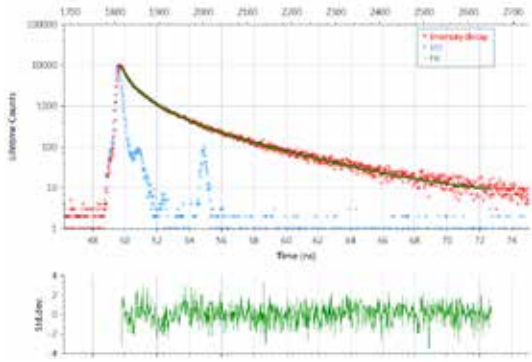

Figure 5: Multi-exponential decay of convallaria in log scale, with emission at 562 nm. (Excitation light source = DeltaDiode laser of 481 nm, fiber-coupled. Repetition rate = 10 MHz. Time range = 100 ns. Objective = 40x. Slit = 300 µm.)

	Lifetime (ns)	Standard Deviation	Normalized B	Relative Amplitude
τ_1	1.25	0.041	0.036	45.42
τ_2	4.11	0.048	0.09	36.06
τ_3	0.32	0/005	0.56	18.52

Table 1: Multi-exponential analysis of convallaria with emission at 562 nm.

The third sample was a Mo substrate with various flakes on the surface. The different flakes showed different PL and TCSPC spectra. The vision camera image of three flakes (Figure 6) was observed with the 20x objective. The lifetime measurement of each flake at 565 nm is shown in figure 7b. The experimental data from top to bottom are for white, black and third flake, respectively.

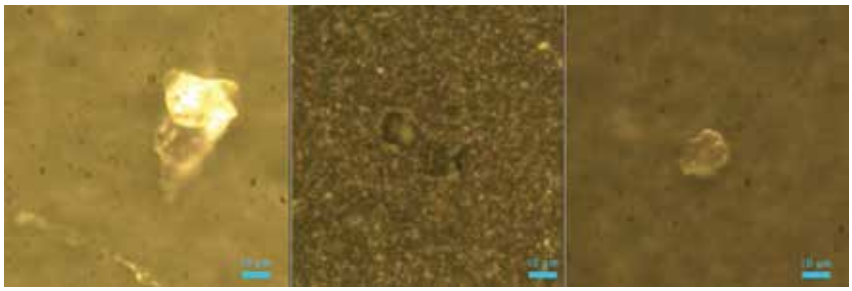

(a) (b) (c)

Figure 6: Three different flakes presenting different PL spectra observed by top illuminator and 20x objective. (a) White flake. (b) Black flake. (c) Third flake.

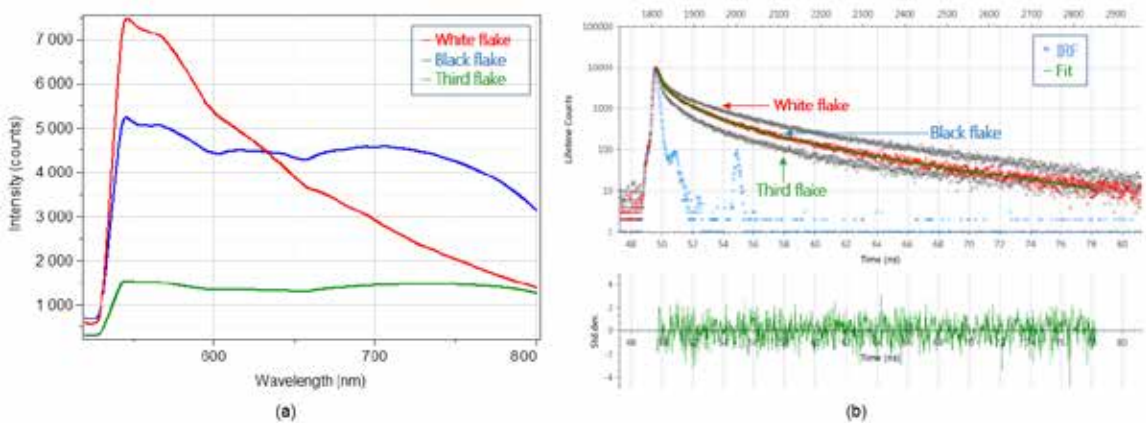

Figure 7: (a) Steady state of three flakes. (b) Lifetime measurement of three flakes at 565 nm. The green line is the fitted curve of the black flake as a four-decay-time model. (Excitation light source = DeltaDiode laser of 481 nm, fiber-coupled. Repetition rate = 10 MHz. Time range = 100 ns. Objective = 20 x. Slit = 500 µm.)

EzTime was used to analyze the data as well, and a four-decay-time model resulted in best fit for each curve. The parameters of the fitted curves are listed in Table 2.

	White flake				Black flake				Third flake			
	Lifetime (ns)	**Std. Dev.**	**Nor. B**	**Rel. Amp.**	**Lifetime (ns)**	**Std. Dev.**	**Nor. B**	**Rel. Amp.**	**Lifetime (ns)**	**Std. Dev.**	**Nor. B**	**Rel. Amp.**
τ_1	1.15	0.077	0.29	18.81%	1.03	0.059	0.36	26.96%	0.93	0.043	0.2	27.59%
τ_2	3.69	0.167	0.21	43.99%	3.44	0.242	0.14	42.08%	3.3	0.168	0.07	35.87%
τ_3	11.82	0.445	0.05	32.23%	14.05	1.593	0.02	20.53%	19.01	3.942	0.01	17.74%
τ_4	0.19	0.006	0.46	4.97%	0.21	0.004	0.56	10.43%	0.18	0.002	0.72	18.80%
$\bar{\tau}$= 1.79 ns x_2 = 1.14					$\bar{\tau}$ = 1.25 ns x_2 = 1.06				$\bar{\tau}$ = 0.74 ns x_2 = 1.07			

Table 2: Multi-exponential analysis of three flakes with emission at 565 nm.

The above procedure validates the capability of the SMS system with TCSPC components for both steady state and time-resolved micro PL measurements on the same platform. The LabSpec software provides accurate manipulations of samples and spectrometer, and the EzTime software provides a powerful tool to analyze and present time-resolved results.

References

(1) Joseph R. Lakowicz, *Principles of Fluorescence Spectroscopy*, Third Edition (Springer, New York, 2010)
(2) www.thermofisher.com/order/catalog/product/A1301

Minority Carrier Lifetime and Diffusion Length Characterization of LEDs and Other Semiconductor Materials by Lifetime Measurement

Introduction

Minority carrier lifetime and diffusion length are essential factors to understand the device quality and expected performance of optoelectronics devices, particularly for thin film solar cells with bandgaps covering visible to near-infrared ranges. Among several available characterization methods [1-5] time correlated single photon counting (TCSPC) is a popular candidate for the measurement of time-resolved photoluminescence (TRPL) and direct determination of effective minority carrier lifetimes along with carrier diffusion length. This method is fast, easy, contactless, calibration-free and can be used with either opaque or transparent samples [6-7] .

TCSPC is a pulsed technique that builds up a histogram of photon arrival times from successive excitation-collection cycles. The histograms obtained give an immediate qualitative indication of lifetime and can show the presence of more than one decay pathway. It can be fitted with an appropriate decay model to quantify the lifetimes.

In semiconductor materials, photoexcitation with above bandgap light usually results in creation of electron-hole pairs. These charge carriers diffuse from the point of generation and if not collected by an external circuit, will fall back to their ground state through recombination. The charge carrier lifetime is the time that it takes for photo-generated electrons and holes to recombine. Charge carrier lifetime is a statistical value that involves large numbers of electrons and holes, all recombining at different times via various pathways. As a result, it can be complicated to measure directly. Time-resolved PL offers one way to characterize carrier lifetimes.

The PL signal is directly related to excess carrier concentration Δn, and the continuity equation for semiconductors [8] adequately describes the excess carrier dynamics following photoexcitation:

$$\frac{\partial(\Delta n)}{\partial t} = G - R + D\frac{\partial(\Delta n)}{\partial x^2} + \mu E\frac{\partial(\Delta n)}{\partial x}$$

Δn: Excess carrier concentration; D: Diffusivity, μ: Charge carrier mobility, E: Electric field, x: Distance, t: Time.
It can be shown that under conditions of low high charge injection, this equation admits a simple decaying exponential solution [8], where the exponent includes the lifetime of excess carriers:

$$PL \sim \Delta n \sim \exp\left(-\frac{t}{\tau}\right) \quad \text{(Low charge injection)}$$

$$PL \sim \Delta n^2 \sim \exp\left(-\frac{2t}{\tau}\right) \quad \text{(High charge injection)}$$

So, by measuring the decay lifetime of the photoluminescence, the lifetime of the minority carriers could be indirectly inferred. The diffusion length is calculated using the following formula:

$$L = \sqrt{D\tau}$$

Where L is diffusion length, D is diffusivity and τ is the carrier lifetime. Diffusivity is a measure defined as how quickly a group of particles can fill up a space and is material dependent.

Experimental setup

In this paper, we focus on the use of the TRPL technique to measure minority carrier lifetimes using our Standard Microscope Spectroscopy (SMS) system. The SMS system equips most standard microscopes with various microspectroscopy techniques including time-resolved PL, Raman, reflectance, etc., all without compromising the existing functionality of the microscope. In this instance, our setup is capable of measuring samples with a minority carrier lifetime of 25 picoseconds to several seconds using the same electronics. It included a fast PPD-650 PMT detector and a 375 nm DeltaDiode laser as an ultrafast-pulsed excitation source with 45 ps pulse width and maximum repetition rate of 100 MHz. The PL measurement was performed at room temperature.

Results

The measurement was done by a succession of short-pulsed excitations of the sample, followed by exponential decay of the luminescence after each pulse. The TCSPC technique randomly detects single photon luminescence events and builds a histogram of arrival times of the luminescence photons. A fit to this data gives the luminescence lifetime. The PL decay is directly related to the effective carrier lifetime as explained in the introduction.

Figure 1 shows PL measurements for two locations marked as 1 and 2. Location 1 is selected at the edge of the device and location 2 is closer to the center between the two metallic fingers where the PL peak intensity is maximum. As can be seen in figure 2, the data is fitted for decays attributed to position 1 and 2. Decay spectra in figure 2 contain multiple carrier lifetime components.

Table 1 shows lifetime values after fitting the decay by EzTime software and the corresponding values for the goodness of fit (chi sq.). It was expected to observe a shorter lifetime for the PL peak at the edge of the device (1.01 ± 0.78 ns) compared to the center (5.98 ± 0.23 ns) due to the observed higher concentration of defects in the PL map. The reason for this phenomenon is that the lifetime of the excess carriers strongly depends on the

concentration of the defects present in the semiconductor device. The defect points introduce intermediate states between the conduction and valence bands therefore acting as recombination centers in the bandgap and making the carrier lifetimes shorter.

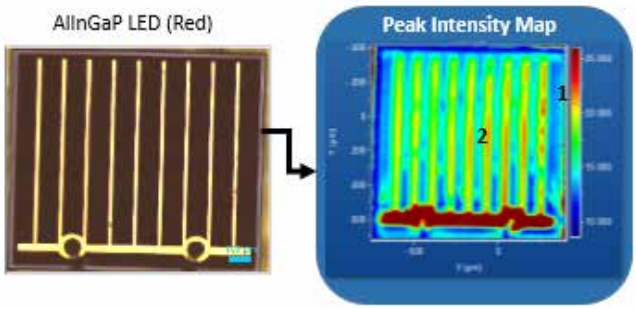

Figure 1: PL peak intensity map for AlInGaP LED (red).

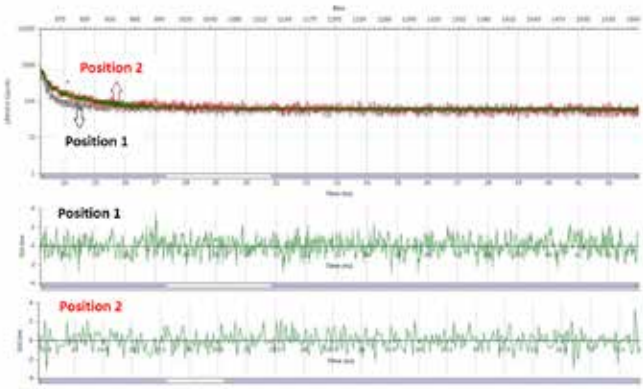

Figure 2: Experimental and simulated intensity decay of AlGaInP (red) LED in log scale, with emission at 630 nm.

Results for position 1 (chi sq. = 0.93)			
Name	Value	Std Dev	Units
T1	0.26	0.03	ns
T2	1.97	0.57	ns
Average Lifetime	1.01	0.78	ns
Results for position 2 (chi sq. = 1.07)			
T1	1.09	0.14	ns
T2	7.92	0.26	ns
Average Lifetime	5.98	0.23	ns

Table 1: Calculated lifetimes by EzTime for the AlGaInP (red) LED

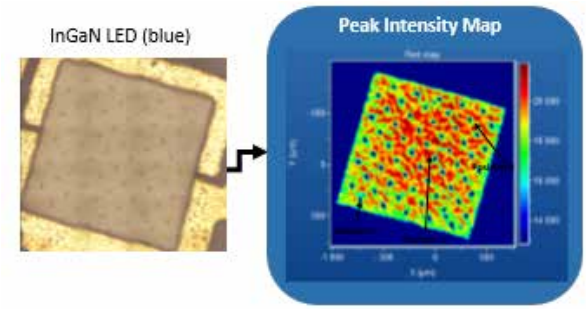

Figure 3: PL intensity map for InGaN LED (blue).

Figure 4 shows the lifetime decays for a blue LED (InGaN) at 3 locations marked in Figure 3 PL intensity map. These decays were recorded for 450 nm PL peak emission. Location 1 is at the center of the device where PL peak is strong and narrow: location 2 is on the messed contact pattern on the surface where PL peak is much weaker: and location 3 is on the side of the device where a visual defect was observed. After fitting the decay spectra, the longest excess carrier lifetime belongs to position 1 at the center of the device with average lifetime of 27.93 ± 2.69 ns. Meshed pattern on the surface displayed shorter average lifetime of 19.89 ± 1.67 ns and the visual defect on the side of the device had the shortest lifetime of 3.86 ± 2.62 ns. The shorter lifetime caused by presence of the defect in the structure is maybe due to the trap-assisted recombination process that happens when an electron falls into an energy level within the bandgap (traps) introduced by the presence of a defect or foreign atoms like doping [9]. For all the decays several lifetime components were observed as shown in Table 2 which can be due to the inhomogeneous distribution and phase segregation of the indium in InGaN structure of the blue LED.

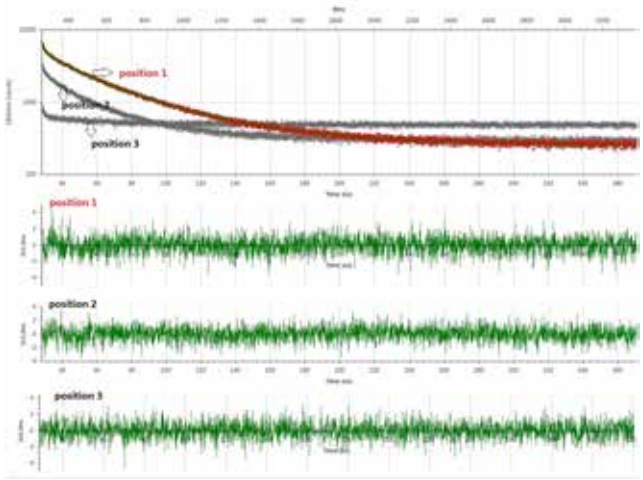

Figure 4: Experimental and simulated intensity decay of InGaN (blue) LED in log scale, with emission at 450 nm.

Results for position 1 (chi sq. = 1.05)			
Name	Value	Std Dev	Units
T1	24.00	2.38	ns
T2	55.74	1.23	ns
T3	2.18	0.23	
Average Lifetime	27.93	2.69	ns
Results for position 2 (chi sq. = 1.09)			
T1	18.39	3.05	ns
T2	1.73	0.30	ns
T3	46.36	2.01	ns
Average Lifetime	19.89	1.67	ns
Results for position 3 (chi sq. = 1.02)			
T1	0.04	0.2	ns
T2	1.61	0.64	ns
T3	37.57	4.57	ns
Average Lifetime	3.86	2.62	ns

Table 2: Calculated lifetimes by EzTime for the InGaN (blue) LED

Conclusion

In this paper, we demonstrated the ability to perform minority carrier lifetime measurement on different commercial LED devices by time-resolved photoluminescence using time-correlated single photon counting. The sample luminescence was resolved spectrally and spatially and lifetime of the luminescence was studied. Multiple time spectra at different photon emission energies was recorded. These time spectra showed multiple exponential decays. The effective lifetimes was estimated from fitting the exponential decay of the TRPL signal. It was observed that the presence of defects shortens the excess carrier lifetimes perhaps due to the trap-assisted recombination process caused by an electron falling into an energy level within the bandgap. These traps are introduced by the presence of defects or foreign atoms, like doping. This method can be used as a complementary technique for PL measurement to provide more information regarding the device degradation and defects. TCSPC is useful for evaluation of very short (picoseconds) to long minority carrier lifetimes and diffusion lengths knowing the material parameters.

References

(1) Jaramillo, R.; Sher, M.-J.; Ofori-Okai, B. K.; Steinmann, V.; Yang, C.; Hartman, K.; Nelson, K. A.; Lindenberg, A. M.; Gordon, R. G.; Buonassisi, T. Transient Terahertz Photoconductivity
Measurements of Minority-Carrier Lifetime in Tin Sulfide Thin Films: Advanced Metrology for
an Early Stage Photovoltaic Material. J. Appl. Phys. 2016, 119 (3), 35101.

(2) Ahrenkiel, R. K.; Call, N.; Johnston, S. W.; Metzger, W. K. Comparison of Techniques for
Measuring Carrier Lifetime in Thin-Film and Multicrystalline Photovoltaic Materials. Sol.
Energy Mater. Sol. Cells 2010, 94 (12), 2197–2204.

(3) Orton, J. W.; Blood, P. The Electrical Characterization of Semiconductors: Measurement of
Minority Carrier Properties; Academic Press: London; San Diego, 1990.

(4) O'Connor, D. V.; Phillips, D. Time-Correlated Single Photon Counting; Academic Press, Inc:
London, UK, 1984.

(5) Bruggemann, R. Steady-State Photocarrier Grating Technique for the Minority-Carrier
Characterisation of Thin-Film Semiconductors. J. Phys. Conf. Ser. 2010, 253 (1), 12081.

(6) O'Connor, D. V.; Phillips, D. Time-Correlated Single Photon Counting; Academic Press, Inc:
London, UK, 1984.

(7) Stéphanie Parola, et al. "Study of photoluminescence decay by time-correlated single photon
counting for the determination of the minority-carrier lifetime in silicon" Energy Procedia 55 (2014) 121 – 127

(8) Jeremy R. Poindexter, et al. "Charge-carrier lifetime measurements in early-stage photovoltaic
materials: intuition, uncertainties, and opportunities"

(9) Queisser, Hans J., and Eugene E. Haller. "Defects in semiconductors: some fatal, some vital." Science 281.5379 945-950 (1998).

Introduction to Reflectance & Tranmittance

Reflectance is a measure of the fraction of incident radiant energy that is reflected off a surface or a series of optical interfaces. Transmittance measures the fractional radiant energy transmitted through an optical material. These parameters are often measured as a function of wavelength – hence, reflectance and transmittance spectroscopy. Both of these spectroscopies are some of the earliest studied due partly to the simplicity in observation of the phenomenon. Their usefulness derives from the fact that light interaction with matter, whether in reflection or transmission modes, often carries signatures of the material in the reflected or transmitted emission and therefore provides a simple, non-contact method of characterizing such materials.

Absorbance and Transmittance

Transmittance is a derived observation from light scattering and absorption. In other words, when light is incident on a material, some of it is scattered at interfaces and another portion gets absorbed. What is left goes through the material and comes out as transmitted light. Therefore, transmittance light indirectly measures the absorbance of the material. Indeed, these two are related as shown below:

$$A = -Log\,(T) = -Log\,(\frac{I_t}{I_o}) \qquad (1)$$

Where,
A is the absorbance, T is the transmittance (which is the ratio of the transmitted light intensity I_t) and the incident light intensity I_o.

In terms of intrinsic material properties, absorbance is a result of the quantized energy states of matter and the base components of matter residing in these states can absorb energy and go from their default ground state to higher energy levels as shown in figure 1. In this instance, the energy difference between the ground state and an excited state is provided by an absorbed photon as described by equation 2.

$$E = \frac{hc}{\lambda} \qquad (2)$$

Where,
E is the energy difference between the ground and excited states of the absorbing species, h and c are constants, and λ is the wavelength of the absorbed photon.

Because the energy states of matter are discrete, it follows from equation 2 that only photons of a certain energy can cause transitions between any given states – other selection rules apply that can further limit the possibility of a photon causing a transition. Even though the energy levels are discrete, for many materials, these levels are often close enough that transitions between them appear as a broad continuum when looking at the absorption spectrum as shown in figure 2. This is particularly true at high temperatures when the energy transition selection rules are less stringent.

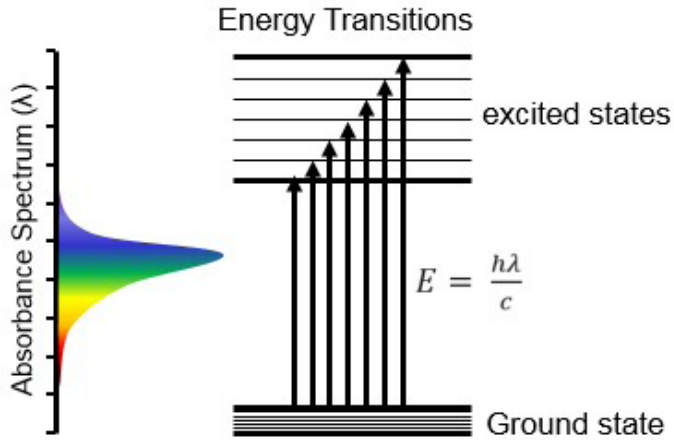

Figure 1: Illustration of energy transitions resulting in absorbance spectrum

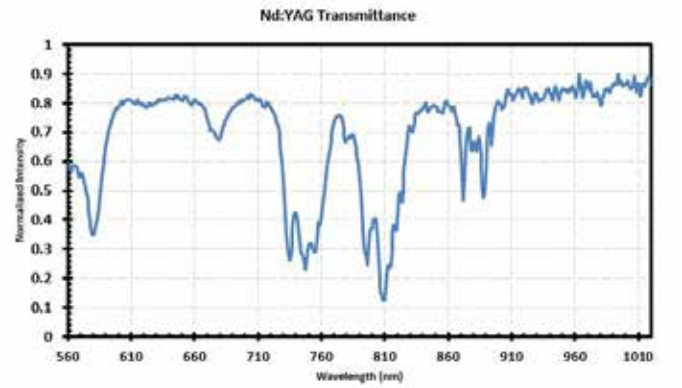

Figure 2: Example transmittance spectrum for Nd:YAG glass

Although the transmittance is usually the measured quantity, the interest is often in understanding the absorbance of the material as that has direct correlations to material properties. This relation to material properties takes different forms, such as the Lambert-Beer's law below in equation 3, that relates absorbance (A) to transmittance (T) and to the concentration (c) of liquids under study.

$$A=-Log\,(T)= \varepsilon l c \qquad (3)$$

Where,
ε and *l* are the material absorptivity and optical path lengths respectively.

$$\eta=n+ik \quad (4) \qquad (4)$$

Where,
n is the real refractive index and k is the imaginary index that describes the absorptive properties of the material. For reflectance, the focus is usually on the real part of the index n although there are advanced techniques that characterize material absorption properties through reflectance measurements.

One of the simpler measurement implementations defines reflectance R as the fractional power reflected from a sample as shown in equation 5.

$$R = \frac{P_r}{P_i} = \frac{I_r - I_{BG}}{I_i - I_{BG}} \qquad (5)$$

Where,
P_r and P_i are the reflected and incident powers on the sample.

Although simple in its definition, the measurement of micro reflectance is often rendered complex in practice due the challenges involved in accurately collecting all the reflected light. This difficulty results from the fact that reflectance actually has two components: Diffuse and Specular reflectance. Diffuse reflectance refers to scattering reflectance from rough surfaces, which tends to be isotropic in the directionality of the scattered light. Specular reflectance refers to the directional reflectance from smooth or shiny surfaces where the angle of incidence is equal to the angle of reflection (Snell's Law). Furthermore, in micro reflectance measurements, the light is incident on, and collected from, the sample through a focusing objective. Since the objective is a focusing optics, it means the incident light has many different angles of incidence and the angles of reflection can be vastly different, especially if it is a scattering sample, as shown in figure 3.

Figure: 3 Illustration of micro reflection for a scattering sample – showing that the ability to collect reflected light can depend on NA of the objective for scattering samples.

Applications

Reflectance spectroscopy is used in many areas of current research interests. Micro reflectance is particularly well suited to thin film characterization, from measuring film thickness to determining optical constants for such films [(1)]. 2D materials are an example of a class of materials where micro reflectance spectroscopy is very popular – this is mainly because the reflectance spectra for a 2D sample changes according to the number of layers of the 2D material [(2)]. Micro absorbance (transmittance) spectroscopy is used in applications such as filter property characterization for imaging and display devices, or concentration determination for liquids and in microfluidic channels. Because absorbance is a function of the energy levels of a material, it is also used in the band structure characterization for micro materials.

References

(1) Y Park et al., "Design, Fabrication, and Micro-Reflectance Measurement of a GaAs/AlAs-Oxide Antireflection Film Journal of the Korean Physical Society, Vol. 40, No. 2, February 2002, pp. 245_249
(2) R. Frisenda et al. "Micro-reflectance and transmittance spectroscopy: a versatile and powerful tool to characterize 2D materials" Journal of Physics D: Applied Physics (2016)

5.3.1 Reflectance & Transmittance

Micro-transmittance Measurement on an SMS System

Introduction

Micro-reflectance (μ-R) is a useful technique for investigating the surfaces and interfaces of micro and nanoscale two-dimensional (2D) materials such as semiconductors, metals, and artificial materials [1, 2]. By this contactless and non-destructive optical method, we can characterize the fine structure and quality of the samples, such as layer thickness, refractive index, etc.

In this work, we provide a method for performing μ-R measurements based on a standard microscope platform. The system described is a comprehensive system and can accommodate the addition of other spectroscopies, such as Raman, photoluminescence (PL), TCSPC spectroscopy, etc.

Method

The reflection spectra were measured using the Standard Microscope Spectroscopy (SMS) system from HORIBA Scientific. The reflectance configuration of the SMS includes a fiber-coupled halogen light source (400 nm - 1100 nm) coupled to the microscope through the universal microscope spectroscopy adapter. The spectroscopy adapter conveys the collimated white light beam to the microscope objective, which focuses the light on to the sample under study. The reflected light from the sample travels backward along the same incident pathway, goes through a beam splitter in the universal microscope adapter, coupled onto the spectrometer (triple grating iHR320 imaging spectrometer). The Synapse CCD on the spectrometer detects the resolved spectrum, and the results are displayed and analyzed in HORIBA LabSpec software.

(a) (b)

Figure 1: Experimental setup for micro-reflectance (μ-R) measurement. (a) Schematic setup. (b) Front view of HORIBA Standard Microscope Spectroscopy (SMS) system, a comprehensive system that accommodates versatile spectroscopies, such as micro-reflectance, Raman, photoluminescence (PL), TCSPC spectroscopy, etc.

Figure 1a illustrates this configuration and figure 1b is a photo of a typical system.

The SMS system can also include an optional motorized XY translation stage, which communicates with the vision camera for sample positioning and scanning. This combination provides reflectance spectral maps, which can be a powerful tool to determine the microstructure of the sample.

Results

Reflectance is defined as the fraction of power in the incident wave that is reflected from the sample. We used an aluminum mirror as the reference sample, providing a measure of the incident light intensity. μ-R is calculated by:

$$R = \frac{P_r}{P_i} = \frac{I_r - I^{BG}}{I_0 - I_0^{BG}}$$

Where P_r and P_i are the powers of reflected and incident light, respectively – corrected by subtracting their corresponding background measurements taken with the incident light off. I and I_0 are the intensities of light reflected by the sample and the reference mirror, respectively. I^{BG} and I_0^{BG} are the intensities when the incident light is off.

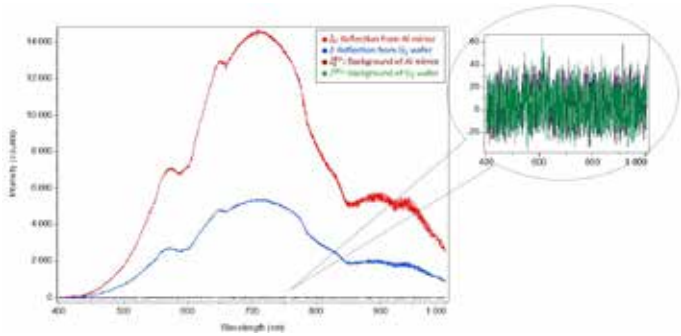

Figure 2: Reflection spectra of Si wafer and Al mirror detected by 60x objective.

Figure 2 shows typical measured spectra from a silicon sample and reference mirror, as well as the background spectra. They were used to calculate µ-R for the sample, shown by the blue curve in figure 3. It is interesting to note the difference in results from this micro measurement and a similar macro measurement made on a silicon solar cell shown by the red curve in figure 3. This difference results from the fact that in the latter case the measurement is done in collimated space and therefore mainly shows the specular reflectance of the sample, while the former measurement shows both specular, as well as the diffuse reflectance components of the sample.

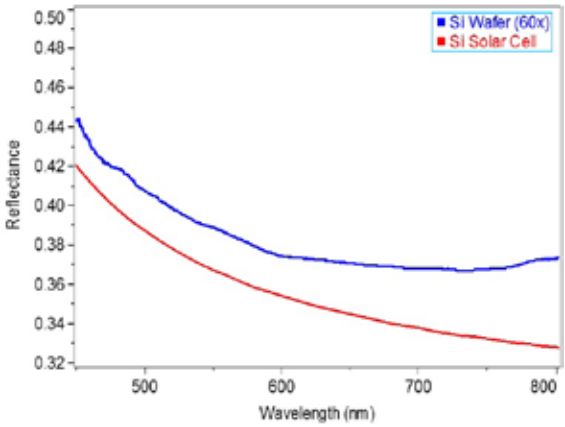

Figure 3: µ-R spectra of Si wafer obtained by 60x objective, compared with macro reflectance measured on Si solar cell (3).

Figure 4 shows the reflectance map of a patterned silicon sample – with HORIBA logo etched in gold lettering on a silicon substrate. Micro reflectance mapping is useful for determination of the sample structure or detection of defects. The spot size of the white light source was 1.3 µm, the spatial resolution of the image is 0.8 µm. The specular surface of the metal area shows much higher reflectance close to µ-R=1, while the silicon substrate surface, as well as areas with surface defects (scattering centers), showed weaker reflectance. It is also important to note how the blemishes on the sample show with higher contrast in the micro reflectance map. This is because these blemishes serve as strong scattering centers for the micro incident beam The silicon substrate has relatively constant reflectance around µ-R=0.4, as expected.

Figure 4: Optical image of the sample (top), and the reflectance mapping of silicon sample with metal plating on surface (bottom), obtained by 60x objective at the wavelength of 550 nm.

Summary

In this work, micro-reflectance spectroscopy as a contactless and non-destructive optical method is shown using a silicon sample with metal plating on the surface. The Standard Microscope Spectroscopy (SMS) system from HORIBA Scientific provides a solution accommodating almost all major spectroscopies, such as micro-reflectance, Raman, photoluminescence (PL), TCSPC spectroscopy, etc. The major components used in this work are listed below.

Part No.	Description
HL-2000-LL	Ocean Optics Long Lifetime Tungsten Halogen light source.
BX-53-MIC	Olympus BX-53 Upright microscope
VIS-CAM	Vision camera for microscope.
XY75x50SWIFT	Motorized XY stage for sample positioning and fast imaging.
IHR320 Core 3	iHR320 f/4.1, imaging spectrometer, including patented kinematic triple grating turret with three specified gratings.
SYNCER-1024x256-OE	Syncerity CCD head thermoelectrically (TE) cooled to -60° C using E2V manufactured, spectroscopy grade 1, 1024 x 256 pixel open electrode CCD chip with 26 µm x 6 µm pixels and overall format of 26.6 mm x 6.6 mm.
LabSpec 6	LabSpec Software for Windows XP and above permitting the control of the spectrometer, data acquisition and a wide range of data treatment and storage options.

References

(1) Y. Park et al., J. Korean Phys. Soc., 40, 245 (2002)
(2) R. Frisenda et al., J. Phys. D: Appl. Phys. 50, 074002 (2017)
(3) M. A. Green, Solar Energy Materials and Solar Cells, 92, 1305 (2008)

5.3.2 Reflectance & Transmittance

Influence of Numerical Aperture (NA) on Micro-reflectance Spectroscopy

Introduction

Micro-reflectance (μ-R) is the measurement of reflectance for microscopic samples. It's a suitable technique for investigating the surfaces and interfaces of micro-scale two-dimensional (2D) materials such as semiconductors, metals, and artificial materials [1, 2]. By this contactless and non-destructive optical method, we can characterize the fine structure and quality of the samples.

In this paper we describe a setup for performing μ-R measurements based on a standard microscope. Specifically, we discuss some challenges presented by the numerical aperture (NA) of the objectives that is peculiar to such microscopic measurements. The system described is a comprehensive system and can accommodate the addition of other spectroscopies, such as Raman, photoluminescence (PL), TCSPC spectroscopy, etc.

Experiment

In macro reflectance measurement on a shiny surface as shown in Figure 1 (a), the signal detected by the detector is mainly from specular reflection. Meanwhile a rough surface presents both specular and diffused (scattering) reflectance as shown in Figure 1 (b). To measure the complete reflectance for such rough samples, it is common to use techniques of variable angle reflectance that has a detector on a goniometer or uses an integrating sphere to capture the scattered reflectance.

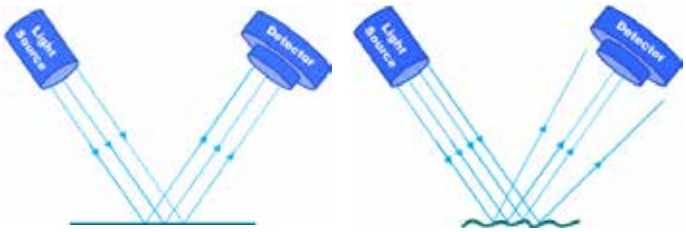

Figure 1: Macro reflection measurement on different sample surfaces. (a) Shiny surface; (b) Rough surface.

In μ-R measurement (Figure 2), both specular and diffused reflectance need to be considered as well. The total reflectance is the sum of specular and diffused reflectance in μ-R measurements:

$$R_{Total} = R_{Specular} + R_{Diffused}$$

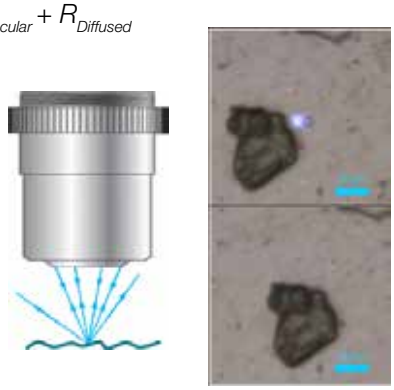

(a) (b)

Figure 2: Micro-reflectance measurement using an objective. (a) Reflection captured by an objective, (b) Images of a white light spot focused by 10x objective, on the specular substrate (top), and on a scattering surface of MoS_2 flake (bottom) – In this case the scattering is strong enough, so one can barely see the incident white light spot.

The ability of an objective to capture reflected light over a range of angles is determined by its numerical aperture (NA). Therefore, it is expected that a larger μ-R can be obtained by using a higher NA objective. This is because a higher NA enables a more accurate determination of R_Diffused. In order to compare the influence of NA on different samples, we tested a silicon wafer sample with a shiny surface and a MoS_2 flake with a scattering surface, using various objectives with different NA. Since reflectance is the fraction of power in the incident wave that is reflected, an aluminum mirror is used to provide the reference signal. It has a high reflection coefficient in the visible spectral range. The setup is illustrated by figure 3.

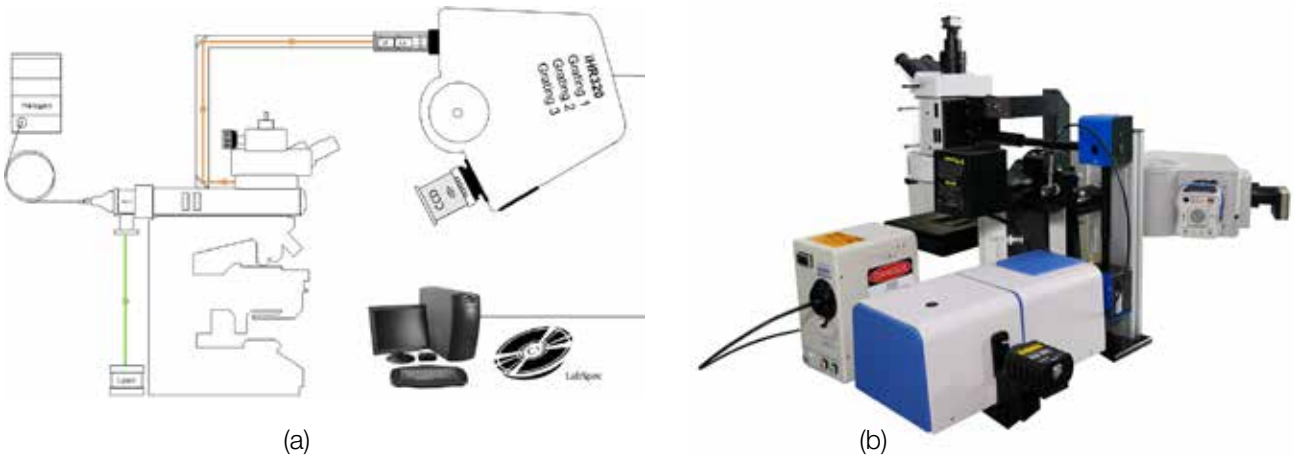

(a) (b)

Figure 3: Experimental setup for micro-reflectance (μ-R) measurement. (a) Schematic setup. (b) Rear view of HORIBA Standard Microscope Spectroscopy (SMS) system, a comprehensive system enabling different spectroscopies, such as Micro-reflectance, Raman, photoluminescence (PL), TCSPC spectroscopy, etc.

A halogen light source with spectral coverage of 400 ~ 1000 nm was coupled into the microscope by a fiber with core size of 10 µm. The objective focused the incident light onto the sample surface. The motorized XY translation stage, a tool to determine the micro-structure of the sample and map the spectra, was used to locate the region of interest at the focal point of incident light. A comparison of spot size achieved by different objectives is shown in figure 4.

Figure 4: White light spot focusing on specular surface by various objectives.

The reflected light was collected by the objective and collimated into the iHR320 imaging spectrometer (600 gr/mm grating, blazed at 750 nm). The resolved spectrum is detected by a Synapse CCD. The results are displayed and analyzed by HORIBA LabSpec software.

Analysis

The µ-R is calculated by:

$$R = \frac{P_r}{P_i} = \frac{I_r - I^{BG}}{I_0 - I_0^{BG}}$$

where P_r and P_i are the powers of reflected and incident light, respectively, corrected by subtracting their corresponding background measurements taken with the incident light off. I and I_0 are the intensities of light reflected by the sample and the reference mirror, respectively. I^{BG} and I_0^{BG} are the intensities when the incident light is off.

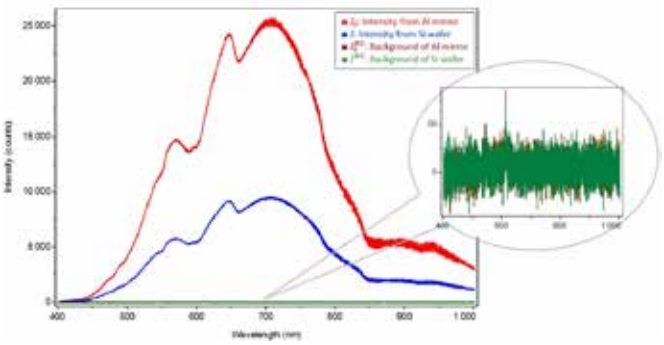

Figure 5: Reflection spectra of Si wafer and Al mirror detected by 10x objective.

Figure 5 shows an example of reflection spectra on the sample and reference mirror, and the background spectra used to calculate the reflectance. µ-R spectra of the two samples are shown in figure 6. The reflectance on the shiny surface of the Si wafer is much larger than that of the rough surface of the MoS_2 flake. On the Si wafer surface, the objectives collect almost all the specular reflection and diffusion; the reflectance value is larger than macro reflectance measured on the solar cell surface. However, µ-R does not follow a clear sequence of objective NA on the specular surface. As expected, for MoS_2, µ-R increases with the increasing of the objective's NA. This is a result of the larger NA objectives having an increased ability to collect diffused reflectance due to their wider collection angle.

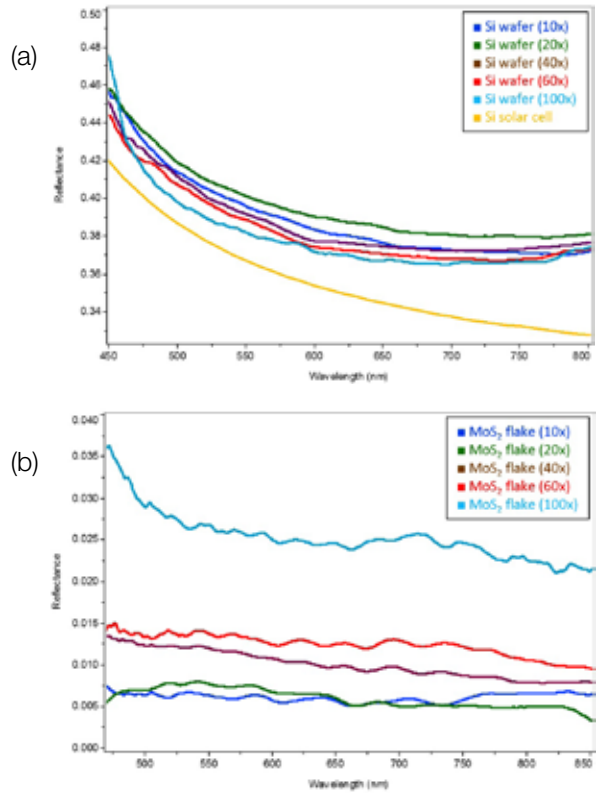

Figure 6: µ-R spectra obtained by 10x (0.3), 20x (0.5), 40x (0.65), 60x (0.9), 100x (0.95) objectives, respectively. (a) Si wafer with highly reflective surface, compared with macro reflectance measured on Si solar cell (3). (b) MoS_2 flake with highly scattering surface.

The normalized reflectance at various wavelengths as a function of the objectives NA is illustrated in Figure 7. The Si wafer presents relative insensitivity to NA, while for the MoS_2 flake, the reflectance increases with NA, as expected.

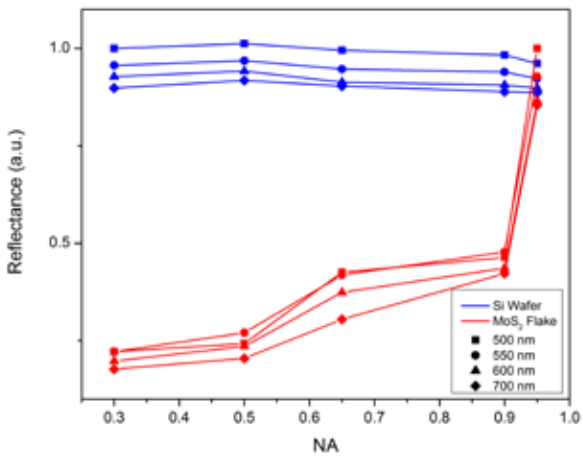

Figure 7: µ-R for each wavelength measured on Si wafer and MoS_2 flake, respectively, as a function of objective's NA.

In order to numerically compare the influence of the objective's NA, we calculated the difference-to-average reflectance ratio at each wavelength, which is determined by:

$$\mu\left(\frac{\Delta R}{R}\right) = \frac{|R_1 - R_2|}{(R_1 + R_2)/2} \times 100\%$$

where R_1 and R_2 are the reflectance measured by two different objectives at each wavelength. We call it Micro-reflectance Difference (μ-RD), the results calculated between largest and smallest μ-R for each sample are listed in the table below. μ-RD for the Si wafer, ideally to be zero, was actually affected by uncertainty of the experimental conditions. For the MoS_2 flake, μ-RD was about 30 times larger in this experiment.

Si Wafer		MoS_2 Flake	
Wavelength	μ-RD (%)	Wavelength	μ-RD (%)
500 nm	3.94	500 nm	127.48
550 nm	4.85	550 nm	122.89
600 nm	4.72	600 nm	125.73
750 nm	3.48	750 nm	122.88

Conclusion

We describe the Standard Microscope Spectroscopy (SMS) platform from HORIBA Scientific. The SMS platform enables the addition of various spectroscopies to most standard microscopes including micro-reflectance. Accurate measurement of micro-reflectance depends on the NA of objective, and in this work, we characterize the influence of the objective's NA on such measurements. On a highly reflective surface such as an Si wafer, μ-R presents insensitivity to objective NA. For a highly scattering surface such as a MoS_2 flake, μ-R measurement has a stronger dependence on the objective NA. For such high scattering samples, measurement accuracy of reflectance increases with NA.

References

(1) Y. Park et al., J. Korean Phys. Soc., 40, 245 (2002)
(2) R. Frisenda et al., J. Phys. D: Appl. Phys. 50, 074002 (2017)
(3) M. A. Green, Solar Energy Materials and Solar Cells, 92, 1305 (2008)

5.3.3 Reflectance & Transmittance

Robust Micro-reflectance Measurement using Wide-field Illumination

Introduction

As mentioned in section 5.3.1, micro-reflectance (μ-R) provides a contactless and non-destructive technique for investigating the surfaces and interfaces of materials, which is useful for obtaining material properties such as layer thickness, refractive index, etc. In this work, we elaborate on another robust method of μ-R measurements using a standard upright microscope. Measuring μ-R by using an illumination beam focused on the sample using an objective, as described in section 5.3.1, can be a delicate technique, requiring a matching of the NA of excitation and collection. In comparison, the method described here places less importance on the properties of incident illumination. Instead, the objective is used to capture and measure reflected light from a defined spot or area of the sample. In this sense, the measurement can be more robust.

We tested the point μ-R measurement on the polished silicon substrate, as well as μ-R mapping on the patterned silicon sample – with the HORIBA logo etched in metal lettering on the same silicon substrate. The results are compared to the other method, by which μ-R is measured based on just using a standard objective for excitation and reflection without any additional beam sampling.

Method

The measurement was done on the HORIBA SMS system that enables the addition of various spectroscopies to most standard microscopes. The configuration is illustrated in figure 1. The illumination is a standard halogen lamp integrated on the microscope covering 500 ~ 1000 nm. The microscope objective collects the reflected light from the wide-field illumination of the sample. At the exit of the microscope trinocular, the reflected light is focused onto a collection fiber through a pinhole. The pinhole serves to block light from all but a small micro spot on the sample, thereby offering spatial resolution. The spatially resolved reflected light travels via the multimode fiber and couples onto the iHR320 spectrometer (a triple grating iHR320 imaging spectrometer). The CCD detects the reflection spectrum resolved by the spectrometer, and the results are displayed and analyzed in HORIBA LabSpec software. The setup is illustrated in figure 1a.

In order to determine the location and size of the spot on the sample from which the reflected light is collected, the spectrometer end of the collection fiber is temporarily connected to a white light source so that an image of the fiber core at the exit of the microscope is projected on the sample, as shown in figure 1b.

An optional motorized XY translation stage could be added to the SMS system, as well. The stage communicates with the vision camera for sample positioning and scanning. This combination provides reflectance spectral maps, which can be a powerful tool to determine the microstructure of the sample.

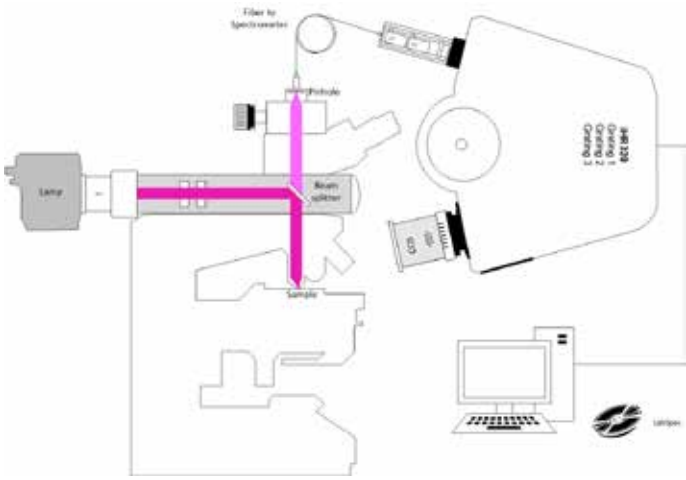

Figure 1a: Schematic setup of robust micro-reflectance (μ-R) measurement using wide-field illumination, based on the HORIBA Standard Microscope Spectroscopy (SMS) system, a comprehensive system that adds various spectroscopies, such as micro-reflectance, micro-transmittance, Raman, photoluminescence (PL), TCSPC spectroscopy, etc. to most standard microscopes.

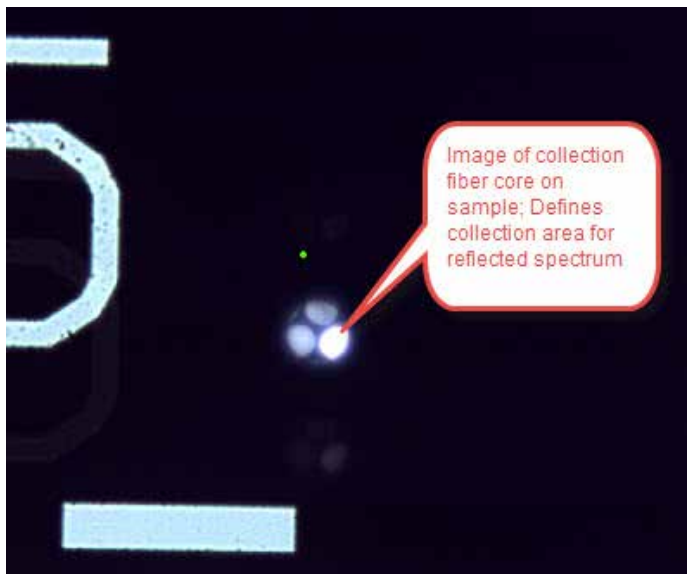

Figure 1b: The location and size of the spot on the sample from which reflected light is collected is determined by imaging the collection fiber core on the sample using white illumination at the spectrometer end of the fiber. This serves to establish a coordinate system for reflectance mapping measurements

Results

Different types of lamps can be used for reflectance

measurements. The important consideration is to ensure that the lamp spectrum has a good intensity in the spectral region of interest. Figure 2 shows the spectral output of two different lamps that we have used for reflectance measurements. In this work, we used the illumination lamp that comes integrated with the microscope. Its spectrum is red shifted relative to another external white light source that was used in another study to provide more intensity in the blue region of the spectrum. In order to compare the methods, we perform a comparison of the reflectance measurement in the region of the spectrum where these two lamps overlap.

Reflectance refers to the ratio of reflected to incident light, calculated by:

$$\mu\text{-}R = \frac{P_r}{P_i} = \frac{I_r - I^{BG}}{I_0 - I_0^{BG}} \qquad (1)$$

Where, P_r and P_i are the powers of reflected and incident light, respectively, corrected by subtracting their corresponding background measurements taken with the incident light off. The reference signal reflected from the aluminum mirror provide a measure of the incident light spectra. I and I_0 are the intensities of light reflected by the sample and the mirror, respectively, while I^{BG} and I_0^{BG} are the background intensities measured when the incident light is off. Figure 3 shows an example of measured spectra (I, I_0, I^{BG} and I_0^{BG}) from the silicon sample and reference mirror, which are used to calculate μ-R by Eq. (1).

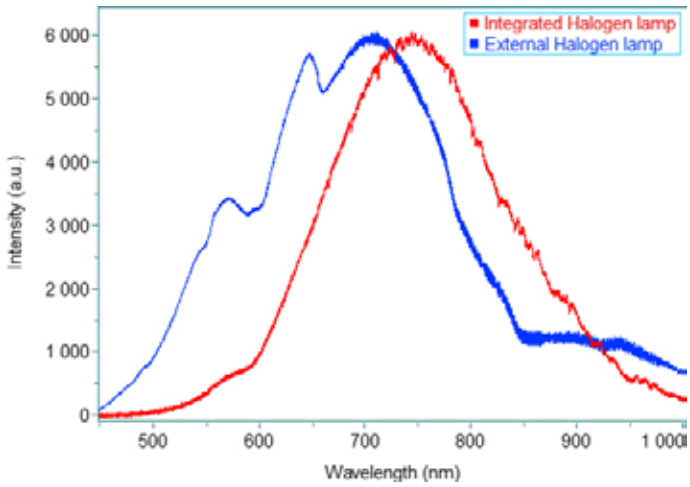

Figure 2: Reference spectrum of an integrated halogen lamp reflected from an aluminum mirror (red), comparing with the normalized spectrum of an external halogen lamp used in the other method (blue), obtained by 10x objective.

The calculated μ-R curve using wide-field illumination is shown in Figure 4. The result using the other method, by which external incident and reflected light are focused and coupled by the objective, is also shown in Figure 4 for comparison. The fluctuation of the difference between the two methods is within the uncertainty of experimental conditions. Both methods provide accurate μ-R measurements.

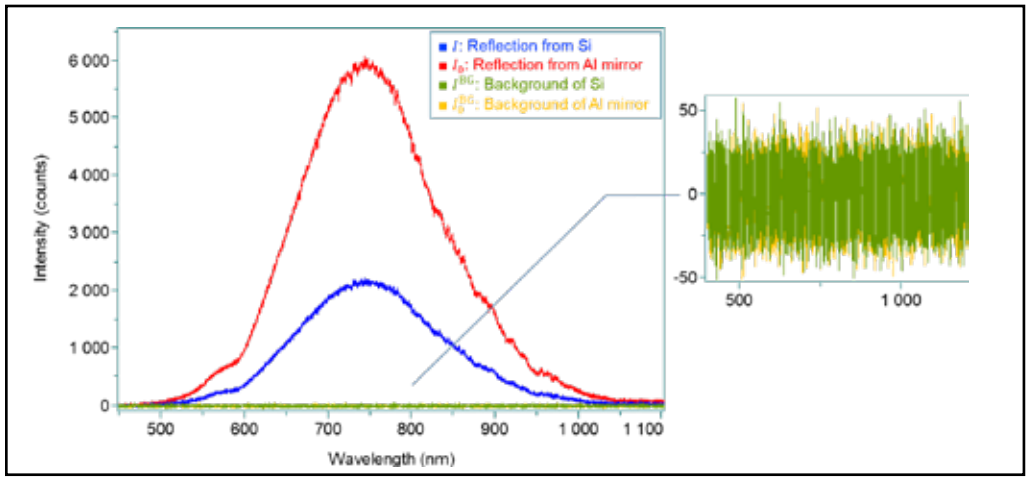

Figure 3: Reflection spectra of asilicon substrate and aluminum mirror detected by a 10x objective.

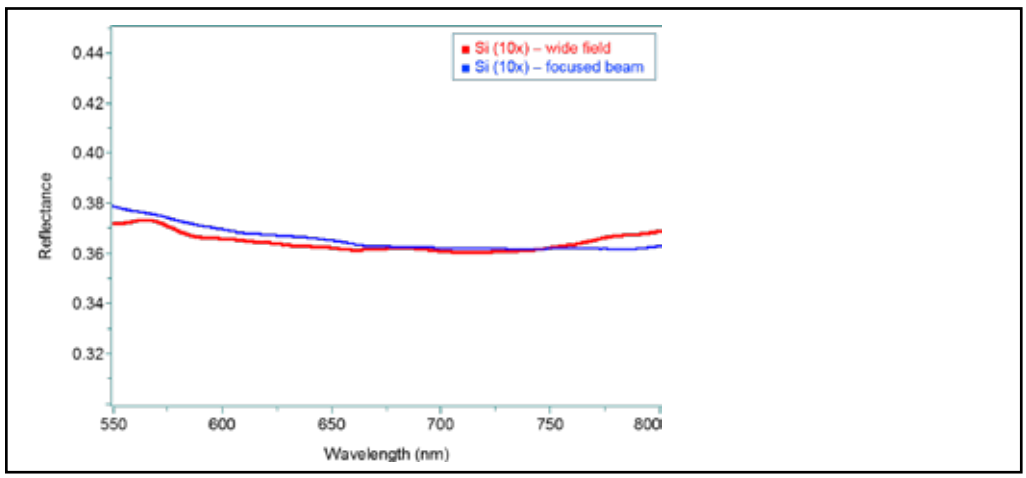

Figure 4: μ-R spectrum of a silicon sample using wide-field illumination obtained by a 10x objective (red), comparing with μ-R spectrum based on just using a 10x objective for excitation and reflection without any additional beam sampling (blue).

In order to assess the system's capability, the μ-R mapping was performed on the surface of the patterned silicon sample – with the HORIBA logo etched in metal lettering on a silicon substrate, as shown in Figure 5. The spatial resolution of this method is determined by the pinhole size, which could achieve less than 1 μm. For the other method using a focused beam, the spot size could be limited by the diffraction limit, especially when using a high NA objective. Same as the other method, the specular surface of the metal area shows much higher reflectance close to μ-R=1, while the silicon substrate surface presents relatively constant reflectance, around μ-R=0.4, and the blemish areas with a high scattering feature show the weakest reflectance.

Figure 5: The μ-R mapping of a silicon sample with metal plating on surface, obtained by a 50x objective at the wavelength of 600 nm, pixel size = 1 μm.

Summary

In this work, the robust method for μ-R measurement using wide-field illumination is introduced. Although comparable in accuracy to other methods, the wide-field illumination method described here is a more robust implementation. The μ-R mapping provides a powerful technique to investigate the sample surface, and quickly determine the structure and quality. The Standard Microscope Spectroscopy (SMS) system from HORIBA Scientific provides a solution that adds various spectroscopies, such as micro-reflectance, Raman, photoluminescence (PL), TCSPC spectroscopy, etc. to most standard microscopes. The major components used in this work are listed to the right.

Part No.	Description
BX-53-MIC	Olympus BX-53 Upright microscope
VIS-CAM	Vision camera for microscope.
XY75x50SWIFT	Motorized XY stage for sample positioning and Fast imaging.
IHR320 Core 3	iHR320 f/4.1, imaging spectrometer, including patented kinematic triple grating turret with three specified gratings
SYNCER-1024x256-OE	Syncerity CCD head thermoelectrically (TE) cooled to -60° C using E2V manufactured, spectroscopy grade 1, 1024 x 256 pixel open electrode CCD chip with 26 μm x 6 μm pixels and overall format of 26.6 mm x 6.6 mm.
LabSpec 6	LabSpec Software for Windows XP and above permitting the control of the spectrometer, data acquisition and a wide range of data treatment and storage options.

5.3.4 Reflectance & Transmittance

Combined Micro-reflectance and Raman or PL Spectroscopy on an SMS System

Introduction

Micro-reflectance (μ-R) is a useful technique for investigating the micro surface characteristics, such as fine structure and quality of the sample. Different from micro Raman and micro photoluminescence (PL) spectroscopy, which are also popular contactless and non-destructive optical methods, μ-R usually uses a broadband light source and can provide complementary insights into a sample that are not readily provided by Raman or PL. One of the main advantages of a modular spectroscopy system is the ability to provide multiple spectroscopies on the same platform. Beyond the cost advantages of doing so are such benefits as co-location, which is the ability to perform different measurements at the same location on a sample. In this work, we add the function of micro-reflectance spectroscopy to our modular turnkey system that equips a standard microscope with components for micro Raman or PL spectroscopy measurements. In order to assess the system's capabilities, we tested a silicon sample with micro scale gold etchings for μ-R measurements. A carbon nanotube sample was tested for micro Raman measurement, and a convallaria specimen, for micro PL, all on the same system.

Method

Figure 1 illustrates the configuration and a picture of the Standard Microscope Spectroscopy (SMS) system for micro-reflectance and micro Raman / PL spectroscopy. A single wavelength laser was used as the excitation light source of micro Raman / PL spectroscopy and a halogen lamp for micro reflectance. Both sources could be coupled by either free-space or fiber-coupled into the microscope through the universal microspectroscopy adapter from HORIBA. The SMS system included a vision camera and illumination to visualize the sample under test. The objective focuses either the laser or white light beam onto a micro spot on the sample surface, and collects the emission or reflected light from the sample. The emission is collimated and focused into the iHR320 spectrometer. The Syncerity CCD, working together with the motorized stage, detects the spectra at selected points or mapping grid on the sample.

(a) (b)

Figure 1: Experimental setup for micro-reflectance and micro Raman / PL spectroscopy on a standard microscope. (a) Schematic setup. (b) Front view of HORIBA Standard Microscope Spectroscopy (SMS) system.

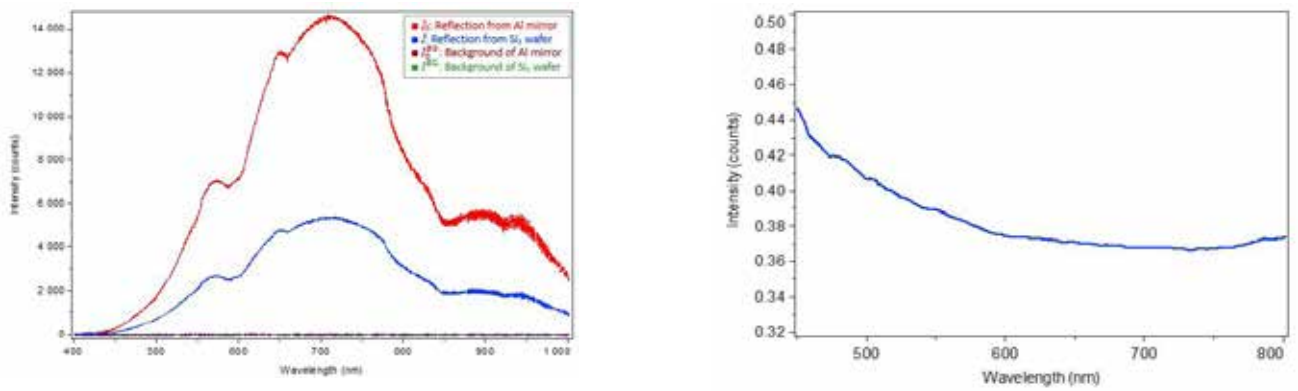

(a) (b)

Figure 2: (a) Reflection spectra of Si and Al mirror detected by a 60x objective. (b) μ-R spectra of Si obtained by a 60x objective, compared with macro reflectance measured on a Si solar cell (1).

Results

1. Micro reflectance (μ-R)

An aluminum mirror is used as the reference signal for its high reflection efficiency at visible spectral range. The spectra from the Si and Al mirror are shown in Figure 2(a) - corrected by subtracting their background signal taken with the incident light off. The μ-R spectrum is shown in figure 2(b) for a bare silicon sample and a Si-based solar cell.

The μ-R mapping is illustrated in figure 3. The 10 μm core size fiber and 60x objective focus the spot size of the white light source to 1.3 μm, the spatial resolution of the mapping is 0.8 μm. With an integration time as 0.05s per point, the total 311 × 92 map grid takes approximately 50 minutes to complete the mapping process.

Figure 3: Optical image of the sample (top), and the reflectance mapping of silicon sample with metal plating on surface (bottom), obtained by 60x objective at the wavelength of 550 nm.

2. Micro Raman

The micro Raman spectroscopy measurement was performed by the same system using a 532 nm cw laser and corresponding Raman filter and dichroic. The Raman spectrum of a carbon nanotube sample and the spatial distribution of Raman spectral intensity around 1600 cm^{-1} are shown in Figure 4.

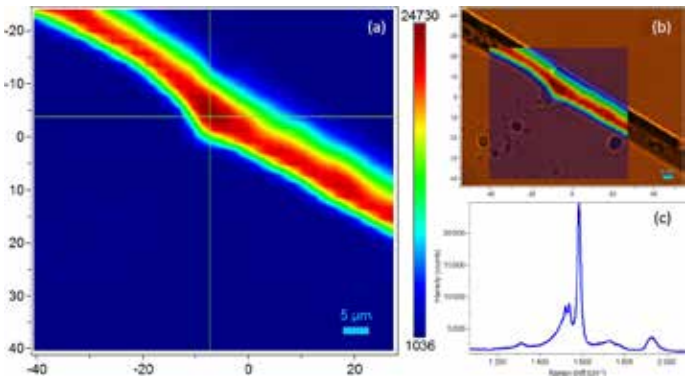

Figure 4: (a) Micro Raman mapping of carbon nanotube sample around 1600cm^{-1}, observed by 60x objective, excitation wavelength = 532 nm, integration time = 0.1s. (b) Optical image of carbon nanotube sample with Raman mapping overlaid. (c) Raman spectrum at the cursor.

3. Micro photoluminescence (PL)

Without modifying the system, the PL spectroscopy measurement was performed simply by switching to PL filters on the universal microspectroscopy adapter. Figure 5 illustrates the PL spectrum of the convallaria specimen stained by acridine orange [2], as well as the spatial distribution of PL intensity around 566 nm, with the area of 258 × 275 pixels and the resolution of 1 μm.

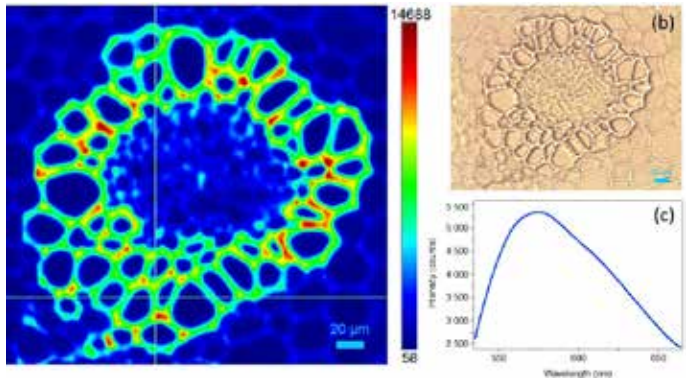

Figure 5: (a) PL mapping of the convallaria sample observed by 20x objective (excitation wavelength = 532 nm, emission wavelength ~ 566 nm, integration time = 0.01s). (b) Optical image of convallaria sample observed by 20x objective. (c) PL spectrum at the cursor.

Summary

In this work, we demonstrate the combination of μ-R and Raman / PL spectroscopy on the same platform of a standard microscope. This microscope equipped with an iHR320 and CCD provides key benefits for multimodal spectroscopic solutions, such as high efficiencies, cost effectiveness, sample co-location, etc. The SMS system from HORIBA Scientific provides a solution accommodating many popular spectroscopies, such as micro-reflectance, Raman, photoluminescence (PL), TCSPC spectroscopy, etc. on one platform. The major components used in this work are listed below.

Part No.	Description
LCX-532S-500-CSB-PPA	Laser - 532 nm, 500 mW, SLM DPSS.
DH-2000	Halogen white light source, 215-2500 nm
BX-53-MIC	Olympus BX-53 Upright microscope.
VIS-CAM	Vision camera for microscope.
IHR320 Core 3	iHR320 f/4.1, imaging spectrometer, including patented kinematic triple grating turret with three specified gratings.
SYNCER-1024x256-OE	Syncerity CCD head thermoelectrically (TE) cooled to -60° C using E2V manufactured, spectroscopy grade 1, 1024 x 256 pixel open electrode CCD chip with 26 μm x 26 μm pixels and overall format of 26.6 mm x 6.6 mm.
LabSpec6	LabSpec Software for Windows XP and above permitting the control of the spectrometer, data acquisition and a wide range of data treatment and storage options.

References

(1) M. A. Green, Solar Energy Materials and Solar Cells, 92, 1305 (2008)
(2) www.thermofisher.com/order/catalog/product/A1301

5.3.5 Reflectance & Transmittance

Robust Micro-reflectance Measurement using Wide-field Illumination

Introduction

Micro-transmittance (μ-T) is a powerful technique for investigating both bulk and interfaces features of micro and nanoscale two-dimensional (2D) materials. By this contactless and non-destructive optical method, we can characterize the fine structure and quality of the samples, such as layer thickness, refractive index, etc.

In this work, we discuss a robust method for performing μ-T measurements based on a standard microscope platform. μ-T is usually done with a focused beam [1], which is a delicate technique requiring a matching of the NA of excitation and collection. The method described here uses only one objective on the collection side while using wide-field illumination on the input side to the sample. This method enhances the robustness of this implementation since it does not depend on the delicate matching of the NA and spot location of the other method that uses a focusing objective on the input and collections sides of the sample. We tested two types of samples here. One type is the optical filter, whose transmittance over wavelength is one of the most important specifications. The other sample is a mica flake that has been used in various applications, from electronic and electrical industries due to its unique physical properties, such as dielectric, insulating, refractivity, etc. Especially, the range in opacity from transparent to opaque makes mica a critical heat insulating material in aeronautics and astronautics.

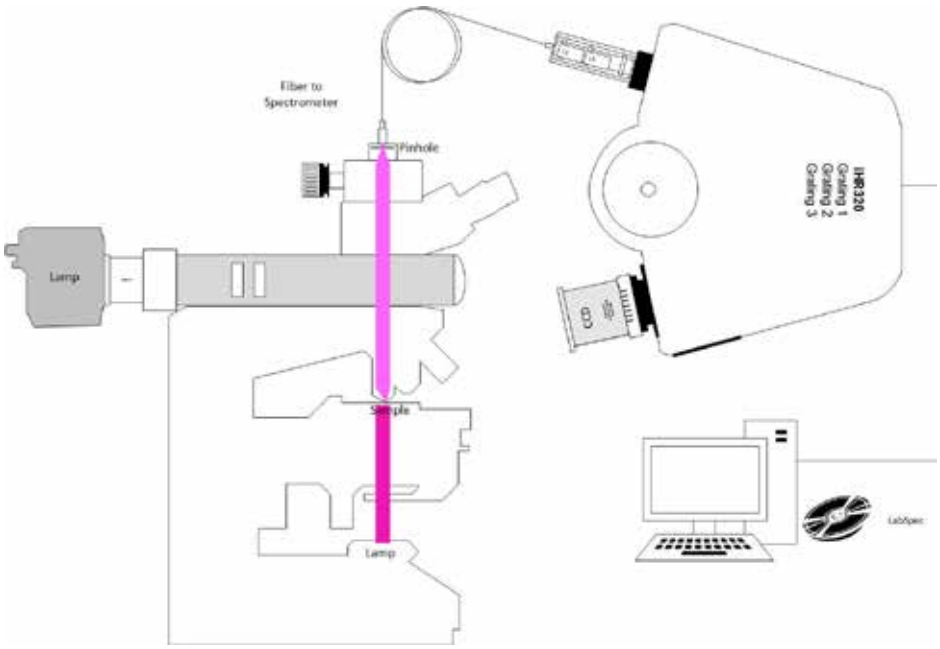

Figure 1: Schematic setup for micro-reflectance (μ-T) measurement using HORIBA Standard Microscope Spectroscopy (SMS) system, a comprehensive system accommodate versatile spectroscopies, such as micro-reflectance, micro-transmittance, Raman, photoluminescence (PL), TCSPC spectroscopy, etc.

Method

The transmission spectra were measured using the Standard Microscope Spectroscopy System (SMS) from HORIBA Scientific, as shown in figure 1.

We used the bottom halogen lamp integrated in the microscope as a light source for transmission illumination. The spectral range covers 500 ~ 1000 nm. The transmitted light from the sample is collected by the microscope objective. At the exit of the microscope, the transmitted light is focused onto a collection fiber through a changeable pinhole. The pinhole serves to block all but light from a small micro location on the sample thereby offering spatial resolution. The transmitted light travels via the multimode fiber and couples onto the iHR320 spectrometer (triple grating iHR320 imaging spectrometer). The resolved transmission spectrum is detected by the CCD on the spectrometer, and the results are displayed and analyzed in HORIBA LabSpec software. An optional motorized XY translation stage could be added to upgrade the SMS system for a transmittance spectral map, which provides a more powerful tool to determine the microstructure of the sample.

Results

Transmittance indirectly characterizes light loss due to phenomena such as absorption, scattering and reflection. It is defined as the ratio of transmitted to incident light. The calculation of μ-T is expressed by:

$$\mu\text{-}t = \frac{P_t}{P_i} = \frac{I_r - I^{BG}}{I_0 - I_0^{BG}} \qquad (1)$$

Where P_t and P_i are the measured powers of transmitted and incident light respectively – corrected by subtracting their corresponding background measurements taken with the incident light off. I and I_0 are the intensities of light transmitted from the sample and the transparent slide, respectively. I^{BG} and I_0^{BG} are the intensities when the incident light is off.

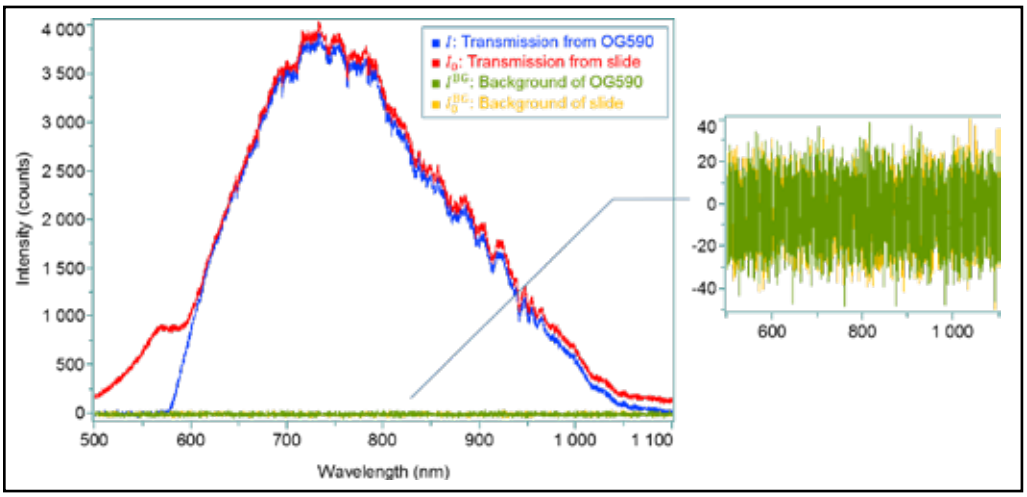

Figure 2: Transmission spectra of 590 nm long pass filter and transparent slide detected by 10x objective.

Two long pass filters were used as samples for transmittance measurement. The intent was to obtain the transmission spectra of these filters. The transmitted spectra of the 590 nm long pass filter and the slide that holds the filter, as well as the background spectra, are shown in Figure 2, which were used to calculate μ-T according to eq.1. Figure 3 shows the μ-T spectra of 590 nm and 610 nm long pass filters, which agree with the reference curves from the provider [2, 3].

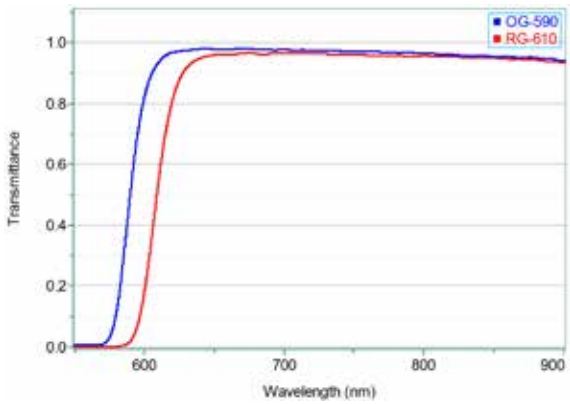

Figure 3: μ-T spectra of 590 nm and 610 nm long pass filters, obtained by a 10x objective.

Another sample tested was a mica flake. The thickness of mica can be determined by measuring the transmittance at certain wavelengths [4]. Here we measured the spatial distribution of μ-T using the software-controlled XY stage. Figure 4 illustrates the μ-T map at 695 nm, as well as the optical image of the mapping area. The μ-T map could identify the sample structure or impurity straightforwardly when compared to the corresponding optical image.

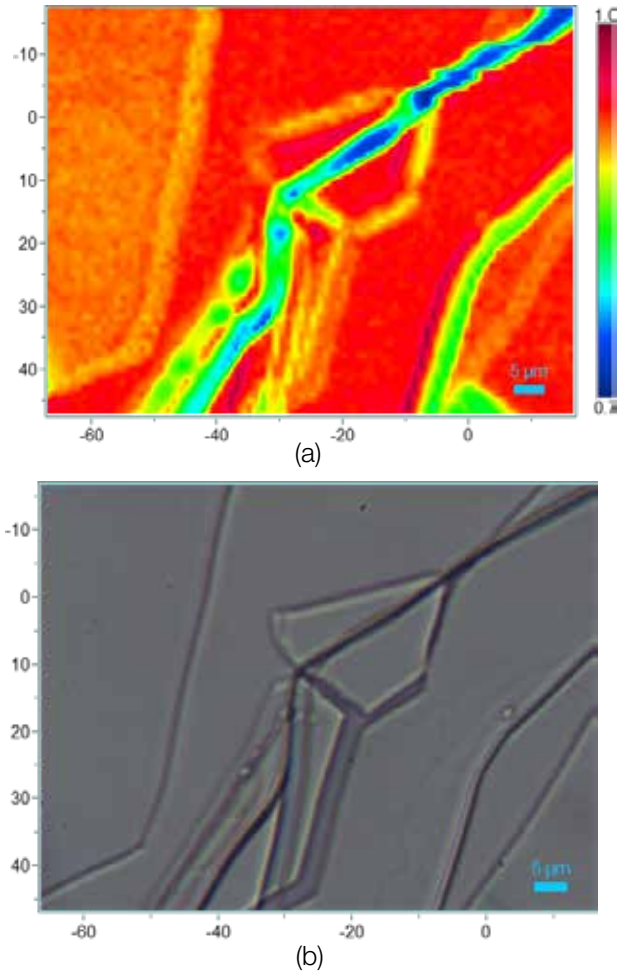

Figure 4: (a) μ-T map of a mica sample, obtained by 50x objective around the wavelength of 695 nm. (b) Optical image of the mapping area of the mica sample.

Summary

In this work, micro-transmittance spectroscopy measurement is illustrated by measuring two commonly used long pass filters and a mica flake. The wide-field illumination micro transmission method described here provides a robust method to determine sample structure and quality. This setup was implemented on the Standard Microscope Spectroscopy (SMS) system from HORIBA Scientific. The SMS provides a comprehensive platform for adding various spectroscopies, such as micro-reflectance, Raman, photoluminescence (PL), TCSPC spectroscopy, etc. to any standard microscope. The major components used in this work are listed below.

Part No.	Description
BX-53-MIC	Olympus BX-53 Upright microscope.
VIS-CAM	Vision camera for microscope.
XY75x50SWIFT	Motorized XY stage for sample positioning and Fast imaging.
IHR320 Core 3	iHR320 f/4.1, imaging spectrometer, including patented kinematic triple grating turret with three specified gratings.
SYNCER-1024x256-OE	Syncerity CCD head thermoelectrically (TE) cooled to -60° C using E2V manufactured, spectroscopy grade 1, 1024 x 256 pixel open electrode CCD chip with 26 µm x 26 µm pixels and overall format of 26.6 mm x 6.6 mm.
LabSpec 6	LabSpec Software for Windows XP and above permitting the control of the spectrometer, data acquisition and a wide range of data treatment and storage options.

References

(1) R. Frisenda et al., J. Phys. D: Appl. Phys. 50, 074002 (2017)
(2) https://www.edmundoptics.com/p/og-590-254mm-dia-longpass-filter/6550/
(3) https://www.edmundoptics.com/p/rg-610-254mm-dia-longpass-filter/6860/
(4) A. P. Bradford, G. Hass and J. B. Heaney, Reflectance, transmittance, and thermal emittance of mica as a function of thickness, Thermophysics of Spacecraft and Planetary Bodies: Radiation Properties of Solids and the Electromagnetic Radiation Environment in Space, (Academic Press, New York, 1967)

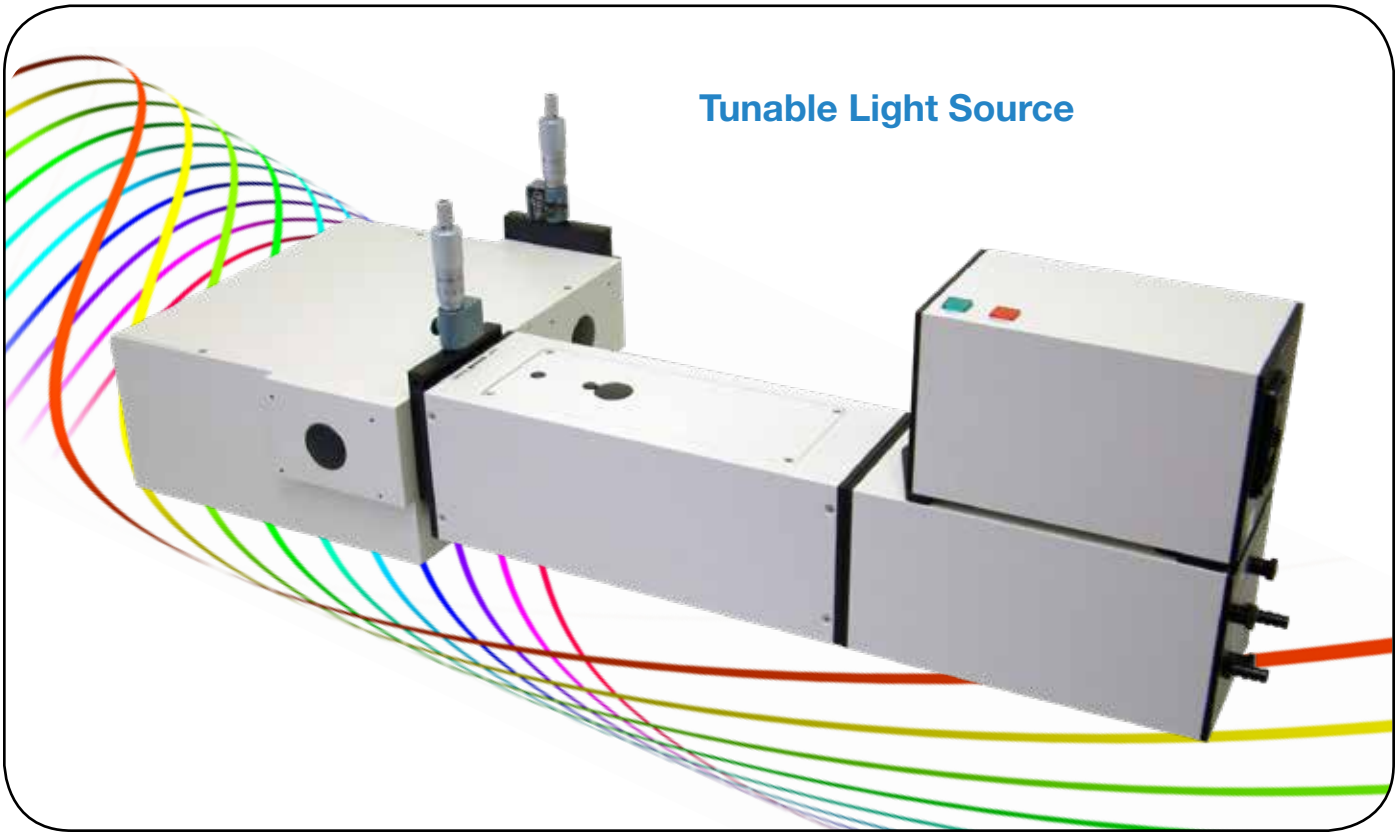

Introduction to Dark Field Scattering

Dark field microscopy was developed primarily as a contrast enhancement technique in microscopy. Its usefulness comes from the fact that image formation comes only from light scattered by the target(s) of interest on the sample. Therefore, the target(s) of interest on the sample show up on the image as bright areas – from the scattered light, against an otherwise dark background, as shown in figure 1 below.

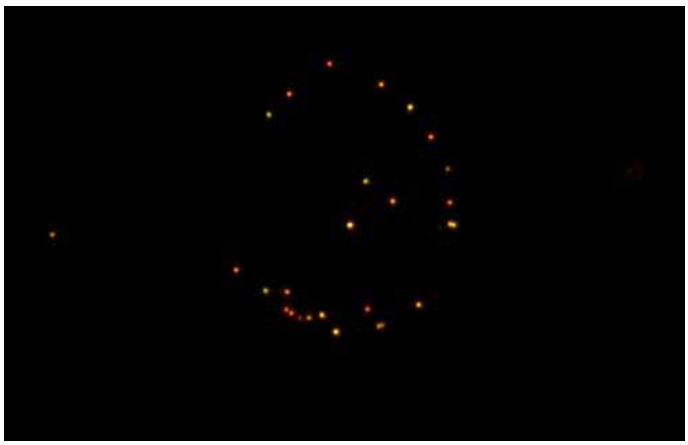

Figure 1: Example of a dark field microscope image of gold nanoparticles

By forming an image using only light that has scattered or interacted with the target in some fashion, dark field imaging succeeds in picking faint objects in a field of view that would otherwise be overwhelmed by the ambient light, as is the case in bright field microscopy.

In this context, the physical phenomena resulting in light scattering by tiny objects in the field of view derives mainly from two effects. For non-conducting particles, scattering is often a result of diffraction through apertures within, or edges around, the particle of interest. It helps that such particles of interest often have sizes that are of the same order of magnitude as the wavelength of light, and the scattering angle $\propto$ is inversely proportional to the size (d) or aperture of the scatter, as approximated in equation 1 below [1].

$$\propto \approx \frac{1.22\lambda}{d} \qquad (1)$$

Where λ is the wavelength of the illumination light.
For conducting particles in the field of view, such as the gold nanoparticles shown in figure 1, the light scattering phenomenon is often from surface plasmon resonances [2]. In an oversimplified sense, the incident light can be thought of as a propagating electric field. Its interaction with the conducting particle causes a polarization of the free electrons in the particle creating electronic dipoles within the particles. These dipoles, in turn, scatter the incident light in different directions, as illustrated in figure 2 above.

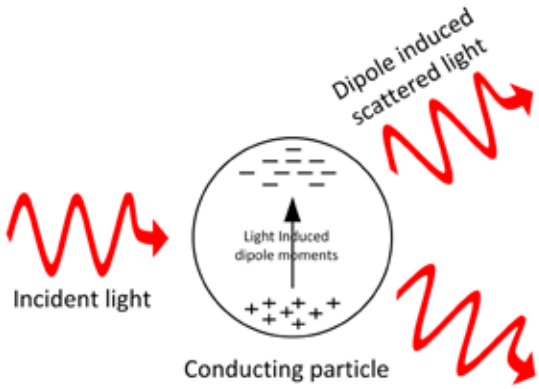

Figure 2: Illustration of light scattering by conducting particle

Applications of dark field scattering spectroscopy

Although developed as a contrast enhancement modality for microscope imaging, dark field has proven to be quite useful as an analytical spectroscopic technique – especially for new developments in micro-and nano-engineered materials. This is because the optical scattering properties of any particle is directly related to the material properties of that particle. Moreover, since the dark field technique only looks at scattered light, spectroscopic analysis of the scattered light can provide a wealth of information about the scattering target - from its size and shape to its composition [3]. Because plasmonic resonances of nanoparticles are sensitive to the ambient environment, they have found much use as nanosensors. This is especially true for label-free biological applications, [4] and their investigation often uses dark field scattering spectroscopy. Finally, metal nanoparticles often produce local field enhancement effects, thereby enhancing response of field intensity dependent effects. This phenomenon has found use in such applications as single molecule fluorescence and Raman applications where functionalized surfaces of nanoparticles serve as hosts for molecular beacons, and the enhanced fluorescence or Raman signal from such single molecule beacons serve to understand various dynamics and location studies in such fields as protein analysis [5].

Implementation of dark field scattering spectroscopy

Dark field imaging and spectroscopy can be implemented on most microscopes using the correct accessories provided by the microscope vendor or third party suppliers. There are also third party home-built systems, but in this context, our interest is mainly in implementations that use a standard microscope from the major microscope vendors. A user needs to first determine whether they want to perform dark field in reflection (or epi) mode or in transmission mode, as this determines largely the illumination and collection accessories required.

Regardless of the specific measurement configuration, the implementation of dark field scattering imaging or spectroscopy relies on ensuring a mismatch between the incidence and collection angles of light going to and coming from the sample. The numerical aperture (NA) of the incidence and collection optics (frequency condenser and objective) succinctly describes this parameter. A mismatch in the NA of the incidence and collection optics ensures that on the collection side of the sample, the unperturbed transmitted incident light and the (usually much weaker) scattered light from the sample are traveling in different directions. This directional separation presents an opportunity to physically block the transmitted unperturbed light from reaching the camera or spectrometer and overwhelm the signal from the scattered light. In the first configuration, the incident light optics has a higher NA compared to the collection optics. Furthermore, the incidence optics uses annular illumination, which blocks incoming light from the central part of the beam so that only high angle illumination rays reach the sample, as shown in figure 3a.

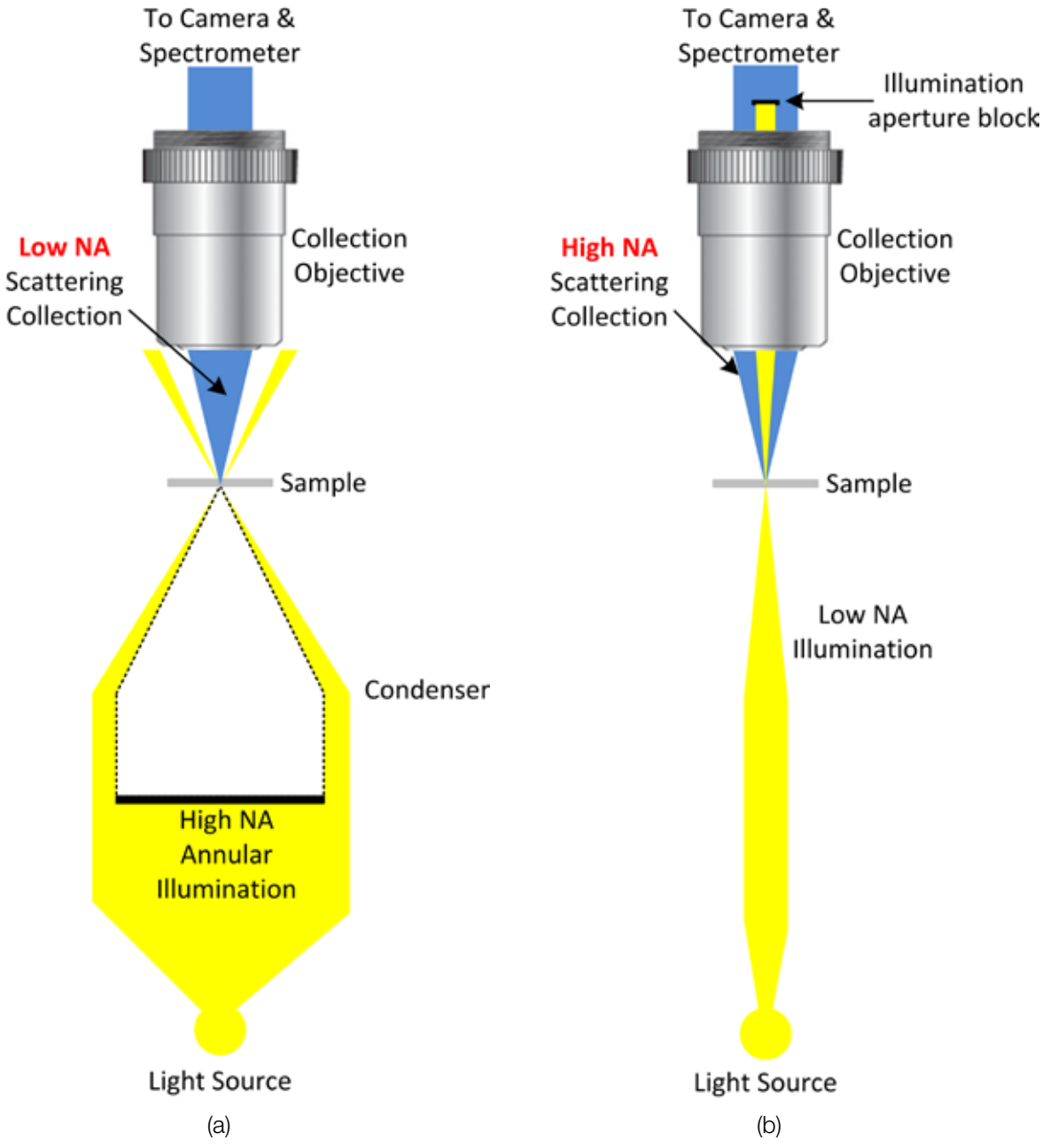

Figure 3: Two implementations of dark field scattering imaging and spectroscopy. Configuration (a) uses a high numerical aperture (NA) annular illumination so that only high angle illumination rays get to the sample. The collection objective has a lower NA, so that only low angle scattered light rays are collected and sent to the camera and spectrometer. Configuration (b) uses a low NA illumination. The collection objective is a high NA objective, collecting both scattered and unperturbed transmitted illumination light. On the back aperture of the collection objective, a narrow blocking aperture is implemented to block the unperturbed transmitted illumination light from reaching the camera or spectrometer.

Of the two configurations shown in figure 3, configuration 3a can be implemented in both transmission and reflection (epi) modes using standard accessories from most microscope manufacturers. Configuration 3b is often implemented in transmission mode as shown, but this design is not common amongst microscope manufacturers.

The Standard Microscope Spectroscopy (SMS) platform from HORIBA is a comprehensive micro spectroscopy system that adds various spectroscopies (including dark field scattering spectroscopy) to most standard microscopes from the major microscope manufacturers. It does so without compromising the other functionalities of the microscope.

Key considerations for a successful implementation of dark field scattering spectroscopy

Perhaps the most important consideration when implementing a dark field imaging or scattering spectroscopy system is the realization that dark field scattering is a relatively weak phenomenon. In fact, the scattering cross section is inversely proportional to the sixth power of the diameter of the scattering particle [5]. This places a lower limit on the size of particles that can be analyzed using this technique. The weakness of the intensity of the observed phenomenon can be compensated by optimizing the optical throughput of the optical collection system and using a highly sensitive detection system. On the collection side, it is helpful to use direct optical coupling to the spectrometer and detection system to avoid coupling and transmission losses that result from fibers and fiber interfaces. It also helps to use a low noise and high quantum efficiency detector to enable high signal-to-noise ratio measurements.

References

(1) https://en.wikipedia.org/wiki/Fraunhofer_diffraction
(2) E S Babich et al. “Dark-field spectroscopy of plasmon resonance in metal nanoislands: effect of shape and light polarization” 2016 J. Phys.: Conf. Ser. 769 012040
(3) Karsten Rebner et al., “Dark-field scattering microscopy for spectral characterization of polystyrene aggregates”, 1 February 2010 / Vol. 18, No. 3 / OPTICS EXPRESS 3116
(4) Vladimir V.Apyari et al., “Label-free gold nanoparticle-based sensing of cysteine: New peculiarities and prospects”, Sensors and Actuators B: Chemical, Volume 260, 1 May 2018, Pages 953-961
(5) Alexander Weigel et al., “ Dark Field Microspectroscopy with Single Molecule Fluorescence Sensitivity”, ACS Photonics 2014, 1, 848–856

6.3.1 Dark field Scattering

Dark field Scattering Spectroscopy and Imaging of Different-sized Gold Nanoparticles by an SMS System

Introduction

Dark field microscopy is primarily a contrast enhancement imaging technique on microscopes. Its contrast enhancement benefit derives from the design of the collection optics of the microscope to only collect scattered light from the target of interest, as shown in figure 1. This design automatically removes the ambient background light that would otherwise overwhelm the image and reduce the image contrast, as in bright field microscopy.

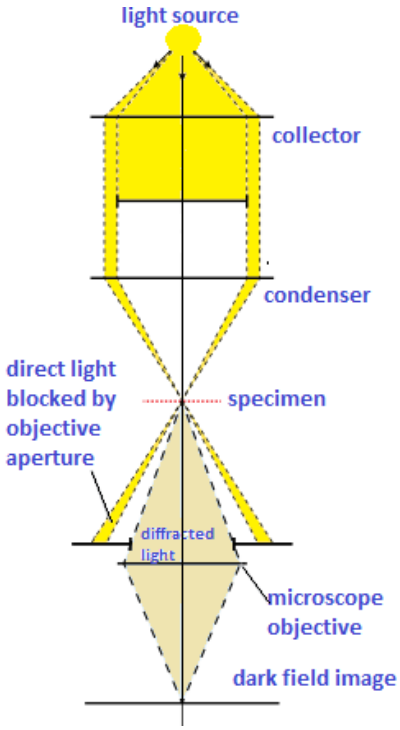

Figure 1: Image showing illumination method in dark field microscopy [1]

Although developed as a contrast enhancement modality for microscope imaging, dark field has proven to be quite useful as an analytical spectroscopic technique - especially for new developments in micro and nano-engineered materials. This is because the optical scattering properties of any particle is directly related to the material properties of that particle. Moreover, since the dark field technique only looks at scattered light, spectroscopic analysis of the scattered light can provide a wealth of information about the scattering target - from its size to its composition [2-4].

Setup

Implementing a dark field scattering spectroscopy system (DFSS) requires connecting a spectrometer to a dark field microscope as well as implementing a method of isolating specific regions of interest in a darkfield image for spectral analysis. The Standard Microscope Spectroscopy (SMS) system from HORIBA offers such capability. The SMS is a modular microspectroscopy solution capable of adding various spectroscopies to most standard microscopes including dark field scattering spectroscopy. Furthermore, the SMS spectroscopy modules add to a microscope in a manner that does not compromise the native functions of the microscope.

The SMS system consisted of a BX53 Olympus microscope equipped with a transmission dark field illuminator and 60x oil immersion objective. The output from the microscope coupled directly to an iHR320 spectrometer and Synapse open electrode detector. The direct coupling of the microscope output to the spectrometer is vital to retain the imaging capability and enable selection of regions of interest (ROI) from the dark field image for spectral analysis using the camera on the spectrometer. If the spectrometer were fiber-coupled, this would simply not be possible – unless the ROI selection happened on the microscope.

Measurements and results

Metal nanoparticles of different morphology have received considerable attention in recent years due to their unique chemical and physical properties. They have found uses from photovoltaics [7] to label-free biological markers [8]. Their appeal derives from the fact that many of these metal nanoparticles display plasmonic resonances [5] that can be tailored to very specific needs by controlling the size and morphology of the nanoparticles [3-6]. Therefore, analysis and control of metal nanoparticle size is of vital interest to practitioners in these various applications, and dark field scattering spectroscopy is a key technique for such analysis. DFSS not only offers the contrast enhancements necessary to see such particles on an optical microscope, but the scattering spectroscopy offers key insights into the particle size and morphology.

The samples studied in this work were gold nanoparticles. Figure 2 shows the gold nanoparticles' darkfield image taken with microscope camera.

Figure 2: Image of gold nanoparticles on the dark field microscope vision camera.

This image shows three particles (labeled boxes in figure 2) marked for scattering spectra characterization. The camera on the spectrometer and horizontal and vertical slit settings at the entrance to the spectrometer are used to define ROIs around each of these particles so that the measured spectrum is only from scattered light coming from each of the particles separately. This is only possible because the microscope is directly (not fiber) coupled to the spectrometer. Figure 3 shows the scattering spectrum for these three particles. As expected, the larger nanoparticles resulted in a red shift of scattering spectrum. By establishing a size calibration using a complementary technique such as AFM, one could use DFSS as a quick and easy non-contact metal nanoparticle size monitoring technique [9]

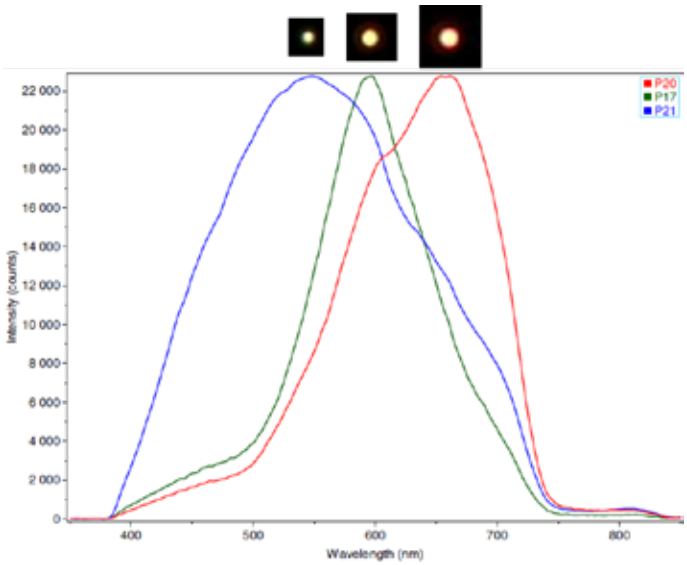

Figure 3: Spectra of individual gold nanoparticles. As the particle size increases, the spectrum shifts to the longer wavelengths.

Conclusion

In this paper, we applied dark field scattering spectroscopy (DFSS) using an SMS platform to study the effect of different gold nanoparticle's sizes on Surface Plasmon Resonance (SPR) scattering spectra. We observed that as the size of nanoparticles increased, the SPR peaks shift to the longer wavelengths. This information combined with AFM and SEM data provides valuable information regarding the morphology evolution and optical properties of nanoparticles for various applications.

References:

(1) https://en.wikipedia.org/wiki/Dark-field_microscopy
(2) Tsutsui Y, Hayakawa T, Kawamura G, Nogami M 2011 Nanotechnology 22 (27), 275203
(3) Aroca R and Martin F 1985 J. Raman. Spectrosc. 16, 156
(4) Klimov V V 2014 Nanoplasmonics (Pan Stanford)
(5) Mie G 1908 Ann. Phys. 25, 377
(6) Nanoscale, 2015, 7, 15209
(7) Atwater H A and Polman A 2010 Nat. Mater. 9, 205
(8) Dieringer J A, McFarland A D, Shah N C, Stuart D A, Whitney A V, Yonzon C R, Young M A, Zhang X and Van Duyne R P 2006 Faraday Discuss. 132, 9
(9) E S Babich, et al., Journal of Physics: Conference Series 769 (2016) 012040

Introduction to Electroluminescence

Electroluminescence (EL) spectroscopy is similar to photoluminescence spectroscopy (PL) in that both measure light emission from matter following excitation to higher energy states. However, unlike PL where excitation is caused by the absorption of light, EL relies on the application of a voltage or electric current across the sample to excite carriers to higher energy states. These carriers then relax to their ground states by the emission of light. Figure 1 illustrates the different excitation processes involved in both PL and EL.

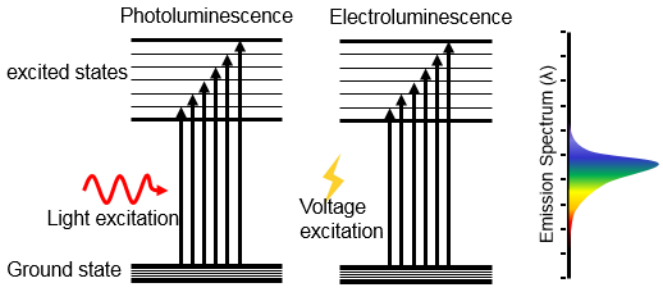

Figure 1: Illustration for photo-excitation for photoluminescence process (left) and voltage or current injection excitation for electroluminescence process. Both phenomena result if light emission during the relaxation process follows excitation.

EL provides complementary information that may not be readily obtained from PL. One reason for this complementarity is that PL is a local phenomenon occurring only where photo-excitation took place. Meanwhile, EL, which is caused by voltage or current flows, can be affected by carrier dynamics further removed from where the luminescence is measured.

Application of electroluminescence spectroscopy

Unlike many of the optical techniques presented here, including PL that are used for material analysis, EL has intrinsic value beyond material analysis in that large industries such as LED lighting are based entirely on the EL phenomena. Because of this intrinsic merit, there is a lot of work in material engineering that targets EL emission of optimal intensity and spectral composition as a desired outcome for lighting and display applications.[1]

As an analytical technique, EL is used heavily in the optoelectronics industry and research to understand and engineer devices that rely on carrier dynamics. In photovoltaics (PV) for example, device performance relies largely on photo-generated carriers traveling from generation site to a battery without recombination. In a laboratory environment, EL can provide a quick and efficient probe of such carrier dynamics in a PV sample (without the need for solar excitation).

Time resolved electroluminescence

Much like PL, EL can also be performed in a time-resolved fashion. Analysis of time-resolved EL measurements (TREL) can indicate fluctuations in the material structure. EL can therefore help in understanding defects or irregularities in the material that may not be evident just from TRPL measurements, and thereby better predict the efficiency of the LED or PV device.[2] Based on the results of TRPL and TREL, improvements can be made to the manufacturing process of LEDs and PVs to make them more robust and efficient. Long-lived (microsecond to seconds) TREL can be measured with fast single channel detectors such as PMTs or even fast CCD array detectors (milliseconds). For short-lived EL phenomena, specialized time resolved techniques such as time correlated single photon counting (TCSPC) are used to resolve the measurement in time [3]. Figure 2 below shows examples of both steady state and time-resolved EL data.

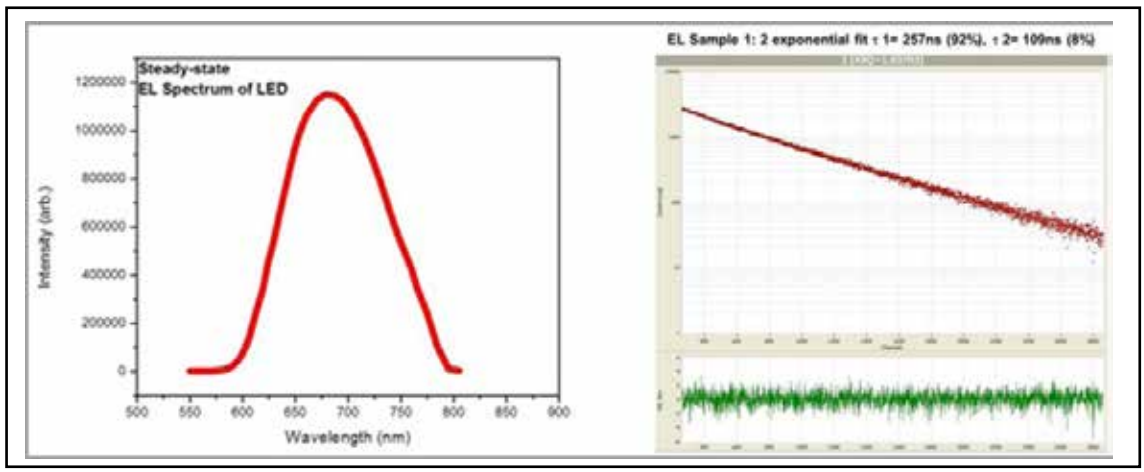

Figure 2: Example of steady state and time-resolved Electroluminescence data. The time-resolved measurement was performed using time correlated single photon counting (TCSPC)

Micro electroluminescence setup

The measurement setup for micro EL (µ-EL) is very similar to that of micro PL except that instead of using a light source for excitation, a source meter is used to inject a voltage (current) into the sample as shown in figure 3.

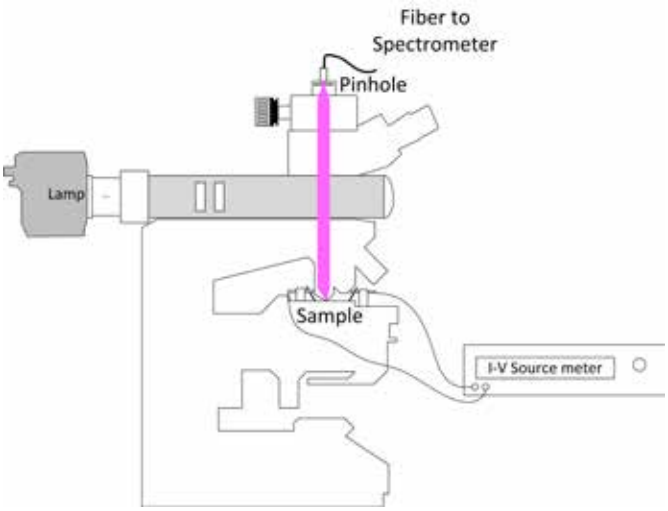

Figure 3: Illustration of micro EL setup on a standard upright microscope.

In figure 3, a current voltage source meter provides the current / voltage excitation to the micro sample via soldered leads or probe pins. The emitted EL light is collected by the microscope objective and reimaged on a pinhole at the exit of the microscope. The pinhole serves to provide spatial resolution as only light from a small micro area on the sample maps onto the pinhole aperture. By raster scanning the sample relative to the pinhole using a motorized stage, an EL map of the sample is generated. The EL light passing through the pinhole at the exit of the microscope is collected by fiber (or free-space coupled) into a spectrometer for analysis.

It is also possible to perform wide-field EL on a microscope as shown in figure 3. In such instances the pinhole assembly is removed so that the wide-field image of the sample can be directed to a camera or spectrometer.

References

(1) D. Han et al., “Enhanced light extraction efficiency of a InGaN/GaN micro-square array light-emitting diode chip”, Vol. 7, No. 9 | 1 Sept 2017 | OPTICAL MATERIALS EXPRESS 3261
(2) T. Kuroda, N. Horio, K. Taniguchi, H. Sato, C. Funaoka, and A. Tackeuchi, Phys. Stat. Sol., 0(1), 25-28, 2002.
(3) Yun-Min Cheng et al., Role of the Charge Generation Layer in Tandem Organic Light-Emitting Diodes Investigated by Time-Resolved Electroluminescence Spectroscopy, J. Phys. Chem. C 2011, 115, 2, 582-588

7.3.1 Electroluminescence

Micro Electroluminescence Characterization of Commercial LEDs on an SMS System

Typical commercial LEDs available in the market are Aluminum Indium Gallium Phosphide (AlInGaP) III-V-compound semiconductors for yellow, orange and red LEDs; and Indium Gallium Nitride (InGaN) alloys for blue, green and white LEDs [1-2]. Making high quality homogeneous ternary and quaternary of semiconductor devices is challenging due to forming local indium or aluminum clusters due to phase segregation [3]. The varying concentrations result in spectral change and broadening of the bandgap altering the local emission spectrum of the diode [4] . All these different challenges during the growth and fabrication of LEDs make it important to monitor and characterize the materials at the various stages in the development and fabrication of a device from growing a wafer, depositing different epilayers and fabricating different device architectures. Electroluminescence (EL) measurement is a popular characterization technique that is performed by current or voltage injection excitation of semiconductor devices. EL data provides useful information regarding the overall device architecture, including the physical structures of the active layers, the electrical properties of the cathode and anode contacts, and the properties of the probes through which the electrical current is injected. Therefore, this technique is capable of determining the injection efficiency of excess carriers through the electrical contacts [5]. In this paper, LEDs of different colors were studied with an SMS setup for device degradation by varying different electrical conditions.

Results

Measurements were made on commercial-grade LEDs of different colors. LEDS operating at longer wavelengths like amber (590 nm) and up, are based on AlInGaP epitaxy devices. Blue and green LEDs are typically made of InGaN-based compound semiconductors. By changing the amount of indium and aluminum, the bandgap of these devices can be altered from 3.49 eV to 0.65 eV covering near infrared to UV spectra. Typically, these LEDs consist of Multi-Quantum Well structures (MQW), that is, thin layers of alternating high and low indium content to trap electrons and holes in a 2-D electron gas to increase the carrier lifetime. Fabrication of a homogeneous epitaxy for high quality LEDs is very challenging due to the phase segregation and clustering of indium for InGaN or aluminum, in the case of AlInGaP. This may result in non-uniform bandgap and spatial inhomogeneity through the LED and change of the local emission of the device.

Figure 1 shows EL spectra for different colors of LEDs, this information later can be used to calculate overall device bandgap.

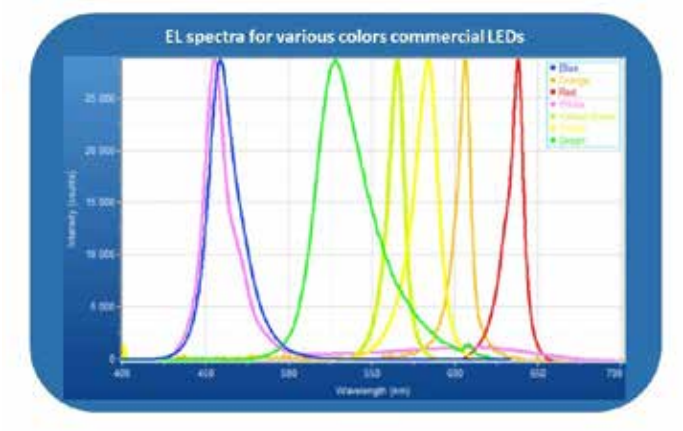

Figure 1: Electroluminescence spectra for different colors of LEDs measured by an SMS system.

The next sample under study was an InGaN LED with royal blue color with a PL peak at 452 nm. GaN LEDs are typically grown by metal-organic chemical vapor deposition (MOCVD) of GaN on sapphire substrates, and the epitaxial structure consists of InGaN/GaN multi-quantum Well (MQW) layers. The processing of these devices conventionally involves (i) patterning the pixels by etching the GaN+MQW stack using a plasma process, (ii) depositing and patterning the P-contact metal pads on the pixels and (iii) depositing and patterning the N-type contact next to the pixel. In some new technologies P and N contacts are positioned in the same side of the device to avoid shadowing caused by wire bonding. Figure 2 shows the electroluminescence image taken with the uEye vision camera on the microscope and a 10x objective. The rough structure of the surface can be due to the removal of the sapphire layer, and the dotted structure with an anode and cathode on the same side is visible. This device is bonded to a package using gold interconnects with no wire going on the top surface of the design for the highest efficiency.

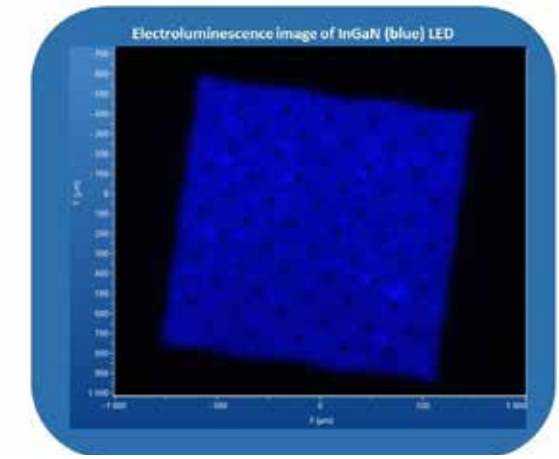

Figure 2: Electroluminescence image of InGaN LED (blue).

Figure 3 shows the EL spectra of the blue LED plotted for different forward injection currents. The EL spectra show a peak centered at 465 nm at 2 µA injection current. However, it slightly shifts to blue with increasing the injection current. The EL peak is centered at 459 nm at 2 mA current. This blue shift may be caused by the super lattice effect, that improves the crystal quality by inducing less strain and piezoelectric field in the LED lattice [2].

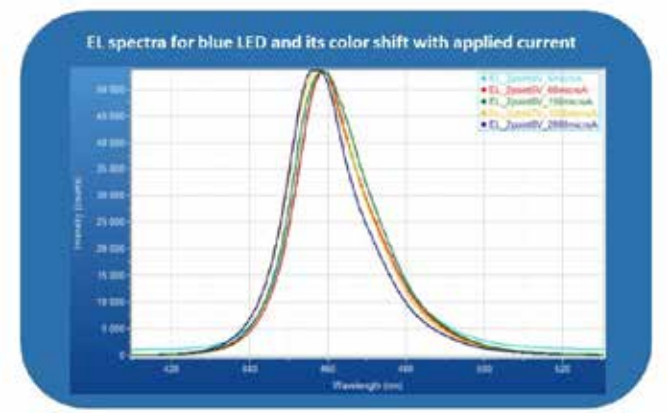

Figure 3: Electroluminescence spectra for the blue LED for different forward injection currents. As the injection current increases the EL peak shifts to the shorter wavelengths from 459 nm to 465 nm.

Figure 4 displays the EL image for a red LED. The shadowing caused by the front contact and wire bonding is obvious in the image.

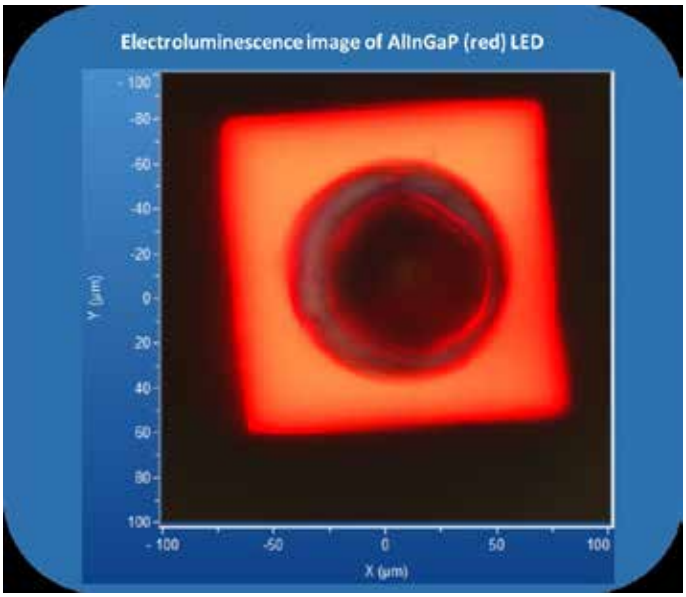

Figure 4: Electroluminescence image of AlInGaP LED (red).

Figure 5 demonstrates different EL spectra for a commercial green LED for different injected currents. It was observed that as the injected current increases, the EL peak shifts to longer wavelengths, therefore its color changes to yellow and orange.

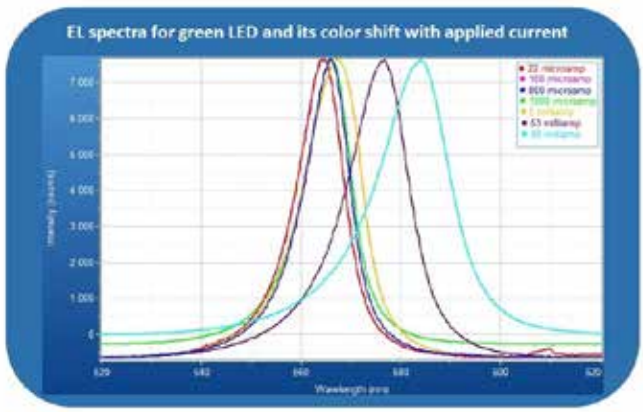

Figure 5: EL spectra for a green LED showing the shift in color from green to yellow and orange by changing the injected current.

Conclusion

In this article, commercial LEDs of different colors were characterized using an SMS setup by varying different electrical conditions. EL images and spectra were obtained for all the samples under different electrical condition. It was observed that the EL spectra shifted slightly to lower wavelengths (blue shift) with an increase in the applied injection current for the blue LED, however this pattern was reversed for the green LED, and a considerable red shift was recorded.

References

(1) Krames M.R. Light-Emitting Diodes: Fundamentals In: Chen J., Cranton W., Fihn M. (eds) [Handbook of Visual Display Technology], Springer, 1719-1734 (2016).
(2) Bourim, E. M., & Han, J. I., "Electrical characterization and thermal admittance spectroscopy analysis of InGaN/GaN MQW blue LED structure, " Electronic Materials Letters, 11(6), 982-992 (2015).
(3) Collazo R. and Dietz N., "The Group III-Nitride Material Class: from Preparation to Perspectives in Photoelectrocatalysis" Preprint of book chapter 8 of "Photoelectrochemical Water Splitting: Issues and Perspectives," ed. H-J. Lewerenz and L.M. Peter, RSC Publishing, pp. 193-222 (2013).
(4) Morkoç H., [Handbook of nitride semiconductors and devices, Materials Properties, Physics and Growth], John Wiley & Sons, 670-750 (2009).

7.3.2 Electroluminescence

Semiconductor Bandgap Determination using Micro Electroluminescence

In Electroluminescence (EL) measurements on semiconductors, a current or voltage is fed into the sample under study and the radiative band-to-band recombination of carriers causes light emission. The emitted EL light carries a wealth of information on the material. For example, the peak wavelength of the EL emission is indicative of the material bandgap for a semiconductor sample. The bandgap information can in turn be used to determine the material composition in the case of semiconductor alloys that are commonly used in LEDs [1] – an important quality control step in the design and fabrication of such devices.

One of the advantages of EL over other techniques such as photoluminescence (PL), is that it is relatively non-local. That is, while an EL measurement could be made at a particular point on a sample, its manifestation depends on carrier dynamics that extend beyond the point of measurement and therefore show more representation of "real life" conditions of device behavior compared to PL. Fortunately, both techniques can readily be implemented on the Standard Microscope Spectroscopy (SMS) system from HORIBA.

Experimental setup

Implementation of EL on the SMS system relies on the use of micro probes either on or around the sample stage to apply a direct current to the sample under study, as shown in figure 1. Of course, this requires the sample to have proper metallization contacts to form a complete current circuit. The EL emission is collected by an objective and channeled through the microscope into a spectrometer for detection and analysis.

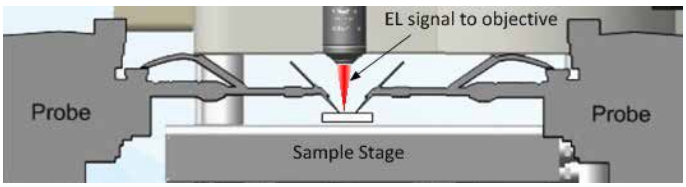

Figure 1: Illustration of EL excitation and collection on an SMS setup

Results

Measurements were made on commercial-grade LEDs of different colors. Figure 2 shows EL spectra for different colors of LEDs as a function of energy (ev). These peaks were fitted using the Gaussian Lorentzian peak fitting model in LabSpec software and the peak position and peak FWHM was calculated for each device and is shown in Table 1. These values identify the energy of the bandgap for each device.

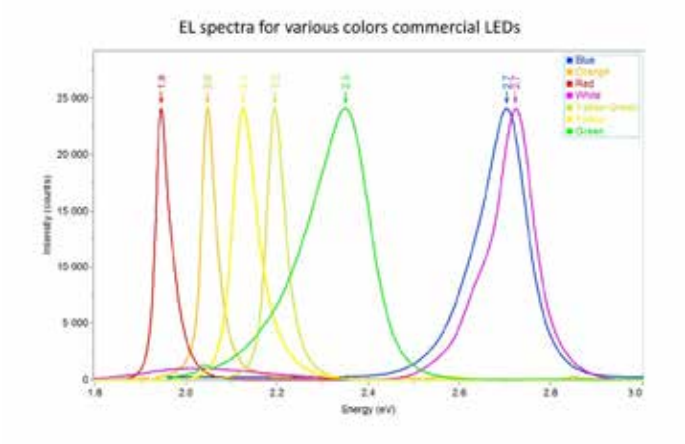

Figure 2: Electroluminescence spectra for different colors of LEDs measured by an SMS system, plotted based on energy.

LED Label	Peak FWHM (ev)	PL Peak Energy = SC bandgap (ev)
White	0.10 & 0.24	2.72 & 2.02
Blue	0.11	2.70
Green	0.13	2.35
Yellow-Green	0.05	2.19
Yellow	0.06	2.13
Orange	0.04	2.05
Red	0.03	1.95

Table 1: EL signal peak position and peak FWHM values extracted from LabSpec peak fitting model. The peak energies are directly related to SC device material bandgaps.

Conclusion

In this article, the Standard Microscope Spectroscopy (SMS) system from HORIBA was used to characterize the EL spectral signatures from a set of commercial LEDs of different colors. The peak position of the measured spectra was used to deduce the material bandgaps of the samples involved. Bandgap determination of this type is important in the device engineering and fabrication process.

References

(1) E. F. Schubert, Light-Emitting Diodes, 2nd ed., Cambridge University Press, Cambridge, NY, (2006)

7.3.3 Electroluminescence

Combined Micro Photoluminescence and Electroluminescence Characterization on an SMS System

Among the different characterization techniques for semiconductors, spatial photoluminescence and electroluminescence measurements are two key techniques for optoelectronic device characterization and failure analysis, providing essential information on critical device factors such as epitaxial layer composition, bandgap and minority carrier lifetime [1-6]. These characterization techniques help to reduce semiconductor devices production cost and performance variance, and allow improved understanding of their physical properties. In addition, these techniques are advantageous since they are non-destructive, and provide rapid, spatially-resolved evaluation of defects and device degradation either at room, or low temperature conditions.

Photoluminescence (PL) is performed by laser excitation and the resultant luminescence emitted from the radiative recombination of photo-generated electrons and holes is detected using multi or single channel detectors. In this method, luminescence peak intensity, width and wavelength location are very good indicators of the grown epitaxial layer quality (defect density, doping levels, etc.) and composition, making this technique an excellent quality control measure for in-line and offline monitoring of semiconductor devices.

Electroluminescence (EL) measurements are performed by current or voltage injection excitation of semiconductor devices. EL data is complementary to PL data, providing useful information regarding the overall device architecture, including the physical structures of the active layers, the electrical properties of the cathode and anode contacts, and the properties of the probes through which the electrical current is injected. Therefore, this technique is capable of determining the injection efficiency of excess carriers through the electrical contacts [7].

A device with high PL efficiency does not necessarily lead to a bright LED with high EL efficiency. Also in some cases, the different emission mechanisms between PL and EL could result in emission wavelength and intensity change between the two datasets. Therefore, fabricated devices could behave very differently from observations using PL during the wafer growth stage. Hence, the necessity to study and characterize samples using both techniques. In this study, we describe an experimental setup to perform both micro PL and EL techniques at the same point on a sample with high spectral and spatial resolution, speed and accuracy. Commercial LEDs of different colors was studied with this setup for device degradation by varying different electrical conditions and PL mapping.

Experimental setup

The SMS setup is described in detail in previous articles. A 375 nm DeltaDiode laser is used as an excitation source for PL, and a voltage source is used for EL excitation.

Results

Measurements were made on commercial-grade red, blue and white LEDs. Figure 1 shows various PL parameters for a commercial red LED (AlInGaP). These parameters include peak intensity, wavelength position, and FWHM of the PL emission that can be correlated to the compositional properties of the wafer. PL peak position change may be attributed to variation of the device active layer thickness, the composition alloys in ternary and quaternary epitaxial layers or changing quantum well widths. PL peak intensity contains information on the purity and quality, i.e. the presence of competing radiative and/or non-radiative recombination centers of semiconductor materials.

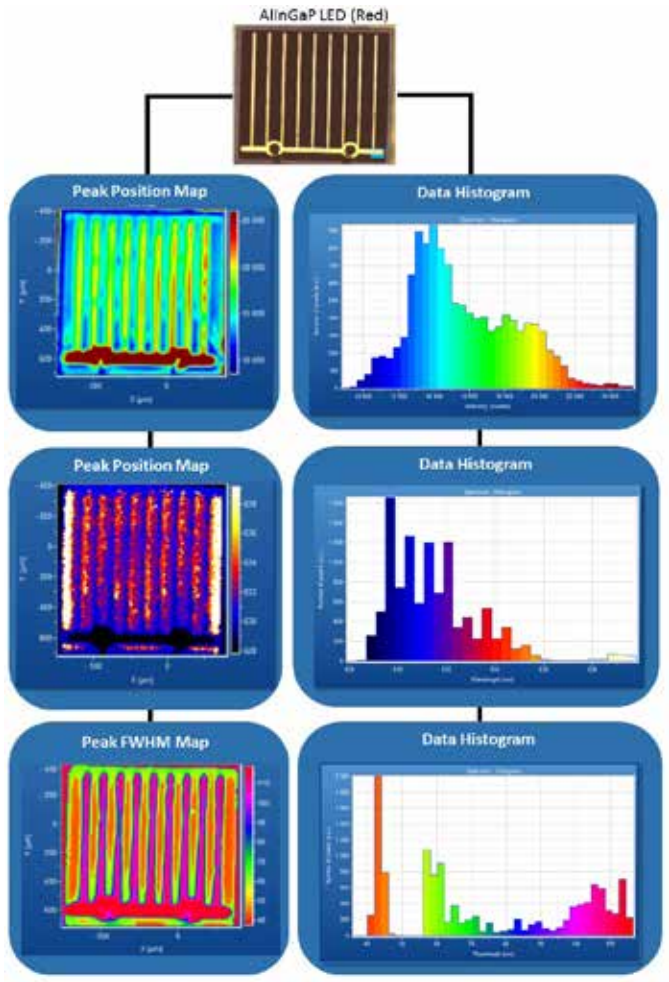

Figure 1: Various PL maps (peak intensity, peak wavelength position, and peak FWHM of the emission) with the associated data histograms for AlInGaP LED (red).

PL peak FWHM is an indicator of a number of factors including doping, layer disorder and layer grading effects [8], and also yields information about changes in the alloy composition of ternary and quaternary materials. It is in many cases a better indicator, at room temperature, than the peak wavelength. The reason for this is that the FWHM is not sensitive to excitation power density, unlike the peak wavelength [9]. The plots on the right hand side of figure 2 show the histogram of the distribution for the mapped data providing very useful statistical information about how non-uniformities affect the device under test. A PL intensity map for this device shows a drop of the peak intensity at the edge of the device, which can be attributed to higher defect density and possible device degradation.

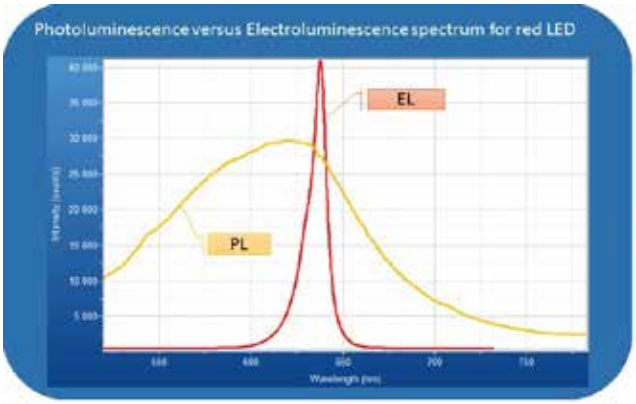

Figure 2: Photoluminescence versus electroluminescence spectrum for AlInGaP (red) LED. These 2 spectra appeared significantly different.

Figure 2 shows Photoluminescence versus electroluminescence spectra for AlInGaP (red) LED. The difference in the two spectra shows the complementarity of PL and EL. The discrepancy between the EL and the PL peak positions may be the result of different radiative transitions [8] . PL reveals the dynamics of excess carrier relaxation between different bands by photon excitation, and is very much localized to the photo-excited site. Meanwhile, for EL, the excess electrons and holes are created by an electric current caused by an externally applied bias. As a result, EL contains information about the injection efficiency of the excess carriers through the electrical contacts which is not shown in PL. In this setup, PL is sampling a very small area of the device (about 5 µm laser spot size) versus EL that is sampling over a larger area (objective field of view of 65 x 50 µm) resulting in less sensitivity to localized defects. This high resolution for PL may lead to defects and dislocations playing more significant roles and altering the PL, such as PL peak broadening and intensity drop.

The next sample under study was InGaN LED with royal blue color and a PL peak at 452 nm. Figure 3 displays the PL map for the same device. The rough structure of the surface is also visible in all of the PL maps (intensity, position and FWHM of the PL peak). PL intensity drops on the messed contact pattern.

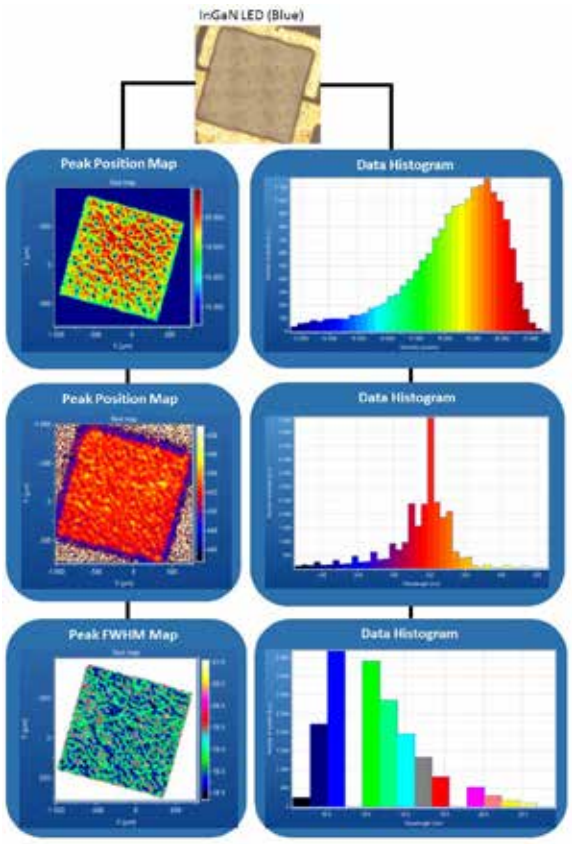

Figure 3: Various PL maps (peak intensity, peak wavelength position, and peak FWHM of the emission) with the associated data histograms for InGaN LED (blue).

Figure 4 displays the photoluminescence and electroluminescence spectra measured for the commercial blue InGaN LED. The EL and PL spectra almost follow a similar pattern with EL slightly shifted to longer wavelengths (red shift). The EL peak red shift may be attributed to the Stark effect caused by the electric field generated by the externally applied bias to the device.

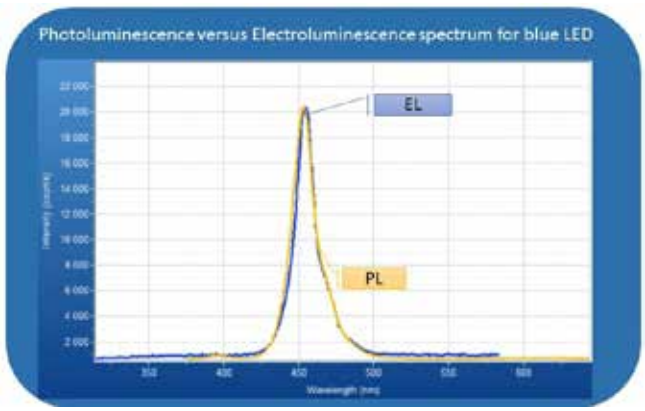

Figure 4: Photoluminescence versus electroluminescence spectra for InGaN (blue) LED. These 2 spectra are similar.

The Stark effect is the shifting and splitting of degenerate energy levels of atoms and molecules due to an external electric field [10]. In addition, PL and EL spectrum have more similarities compared to the same results (figure 2) for red LED, perhaps an indication of a more homogeneous epitaxial layer for blue LED.

Figure 5 demonstrates a normalized PL and EL emission for a commercial white LED. Most of the white LEDs in the market are made using a narrow-band blue emitter by InGaN LEDs plus a broad spectrum yellow emitter by a phosphor coating deposited on the blue die. The blue light generated either passes through the phosphor layer with no alteration or gets absorbed by the phosphor and converted to yellow. The combinations of the blue and yellow photons generates white light [2,11]. The thickness and composition of the phosphor layer determines the position and FWHM of the yellow peak and is often used to tailor the white color to warmer or cooler shades.

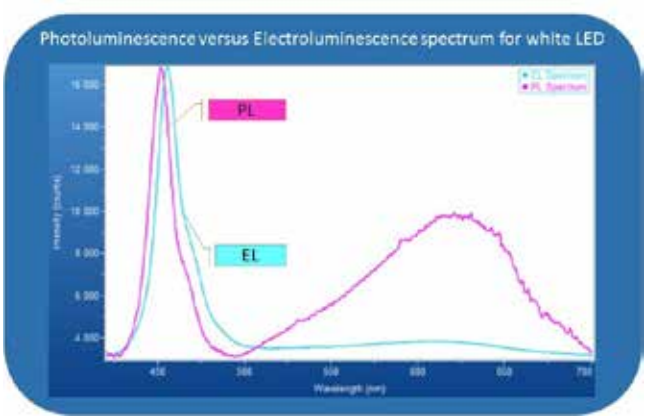

Figure 5: Photoluminescence versus electroluminescence spectra for white LED. El peak has a shift to the longer wavelengths compared to the PL peak for the blue peak at 450 nm. The broad yellow peak is much stronger for PL compared to EL

Conclusion

In this article, a multimode configuration of the SMS microspectroscopy system is used to characterize commercial LEDs. This tool enables the user to collect both EL and PL from the same spot on the device under the test with high spectral and spatial resolution, speed and accuracy. The luminescence measurements can improve the user's knowledge of the underlying material as well as device quality, in order to either monitor or optimize a process, or have a fundamental understanding of a material structure. The setup was used to study different commercial LEDs of different colors – collecting EL data under varying electrical conditions and mapping the PL peak. It was observed that the EL spectra were different from the PL spectra in some cases, emphasizing that they are often representative of different physical phenomena and provide complementary information.

References

(1) C. Licitra, N. Rochat, N. Gambacorti, S. David, G. R. Muthinti, F. Olivier, A. Faujour and A. Chabli, "Contribution of Luminescence Techniques for the Characterization of Materials and Devices at the Nanoscale" FCMN 135-138 (2017).
(2) Sung, H.J., Cho, Y.S., Huh, Y.D. and Do, Y.R., "Preparation, characterization and photoluminescence properties of Ca 1-x Sr x S: Eu red-emitting phosphors for a white LED," Bulletin of the Korean Chemical Society, 28(8), pp.1280-1284 (2007).
(3) Prall, C., et al. "In-situ photoluminescence measurements during MOVPE growth of GaN and InGaN MQW structures." Journal of Crystal Growth 415, 1-6 (2015).
(4) Li, Heng, et al. "Three dimensional characterization of GaN-based light emitting diode grown on patterned sapphire substrate by confocal Raman and photoluminescence spectromicroscopy." Scientific Reports 7, 45519 (2017).
(5) Lien, D.H., Amani, M., Desai, S.B., Ahn, G.H., Han, K., He, J.H., Ager, J.W., Wu, M.C. and Javey, A., "Large-area and bright pulsed electroluminescence in monolayer semiconductors", Nature communications, 9(1), p.1229 (2018).
(6) Lu, T., Ma, Z., Du, C., Fang, Y., Wu, H., Jiang, Y., Wang, L., Dai, L., Jia, H., Liu, W. and Chen, H., "Temperature-dependent photoluminescence in light-emitting diodes." Scientific reports 4, 6131, (2014).
(7) Agostini, G. and Lamberti, C. eds., [Characterization of semiconductor heterostructures and nanostructures] Elsevier, (2011).
(8) Moore, C.J.L., and Miner, C.J., "A Spatially Resolved Spectrally Resolved Photoluminescence Mapping System," Journal of Crystal Growth, Vol. 103, pp. 21-27, (1990).
(9) Bassignana, I.C., Miner, C.J., and Puetz, N., "Photoluminescence and Double-Crystal X-Ray Study of InGaAs/InP: Effect of Mismatch Strain on Band Gap" Journal of Applied Physics, Vol. 65, Issue 11, pp. 4299-4305, (1989).
(10) Mchedlidze, T., Arguirov, T., Kittler, M., Hoang, T., Holleman, J. and Schmitz, J., "Influence of electric field on spectral positions of dislocation-related luminescence peaks in silicon: Stark effect" Applied physics letters, 91(20), p.201113, (2007).
(11) Rao, H., Ding, K., Song, J., Xie, L., Wang, W., Wan, X., Zhou, L. and Liao, J., "Self-adaptive phosphor coating technology for white LED packaging", Frontiers of Optoelectronics, 5(2), pp.147-152, (2012).

For more information visit:

Microspectroscopy.com

info.sci@horiba.com

www.horiba.com/osd

USA:	+1 732 494 8660	**France:**	+33 (0)1 69 74 72 00	**Germany:**	+49 (0) 6251 8475 0
UK:	+44 (0)1604 542 500	**Italy:**	+39 06 51 59 22 1	**Japan:**	+81(75)313-8121
China:	+86 (0)21 6289 6060	**India:**	+91 80 41273637	**Singapore:**	+65 (0)6 745 8300
Taiwan:	+886 3 5600606	**Brazil:**	+55 (0)11 2923 5400	**Other:**	+33 (0)1 69 74 72 00